Université de Montréal

R-2-hydroxyglutarate modulates DNA Replication via Integrated Stress Response

Par

Jyoti Sharma

Département de Biochimie et Médecine Moléculaire

Faculté de Médecine

Mémoire présenté en vue de l'obtention du grade de Maîtrise en Biochimie

August 2023

Université de Montréal

Unité académique : Département de Biochimie et Médecine Moléculaire, Faculté de Médecine

---

Ce mémoire intitulé

R-2-hydroxyglutarate modulates DNA Replication via Integrated Stress Response

Présenté(e) par

Jyoti Sharma

A été évalué par un jury composé des personnes suivantes

Dr. Nicole J. Francis
Président-rapporteur

Dr. Hugo Wurtele
Directeur de recherche

Dr. Frédérick Antoine Mallette
Codirecteur de recherche

Dr. Julianna Blagih
Membre du jury

Résumé

Les gènes de l'isocitrate déshydrogénase (IDH) sont mutés dans 70 à 80 % des gliomes de bas grade. Les enzymes mutantes IDH qui en résultent présentent une activité de gain de fonction, produisant du R-2-hydroxyglutarate (R-2-HG), appelé oncométabolite en raison de son accumulation anormale dans les tumeurs et de ses activités oncogéniques potentielles. Parmi les caractéristiques du cancer telles que la reprogrammation métabolique et épigénétique, le stress réplicatif et la stabilité du génome ont été peu caractérisés dans les cancers IDH-mutants. Par conséquent, cette étude vise à étudier l'impact de l'accumulation de R-2-HG sur la réplication de l'ADN et sa contribution au stress réplicatif dans les cancers IDH-mutants.

Nous avons étudié la dynamique de la fourche de réplication dans des astrocytes humains normaux et confirmé les résultats dans d'autres lignées cellulaires normales et cancéreuses. Nous avons constaté que le traitement exogène par l'octyl-R-2-HG entravait la progression de la fourche de réplication et retardait par conséquent l'achèvement de la phase S. L'évaluation des niveaux de phosphorylation des protéines RPA, CHK1 et H2AX a révélé que la réponse classique au stress réplicatif (RSR) n'était pas activée. Un état cellulaire dans lequel la réplication de l'ADN est altérée sans activation de la RSR a notamment été décrit dans la littérature comme résultant de l'activation de la réponse au stress intégré (ISR). Cependant, l'activation de la RSI dans les cancers mutants IDH n'est pas bien étudiée. En évaluant les marqueurs d'activation de la RSI, tels que la phosphorylation de l'eIF2α et les niveaux de protéines ATF4, nous avons montré que l'octyl-R-2-HG activait la RSI. De plus, le blocage de l'ISR a partiellement sauvé la fourche de réplication et la progression de la phase S. Nous avons répliqué cette étude oncométrique. Nous avons reproduit ce défaut de réplication de l'ADN lié à l'oncométabolite ainsi que l'effet de sauvetage partiel de l'ISRIB lors de l'induction de la surexpression du gène IDH mutant. Nos résultats indiquent que la production de R-2-HG associée à la mIDH peut inhiber la dynamique normale de réplication de l'ADN via la signalisation ISR.

Mots-clés : Isocitrate déshydrogénase, Mutations IDH, Tumorigenèse, Octyl-R-2-HG, Oncométabolite, Réplication de l'ADN, Stress Réplicatif, Réponse Intégrée au Stress, Astrocytes

Abstract

The isocitrate dehydrogenase (IDH) genes are mutated in 70-80% of low-grade gliomas. The resulting IDH mutant enzymes exhibit gain-of-function activity, producing R-2-hydroxyglutarate (R-2-HG), which is referred to as an oncometabolite due to its abnormal accumulation in tumours and potential oncogenic activities. Among the hallmarks of cancer such as metabolic and epigenetic reprogramming, replicative stress and genome stability have been poorly characterized in IDH-mutant cancer. Therefore, this study aims to investigate the impact of R-2-HG accumulation on DNA replication and its contribution to replicative stress in IDH-mutant cancers.

We investigated replication fork dynamics in normal human astrocytes and confirmed the results in other normal and cancer cell lines. We found that exogenous treatment with octyl-R-2-HG impaired replication fork progression and consequently delayed S-phase completion. Assessment of RPA, CHK1 and H2AX protein phosphorylation levels revealed that the classical Replicative Stress Response (RSR) was not activated. Among others, a cell state in which DNA replication was impaired without activation of the RSR has been described in the literature as a result of activation of the Integrated Stress Response (ISR). However, ISR activation in IDH-mutant cancers is not well studied. Hence, by assessing ISR activation markers such as eIF2α phosphorylation and ATF4 protein levels, we showed that octyl-R-2-HG activated ISR. Moreover, blocking ISR partially rescued the replication fork and S-phase progression. We replicated this oncometabolite-related DNA replication defect as well as ISRIB's partial rescue effect upon induction of mutant IDH gene overexpression. Our results indicate that mIDH-associated R-2-HG production possibly inhibits normal DNA replication dynamics via ISR signalling.

Keywords: Isocitrate dehydrogenase, IDH mutations, Tumorigenesis, Octyl-R-2-HG, Oncometabolite, DNA replication, Replicative stress, Integrated Stress Response, Astrocytes

Table of Contents

List of Tables

List of Figures

List of Contributions

- Data used for preparation of the Figure 10A, B and 14A was generated by Dr. Mary McQuaid.
- Editorial review on the following chapters was done by Dr. Hugo Wurtele and Dr. Frédérick Antoine Mallette
    - Chapter 1 – Section – Rationale and Hypothesis
    - Chapter 2 – Materials and methods
    - Chapter 3 – Results
    - Chapter 4 – Discussion
    - Chapter 5 – Conclusion

List of Acronyms and Abbreviations

53BP1	p53-binding protein 1
5caC	5-carboxycytosine
5fC	5-formylcytosine
5mC	5-methylcytosine
a.u.	Arbitrary units
AlkB	Alkylation B
ALT	Alternate lengthening of telomere
AML	Acute myeloid leukemia
ATF4	Activating transcription factor 4
ATM	Ataxia-telangiectasia mutated
ATR	Ataxia telangiectasia and Rad3 related
ATRi	Ataxia telangiectasia and Rad3 related inhibitor
ATRIP	ATR interacting protein
ATRX	Alpha-thalassemia/mental retardation, X-linked chromatin remodeler
BCAT	Branched-chain amino acid aminotransferase
BRCA1	Breast Cancer gene 1
bZIP	Basic leucine zipper domain
CAF1	Chromatin assembly factor 1
Cdc45	Cell division cycle 45
Cdc6	Cell division cycle 6
CDK	Cyclin-dependent kinase
Cdt1	Chromatin licensing and DNA replication factor 1
CHK	Checkpoint kinase 1
CHK1i	Checkpoint kinase 1 inhibitor
CHOP	CCAAT-enhancer-binding protein homologous protein
CIMP	CpG island methylator phenotype
CldU	Chlorodeoxyuridine
CpG	5’-C—phosphate—G-3’
DDIT3	DNA Damage Inducible Transcript 3

DDK	Dbf4-dependent kinase
DDR	DNA damage response
DNMT1	DNA-methyltransferase 1
DTT	Dithiothreitol
EdU	Ethynyl-deoxyuridine
eIF2α	Eukaryotic initiation factor 2 α subunit
FAD	Flavin adenine dinucleotide
FDA	Food and Drug Administration
FH	Fumarate hydratase
FTO	Fat mass and obesity-associated protein
GADD34	Growth arrest and DNA-damaged protein 34
G-CIMP	Glioma - CpG island methylator phenotype
GCN2/EIF2K4	General control nonderepressible 2 / eukaryotic translation initiation factor 2 alpha kinase 4
GDC	Genomic Data Commons
GEF	Guanine nucleotide exchange factor
HDR	Homolog-directed repair
HIF-1α	Hypoxia-inducible factor 1-alpha
HR	Homologous recombination
HRI/EIF2AK1	Heme-regulated eIF2α kinase / eukaryotic translation initiation factor 2 alpha kinase 1
HU	Hydroxyurea
HygR	Hygromycin
IDH	Isocitrate dehydrogenase
IdU	Iododeoxyuridine
iPOND	Isolation of proteins on nascent DNA
IRES	Internal ribosome entry site
ISR	Integrated stress response
ISRIB	Integrated stress response inhibitor
Jak	Janus kinase
JmjC	Jumonji C

JMJD	Jumonji C domain-containing proteins
kDa	Kilodalton
KDM	Lysine demethylase
KLF4	Kruppel-like factor 4
LLG	Low-grade gliomas
m6A	N6-methyladenosine
MCM	Mini-chromosome maintenance
mIDH	mutant-isocitrate dehydrogenase
MRN complex	MRN (Mre11, Rad50 and Nbs1) complex
mTORC	Mechanistic target of rapamycin complex
NADP+	Nicotinamide adenine dinucleotide phosphate
NADPH	Reduced - nicotinamide adenine dinucleotide phosphate
NAP1	Nucleosome assembly protein 1
NCI	National Cancer Institute
Nrf2	Nuclear factor erythroid 2–related factor 2
OCT4	Octamer-binding transcription factor 4
PARP	Poly ADP ribose polymerase
PD-1	Programmed cell death protein 1
PERK/EIF2AK3	Protein kinase R (PKR)-like endoplasmic reticulum kinase / eukaryotic translation initiation factor 2 alpha kinase 3
PERKi	Protein kinase R (PKR)-like endoplasmic reticulum kinase inhibitor
PHD	Prolyl hydroxylase domain
PHF2	PHD Finger Protein 2
PIG3	p53-inducible gene 3
PKR/EIF2AK2	Protein kinase RNA-activated / eukaryotic translation initiation factor 2 alpha kinase 2
PP1	Protein phosphatase 1
R-2-HG	R-2-hydroxyglutarate
R2HGDH	R-2-hydroxyglutarate dehydrogenase
RF	Replication fork
RFC	Replication factor C

ROS	Reactive oxygen species
RSR	Replicative stress response
S phase	Synthesis phase
S-2-HG	S-2-hydroxyglutarate
S2HGDH	S-2-hydroxyglutarate dehydrogenase
SDH	Succinate dehydrogenase
SHH	Sonic hedgehog
SLBP1	Stem-loop-binding protein
SOX2	SRY-box 2
TC	Ternary complex
TCA	Tricarboxylic acid cycle
TET	Ten-eleven translocation
Tg	Thapsigargin
t-NASP	Nuclear autoantigenic sperm protein
TopBP1	DNA topoisomerase 2-binding protein 1
TP53	Tumor protein 53
TRE	Tetracycline-controlled transcriptional activation
YTHDF	YT521-B homology domain family
α-KG	alpha-ketoglutarate

-

Acknowledgement

It is with great gratitude that I thank Dr. Hugo Wurtele and Dr. Frédérick Antoine Mallette for providing me with the opportunity to conduct research in their laboratories, as well as for their guidance, constructive criticism, and development of critical thinking. While I am not certain whether I have become a better researcher in the last 1.5 years, I have become more aware of my true capabilities and my pursuit of knowledge.

A stretch of gratitude goes to Dr. Elliot Drobetsky for his jolly ambience, full of wisdom and constructive feedback during the lab meetings. In particular, I would like to thank Dr. Laura Hulea and her team member Dr. Zaynab Nouhi for their assistance in puromycilation experiments and expertise in Integrated Stress Response. For guiding throughout the microscopy and Incucyte experiments and in general, for his support, I am deeply grateful to Dr Mikhail Sergeev, the coordinator of the microscopy core facility.

Thanks to Dr. Mary McQuaid, a former colleague, for introducing me to the cell culture and experimental methodologies. She helped me sharpen my skills in designing experiments. The research conducted by Mary has been carried forward in this thesis, and I am deeply grateful for the insights and contributions she has made to my research. Edlie Saint Hilaire has been the most helpful member for many reasons. In addition to helping with lab settlement, she has also taught me so much French through her positive enforcement attitude. As well as teaching me how to freeze and thaw human cells and analyse DNA fibres, Sari Gezzar-Dandashi gave me so much technical advice and supported my desire to improve public speaking skills. Dr. Francois Belanger and Dr. Jean Francois Lemay have immensely supported my thesis research with their expertise in the field and lab techniques. Thanks a lot, to Roch Tremblay for helping me understand and troubleshoot my qPCR experiments whenever necessary.

I received massive help from Dr. Laurence M Gagne from Mallette lab, during my first attempt at performing transduction. Her welcoming nature made it so smooth to ask questions about anything. She and Dr. Karine Boulay, also from Mallette lab, have been accommodating throughout my research work. Karine's guidance on annexin staining, primer design, and qPCR troubleshooting was particularly valuable. Dr. Arshad Jilani from Filep lab, deserves a special thank you for his cheerful attitude and moral support. I have been immediately transported back home through his

stories and experiences. I would like to thank all the members from both labs for their support and feedback. A massive shout-out to the student committee at CR-HMR. I had the pleasure of experiencing Sugar Shack, pumpkin carving, and other aspects of Canadian culture through events organized by this committee as an international student and avid traveller.

I am extremely grateful for the opportunity to work part-time at Advocate Simar S Anand's restaurant *Darbar*. This experience has been one-of-a-kind and eye-opening. It would not have been possible for me to complete my studies without Dr. Derek Tannis, who accepted the hitchhiking offer and brought Tim and I back to Montreal from the historic failure of Tesla. I would like to express my gratitude to the members of the Toastmasters - Speak with Style for developing a greater sense of speech writing and speaking skills.

Thanks to *Ma* aur *Papa*, I could not have completed my studies successfully without your support. A special thanks to my father, who has inspired me in many ways. He has instilled in me a greater sense of perseverance through his grounded nature and 'never-say-no' attitude. Thank you so much, *Bhai* for complying to support my crazy endeavours. This is also an opportunity for me to thank my friends and neighbours for their support during my stay in Montreal.

Und vielen Dank, Tim!

Preface – A note to current and prospective graduate students

Whether a local or an international student, we share a passion for learning and discovering science. Therefore, I would like to take the opportunity to reiterate some lessons I recorded during my studies that may or may not be useful when making academic decisions.

1. Determining your lab fitness

The team members may or may not appreciate your potential. The day spent in a laboratory can be a synergistic flow like among comrades or as harrowing as hiking alone in the never-ending Himalayas. Be aware that lab presence is not equal to lab performance. I've come to understand that both the supervisor and the student play a role in determining one's fitness within the team. As a prospective student, it is essential to express your curiosity and motivation to a potential supervisor who will assess your suitability, but prioritizing self-assessment is the most effective approach. Here are some meticulous pointers:

a) **Intellectual compatibility** - By engaging in discussions about your interests, attending relevant seminars, and actively observing the level of expertise displayed during lab meetings, it is possible to identify individuals who share your curiosity. It is advisable to request an opportunity from your potential supervisor to interact with the lab members before making a definitive decision of pursuing studies in a lab.

b) **Quality of interpersonal communications** - Communication effectiveness varies among individuals. When engaging with potential team members, it is valuable to discuss any past communication challenges or conflicts involving students or lab members. Assess the supervisor's role in resolving such issues. Additionally, inquire about any instances where students terminated their studies prematurely and the underlying reasons. The reluctance of individuals to address these inquiries may indicate a lack of communication skills, which could potentially contribute to future conflicts.

c) **Modus operandi of the lab** – As a team-oriented individual, it is crucial to assess whether the lab fosters a collaborative environment. Personally, I encountered challenges working in an isolated setting where peer communication was limited merely to greetings. Consider whether a lab practices an equal division of labour when performing common lab tasks and if the

supervisor or lab manager promotes a code of conduct. Pay attention to the level of respect for the workplace environment, such as discouraging personal calls or disruptive conversations. International students may unintentionally feel excluded if local team members do not consciously communicate in a common language, typically English. Evaluate if the lab culture encourages learning from mistakes and provides recognition for team members' promotions and achievements. Consider how often lab members organize gatherings and whether the supervisor joins in. These aspects contribute to assessing the camaraderie and overall functioning of the lab.

d) **Current students' progress** – Investigate whether students who are currently enrolled or have recently graduated have managed to publish a first-author paper within the designated 5-year duration (in Canada) of their PhD studies. This aspect of their academic journey can provide valuable insights into the efficacy and mentorship of their respective supervisors.

e) **Supervisor's vision** – Within a supervisor **devoid of integrity** lies the capability to partake in both **bullying** and the **misuse of power**. Consider, if the well-being of students' mental health a priority for the supervisor? How does the supervisor address a hostile work environment? How frequently does the supervisor offer opportunities for students to enhance their skills? It is crucial to understand the expectations set for students. Has the potential supervisor maintained long-standing collaborations or formed new partnerships in the past five years? Do undergraduate interns work independently or under constant supervision in the lab? How is authorship determined for future publications? Biased decisions can arise if the supervisor solely determines authorship. Open and inclusive discussions with legitimate reasoning should be encouraged to address these topics, avoiding a closed or one-sided approach.

2. Stipend

My experience has been that initially, the supervisor only offers a minimum stipend of 19-20,000 CAD per year which is currently under the poverty line in Canada. But you have the right to explain if it fits your expenses or not. Especially for international students, if the wage is insufficient to book international tickets, do not hesitate to propose a yearly stipend that can accommodate your travel needs.

3. Upfront Evaluation

As a student, I've noticed that guidance is available when one asks for it. Hence, it's important to be upfront about wanting regular evaluations and setting work objectives. Don't be afraid to question evaluations that impact your growth, especially if you're open about your weaknesses. Both the supervisor and the student want the same thing i.e., the student succeeds as an independent thinker and scientist. And hey, when that happens, the supervisor feels proud of their mentorship. It's a win-win situation!

4. EQUALITY, EQUITY and DIVERSITY

As part of ensuring equity, it is important to observe whether the supervisor allocates sufficient resources and attention to each lab member or student, or if there is a tendency to favour a few. Additionally, consider whether interactions are solely influenced by circumstances such as publications and grant-related concerns, or if they are more broadly inclusive and scheduled in nature.

Developing an understanding of the interpersonal dynamics among lab members beyond their professional roles is beneficial. Frequently, supervisors and team members form personal relationships, whether within the same laboratory or elsewhere. The recruitment process for team members is also influenced by pre-existing or ongoing friendships. I have observed certain instances where personal connections were not formally recognized as potential conflicts of interest within a laboratory. Consequently, it is crucial to be conscious of these affiliations in order to understand the lab's environment and avoid being ensnared in monopolistic situations.

5. Mistreatment, disrespect, or incivility – ZERO TOLERANCE POLICY COMPLIANCE

In any setting, whether you're at your lab bench, pipetting, or in a meeting, it's important to address mistreatment, disrespect, or uncivil behaviour. If you find yourself in such a situation, you should report the behaviour, including the main person involved, as it violates the university's zero-tolerance policy. As a student, the idea of reporting supervisor may be daunting or uncomforting, however, reporting serves as an essential tool to highlight existing problems, which will then be utilized to drive necessary improvements. In more serious cases, you can seek free legal advice from the university's legal clinic. Outside of the university, there are also law firms that handle pro bono cases.

6. Awareness

The prevailing work environment is more challenging and overwhelming than ever. It is essential to be mindful that refraining from asking basic questions may lead to a normalization of this behaviour, potentially making you an outlier for raising concerns. ASK! ASK! And ASK!

Limitations in the Respect and Harassment Office System. How to improve?

If you, as a student, intend to formally submit a report against your supervisor, colleague, or anyone in the workplace, consider the following limitations.

Limitations	Example	How to improve?
Emphasis on legality over human connection	A student feels being unheard and repeating themselves while asking for any information related to their report. The Respect/harassment office strictly act as per the lawyer's suggestions to avoid any unintended complications.	Student must be treated with empathy and given importance over legal consideration. If the office's purpose is to support a victim, it should prioritise human connection over legal counsel.
Lack of transparency	A student is not upfront informed about the actions taken by the office on their report and what will be the outcome of that.	Upfront information on steps/actions taken for the report with justification and implications. Students should have the option to engage in report-related meetings, including confronting the offender. A member of student association must be included at all times of the report processing.
Lack of accountability	A student cannot hold Respect/Harassment office accountable for anything as their steps/actions are not transparent. Any wrongdoings from the side of Respect/harassment office will remain undetected.	Transparency enables students to hold the office responsible for mishandling and misconduct, prevalent in authoritative hierarchical structures.
Ignorance towards student's resolution	Student's resolution is not given importance as the offices strictly runs by the legal counsel and act accordingly.	When students provide evidence of harm, obligate achieving resolution such as apologies or direct meetings, granting students

		the choice to convey their grievances through face-to-face conversations.
Instances of falsification and order legal restrictions	Student receives a legal threat note or direct legal order to not share their experience with anyone otherwise they will be charged for 'reputational damage'.	If an office employee is proven to falsify information with evidence, immediate termination from their position occurs. Instead of legal threats to students, these incidents must be publicly shared to raise awareness among others. Afterall, the public holds the power to decide on one's reputation.
No psychological support for the student/victim from university	Despite experiencing harassment and shortcomings of Respect/Harassment office, university does not provide free psychological support. Moreover, student's health insurance is not fully covering the psychological support.	Health insurance should provide complete coverage for psychological consultations to student victims.

Raising awareness and creating a conducive environment in the educational system lie close to my heart. The three words that are highlighted in the quote below by the journalist and Nobel Peace laureate Maria Ressa are inspiring to me and my future vision.

> "I promised our team **transparency, accountability** and **consistency** because I wanted to create systems that would function regardless of personalities…. They are key to building a functional democracy and resisting the cultlike power of a dictator." – *How to stand up to a dictator* by Maria Ressa

Chapter 1 – Introduction

Cancer is a complex cellular condition characterized by the acquisition of abnormal traits that promote uncontrolled proliferation. Extensive research efforts are dedicated to understanding cancer development and progression mechanisms. The exploration of novel targeted therapies to combat this complex disease is promoted by initiatives that foster collaboration and knowledge exchange among researchers. A prominent sequencing platform, Genome Canada, for example, has played a pivotal role in advancing cancer genomics research through its sponsorship of multiple competitions.

Cancer therapy approaches have been shaped by targeting the fundamental concept of the "hallmarks of cancer". These hallmarks represent a proposed collection of acquired cellular functions that enable human cells to undergo uncontrolled proliferation and transition into a tumorous state. In the past 20 years, Douglas Hanahan and Robert Weinberg's creation of the 'hallmarks of cancer' series depicted the long-established nature of replicative stress and genome instability as well as emerging features such as metabolic and epigenetic reprogramming in cancer (Figure 1). These highlighted features comprise the main elements of our research project.

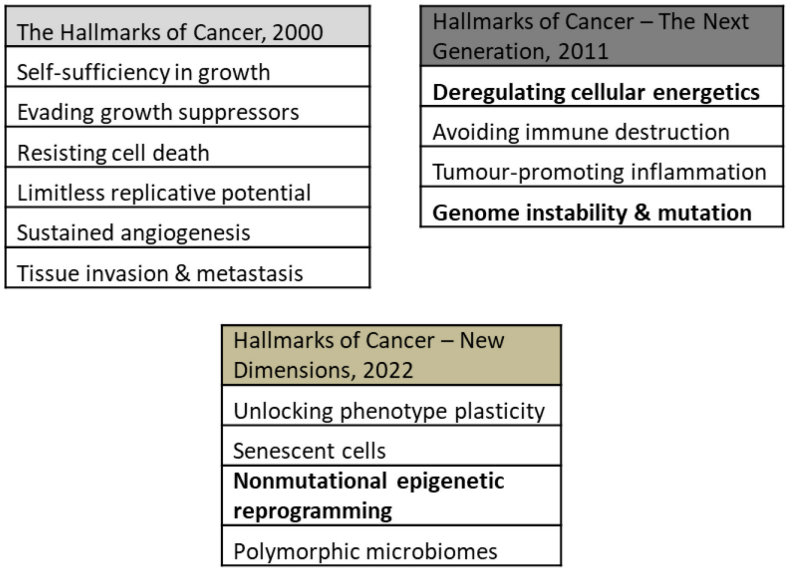

Figure 1 – A glance on emerging features such as 'deregulating cellular energetics' and 'non-mutational epigenetic reprogramming' from Hallmarks of Cancer (Hanahan, 2022; Hanahan & Weinberg, 2000, 2011)

Metabolic reprogramming in IDH-mutant cancer

The metabolic process encompasses a series of biochemical reactions that convert nutrients into energy as well as building blocks readily utilized by other cellular activities. Within a nutrient-fluctuating micro-environment, cell survival is influenced by alterations in gene expression of metabolic enzymes and changes in metabolic activity (Barrio et al., 2014). In the context of cancerous cells, metabolic reprogramming refers to these specific modifications that enable the establishment and support of bioenergetics for tumour development (Gouirand et al., 2018; L. Ma et al., 2013). The long-standing Warburg effect describes characteristics of metabolic reprogramming in cancer as excessive production of lactate, a product of anaerobic glycolysis (fermentation), despite the consumption of oxygen (Liberti & Locasale, 2016). However, recent studies have expanded on this concept, indicating a cancer state in which both fermentation and respiration occur simultaneously. In general, cancer metabolism is a complex phenomenon in which multiple factors may contribute to the process of reprogramming (Faubert et al., 2020; H. Li et al., 2020; McCann & Kerr, 2021; Xie et al., 2022).

Simpler cause-and-effect scenarios of metabolic reprogramming exist in studies focusing on genetic abnormalities. These abnormalities, particularly missense mutations in metabolism genes, are often sufficient to cause the abnormal accumulation of metabolic products, and subsequently leading to metabolic rewiring (Oermann et al., 2012). Among the extensively studied metabolic enzymes, those involved in the tricarboxylic acid (TCA) cycle have been identified as potential oncogenic drivers in human cancer. Mutations in specific enzymes such as isocitrate dehydrogenase 1/2 (IDH1/2), succinate dehydrogenase (SDH), and fumarate hydratase (FH) have been associated with increased accumulation of R-2-hydroxyglutarate (R-2-HG), succinate, and fumarate, respectively (Figure 2). These metabolites in abnormal concentrations are referred to as oncometabolites.

Notably, oncogenic mutations found in IDH genes are characterized as gain-of-function mutations that result in the emergence of neomorphic IDH enzymatic activity, thus producing R-2-HG. The presence of R-2-HG has become a valuable biomarker for the pathological diagnosis of tumours (Nobusawa et al., 2009). The NCI Genomic Data Commons (GDC) analysis indicates that IDH-mutant tumours predominantly originate within the central nervous system, with approximately 70-80% of these cases identified as low-grade gliomas with IDH1 mutations. However, these

mutations have also been observed in other tumour types, such as 6-10% of acute myeloid leukemia (AML) cases and 13% of cholangiocarcinoma.

The catalytic activity of the normal IDH enzyme i.e., the oxidative decarboxylation of isocitrate to form α-ketoglutarate (α-KG) results in a reduced form of NADPH (Nicotinamide Adenine Dinucleotide Phosphate). However, mutant IDH enzymes consume NADPH to convert α-KG to R-2-HG, an irreversible reaction, disrupting the balance between α-KG and NADPH demands (Figure 2). The depletion of α-KG has been extensively studied and is associated with abnormal DNA methylation also known as Glioma – CpG Island Methylator Phenotype (G-CIMP). The underlying mechanism of this epigenetic reprogramming is discussed in a later section.

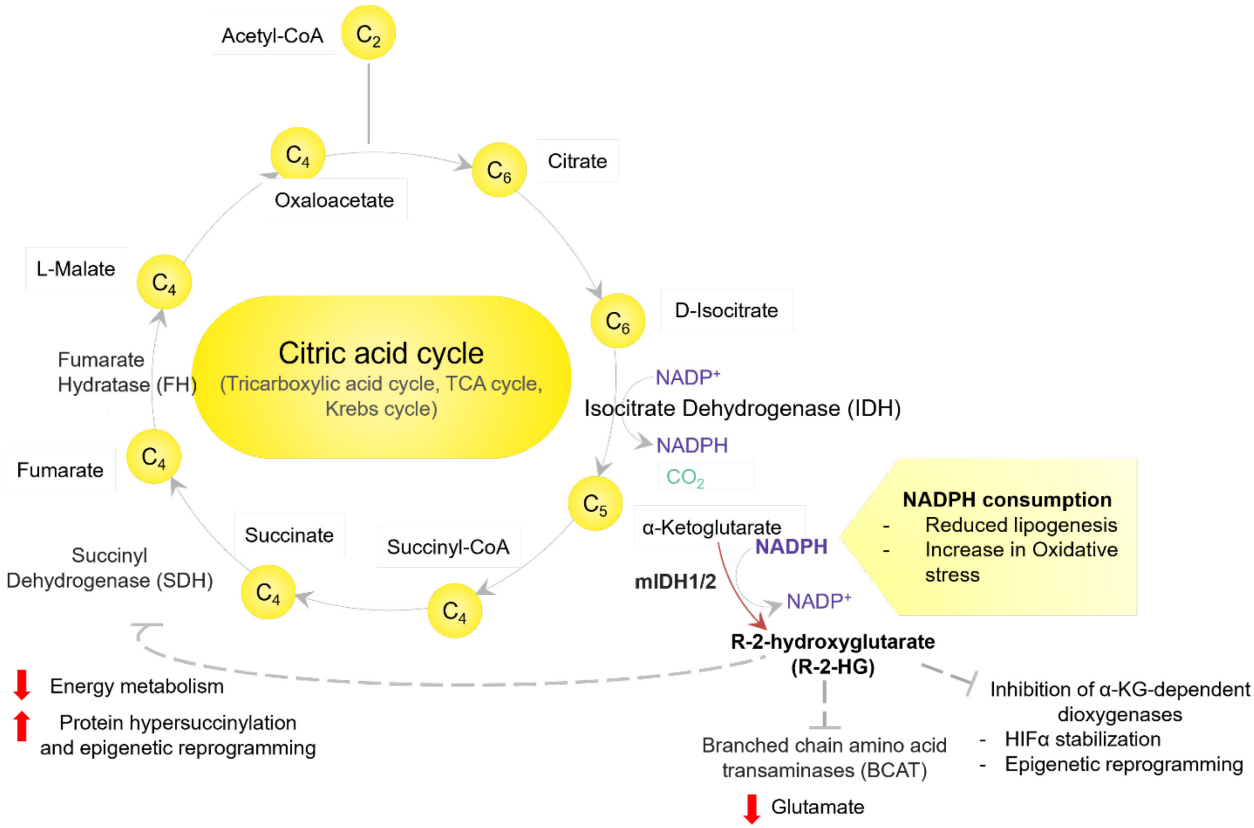

Figure 2 – Mechanisms of metabolic reprogramming by R-2-HG in IDH-mutant cancer (designed using ConceptDraw).

On the other hand, the depletion of NADPH pools both in the mitochondria (IDH2) and cytoplasm (IDH1), has been shown to impact lipid biosynthesis and homeostasis of Reactive Oxygen Species (ROS). NADPH serves as a cofactor for the process of lipogenesis. In heterozygous IDH1 mutant fibrosarcoma, the depletion of NADPH caused by R-2-HG was found to exacerbate cellular growth under conditions of lipid deficiency (Badur et al., 2018). Altered phospholipid profiles have also been reported in IDH-mutant gliomas and chondrosarcomas. Based on S. Li et al., 2019, dysregulated fatty acid metabolism was postulated to alter cellular membrane composition, increase oxidative stress, and modulate apoptosis in a glucose-dependent manner, thereby promoting tumorigenesis.

Similar to the anabolic pathway of lipid biosynthesis, aerobic catabolism also generates ROS, which, when accumulated, can trigger oxidative stress, and cause significant damage to DNA, RNA, and proteins (Castelli et al., 2021; Rodriguez-Fernandez et al., 2013; Tanaka & Chock, 2021; Van Houten et al., 2018). NADPH serves as a crucial reducing agent in multiple antioxidant systems, such as glutathione and thioredoxin reductase, along with NADPH oxidases, enabling effective detoxification of ROS. Hence, the depletion of NADPH resulting from the production of R-2-HG has prompted the exploration of therapeutic approaches targeting an oxidative stress signalling via Nrf2 pathway (Y. Liu et al., 2019). In normal cells, the Nrf2 pathway orchestrates the upregulation of antioxidant systems as a response to oxidative stress. However, in IDH1 mutant cells, Nrf2 knockdown has been demonstrated to enhance the sensitivity to temozolomide, a genotoxic form of chemotherapy (K. Li et al., 2017).

In addition to the metabolic rewiring induced by the production of R-2-HG, the accumulation of R-2-HG also exerts a competitive inhibitory effect on the activity of branched-chain amino acid transaminase (BCAT) and succinate dehydrogenase (SDH). BCAT enzymes play a crucial role in brain metabolism by facilitating the reversible production of glutamate from α-ketoglutarate (α-KG) and branched-chain ketoacids. Glutamate is essential for neural communication and neurotransmission homeostasis. Exploiting the inhibitory effect of R-2-HG on BCAT, glutaminase (produces glutamate from glutamine) inhibitors have been used to enhance the eradication of IDH-mutant gliomas (McBrayer et al., 2018; Zhang, 2018). SDH, on the other hand, normally catalyzes the conversion of succinate to fumarate in the TCA cycle. The inhibition of SDH by the accumulation of R-2-HG has been implicated in the hypersuccinylation-dependent apoptosis

resistance, thereby promoting tumorigenesis. (F. Li et al., 2015). An interesting finding is that IDH1/2 mutant cells with an increased succinylated histones suggest the possibility of genomic instability resulting from the bulky succinyl modification.

IDH-mutant or mIDH-positive brain cancers mainly originate from astrocytes and oligodendrocytes, resulting in infiltrative neoplasms that cannot be completely surgically resected. The initial treatment strategy for mIDH1-positive tumours involved the inhibition of the catalytic activity of the mIDH1 enzyme using the chemical compound AGI 5198 (Popovici-Muller et al., 2012). However, the efficacy of this mIDH inhibitor was considered limited due to the observation of poor pharmacodynamic profiles and its rapid metabolism, and some AML patients even showed resistance to this inhibitor. As a result, an improved version of AGI 5198, AG 120 (Ivosidenib) is approved by FDA and currently undergoing human trials. However, some reports have argued that AG 120 only regresses the cancer phenotype but does not eliminate cancer cells (Gruber et al., 2022; Popovici-Muller et al., 2018; Zhuang et al., 2022). Recruitment for several clinical trials involving combination drugs is curently in progress (Table 1). Although mIDH-positive gliomas have a better survival rate than mIDH-negative cancers, frequent relapses highlight the need for more aggressive treatment options (Molinaro et al., 2019). Therefore, targeted therapies addressing the molecular mechanisms underlying IDH mutation-associated alterations in cell activities are necessary to effectively treat IDH-mutant pathologies.

Table 1 – Ongoing clinical trials for mIDH-positive cancers (clinicaltrials.gov).

Drug (single/combination)	**Drug Action**	**Condition or disease**	**ClinicalTrials.gov ID**
HMPL-306	Dual mIDH1/2 inhibitor	mIDH metastatic solid tumours - cholangiocarcinoma, skeletal chondrosarcoma, low-grade glioma, perioperative low-grade glioma	NCT04762602
Olaparib Durvalumab	PARP inhibitor Immune-checkpoint inhibitor	mIDH glioma & cholangiocarcinoma	NCT03991832

Retifanlimab All-trans retinoic acid	PD-1 inhibitor Retinoid drug	Recurrent mIDH astrocytoma & oligodendroglioma	NCT05345002
Talazoparib	PARP inhibitor	Recurrent mIDH glioma & glioblastoma	NCT04740190
AG-120 (Ivosidenib) Enasidenib Fedratinib	mIDH1 inhibitor Pan-mIDH2 inhibitor Jak inhibitor	mIDH myeloproliferative neoplasm	NCT04955938

Isocitrate Dehydrogenase (IDH) genes and R-2-HG production

The Isocitrate dehydrogenase (IDH) enzymes participate in a biochemical reaction taking place in both the cytoplasm and mitochondria. The human genome encompasses five IDH genes: IDH1 (located on chromosome 2), IDH2 (located on chromosome 15), IDH3A (located on chromosome 15), IDH3B (located on chromosome 20), and IDH3G (located on chromosome X). These genes give rise to the expression of three enzymes: IDH1, IDH2, and IDH3. While IDH1 and IDH2 are homodimeric in nature, IDH3 is a heteromeric protein complex composed of IDH3A, B, and G subunits. The IDH1 and 2 enzymes catalyze the conversion of isocitrate to alpha-ketoglutarate (α-KG) through an oxidative decarboxylation reaction, utilizing one $NADP^+$ per isocitrate and releasing NADPH. IDH1 and IDH2 can reversibly produce isocitrate via reductive carboxylation, however, IDH3 possesses an irreversible activity (T. Ma et al., 2017). IDH2 and IDH3 enzymes function in the mitochondria, while IDH1 operates in the cytoplasm.

Table 2 – Frequency of different IDH mutations in gliomas (Hartmann et al., 2009; Waitkus et al., 2016; Yan et al., 2009).

Gene	Mutation	Amino acid change	Frequency
IDH1	395 G>A	R132H	83-88%
	395 G>T	R132L	0.3-4%
	394 C>T	R132C	3-4%
	394 C>A	R132S	1-2%
	394 C>G	R132G	0.6-1.3%
IDH2	515 G>A	R172K	2.4-2.7%
	515 G>T	R172M	0.8-1.8%
	514 A>T	R172W	0-0.7%
	514 A>G	R172G	0-1.2%

Mutations in the IDH1 and IDH2 genes play a significant role in the development of tumours. Table 2 provides a summary of the most common driver mutations observed in these genes. What makes these mutations particularly intriguing is their occurrence as heterozygous variants within cancer cells that originate from somatic mutations. These mutations manifest as missense mutations (substitution) at the catalytic site of both IDH enzymes. The heterozygous nature of these mutations leads to the formation of heterodimeric protein assembly with neomorphic enzymatic activity, converting α-KG to R-2-HG. Unlike the reversible reaction by the IDH homodimer, this biochemical reaction by the IDH heterodimer depicted in Figure 3 is irreversible in nature

(Leonardi et al., 2012). Notably, 2-HG exists in two enantiomers: R (or D) and S (or L) configurations. However, IDH enzymes are responsible for the production of R-2-HG in the context of IDH-mutant cancers (Gross et al., 2010; Intlekofer et al., 2017). R-2-HG is estimated to be found at concentrations between 1 and 30mM in cancer cells and found to be accumulated in the extracellular matrix (Ježek, 2020).

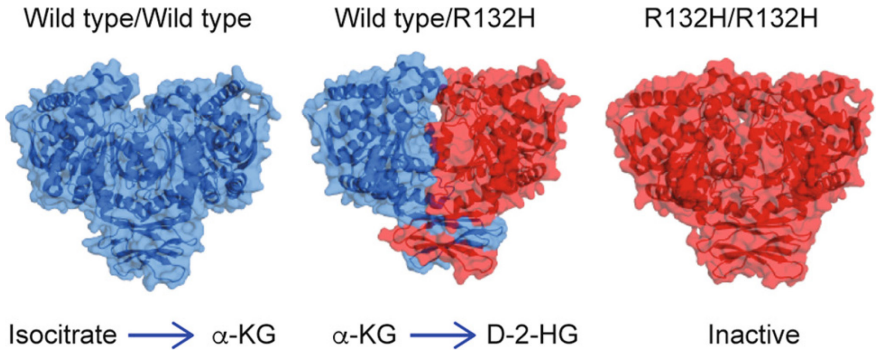

Figure 3 – Heterodimeric nature of IDH-mutant enzymes in cancer (Han et al., 2020). (D in D-2-HG denote D and L chemical configuration)

The enantiomers R and S-2-HG undergo oxidation to produce α-KG by the enzyme R and S-2-hydroxyglutarate dehydrogenase (R2HGDH or S2HGDH), respectively, which belongs to the FAD-binding oxidoreductase/transferase type 4 family of mitochondrial proteins. These enzymes were initially investigated in neurometabolic disorders. Particularly the presence of mutated R2HGDH or S2HGDH led to the accumulation of R and S-2-hydroxyglutaric acid in the urine of affected individuals (Kohlschütter et al., 1982; Kranendijk et al., 2012). However, in the context of malignancy, an aberrant upsurge in R-2-HG occurs primarily due to its elevated production rate rather than its degradation rate (Berger et al., 2019).

Antagonistic effect of R-2-HG promoting tumorigenesis

The role of the normal metabolite α-KG can be broadly divided into two categories: energy metabolism and regulation of cellular activities as a cofactor of dioxygenases. In energy metabolism, α-KG serves as a substrate in the TCA cycle to produce intermediary metabolites that supply ATP and building blocks for cells, such as amino acids and lipids (Figure 2). Additionally, the production of α-KG also generates NADPH, which regulates the antioxidant activity and fatty acid biosynthesis.

Dioxygenases are a type of non-heme iron enzymes that incorporate oxygen atoms into substrates. A subfamily of enzymes referred to as α-KG-dependent dioxygenases require α-KG along with Fe (II) ions as cofactors for their enzymatic activity. However, R-2-HG has been found to competitively inhibit these enzymatic activities due to its poor ligand interactions with Fe (II) ions, crucial for catalysis (Figure 4) (Joberty et al., 2016; Xu et al., 2011). This antagonistic effect of R-2-HG has been speculated to promote tumorigenesis by epigenetic reprogramming and alteration in gene expression (J. W. Park & Turcan, 2019; Ye et al., 2013a). The most studied dioxygenases are described in the following section, emphasizing their role in IDH-mutant tumorigenesis.

TET dioxygenases

The TET family of dioxygenases catalyzes the oxidation of 5-methylcytosine (5mC), an epigenetic marker on DNA. This enzymatic reaction results in the formation of three different cytosine derivatives: 5-hydroxymethylcytosine (5hmC), 5-formylcytosine (5fC), and 5-carboxycytosine (5caC). DNA methylation occurs in approximately 70-80% of the genome. It is particularly prevalent at CpG sites within gene promoters and acts as a transcriptionally ON or OFF marker (Smith & Meissner, 2013). Studies have suggested that the inhibitory effect of R-2-hydroxyglutarate (R-2-HG) on TET enzymes contributes to a hypermethylation pattern observed on CpG islands in glioblastomas and AML cases, known as CpG island methylator phenotype (CIMP) (Figueroa et al., 2010; Noushmehr et al., 2010). The DNA hypermethylation was postulated to alter chondrogenic and osteogenic differentiation by decreasing the transcription of sonic hedgehog (SHH) signalling proteins (L. Liu et al., 2021). In astrocytes, the IDH1 R132H mutation alone was sufficient to induce the CIMP phenotype (Turcan et al., 2012).

DNA methylation deposition and removal are regulated by the interplay between TET demethylases and DNA methyltransferases (DNMT) in a cell cycle-dependent manner. However,

the activity and recruitment of these enzymes are also influenced by histone modifications specifically the histone methylation markers (Y. Li et al., 2021). Interestingly, a considerable amount of research has focused on investigating the antagonistic effect of R-2-HG on histone lysine demethylases (KDM), acting as yet another pivotal point in the dysregulation of gene expression and epigenetics in IDH-mutant cancer.

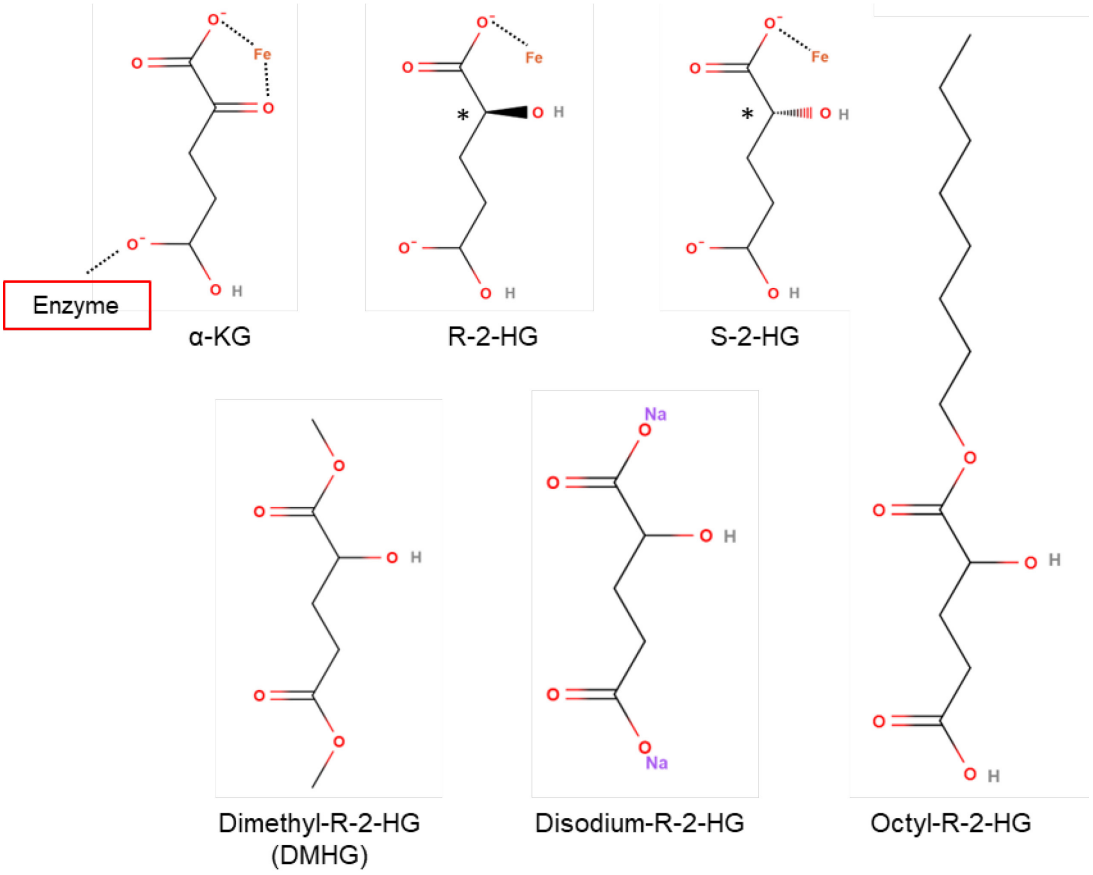

Figure 4 – Chemical structure of metabolites α-KG, R-2-HG and S-2-HG with Fe (II) ion and dioxygenase interaction site are in the top row. Common cell-permeable forms of R-2-HG used in experimental studies are in the bottom row. Structures were designed using MolView. '*' represents the chiral carbon.

Jumonji-C domain-containing lysine demethylases (JMJD-KDMs)

Jumonji C is the signature domain capable of ligand interactions with Fe (II). An important member of the Jumonji C (JmjC) domain-containing protein family is the demethylase that modulate modifications on histone tails therefore also known as KDM proteins. KDM superfamily proteins

are classified as KDM 2 – 8 subfamilies based on their substrate specificity, catalytic activity and structural properties (Table 4). These enzymes are inhibited by metabolites such as fumarate, succinate and R-2-HG and have been implicated in IDH-mutant tumorigenesis (Chowdhury et al., 2011; Sulkowski et al., 2020; Ye et al., 2013). The inhibitory activity of R-2-HG on KDMs alters gene expression and histone modifications profoundly (Janke et al., 2017; Kickingereder et al., 2015). Several studies have indicated that the absence of histone demethylation impairs differentiation and promotes leukemogenesis in mIDH-positive cells (Figueroa et al., 2010; Y. Jin et al., 2015; Losman et al., 2013; Lu et al., 2012). A number of mIDH-positive malignancies have been identified to be defective in the DNA Damage Response (DDR). In one of them, promoter H3K9 hypermethylation was associated with a decreased expression of DNA damage sensor ATM caused by the inhibitory effect of R-2-HG on KDM4A/C (Inoue et al., 2016). A further study speculated that R-2-HG-mediated inhibition of KDM4A and KDM4B was responsible for the suppression of Homologous Recombination (HR) repair or the 'BRCAness' and proposed that the PARP inhibition could be an effective therapeutic strategy against mIDH-positive cancer (Sulkowski et al., 2017). As shown in Table 4 and discussed in the following section, recent advances shed light on the involvement of several KDM enzymes in DNA replication. In summary, KDMs play a critical role in regulating several cellular functions, the alteration of which may contribute to tumorigenesis following IDH mutations and the inhibition of KDMs by the accumulated oncometabolite R-2-HG.

AlkB and FTO dioxygenases

Additional α-KG-dependent dioxygenases, specifically proteins from the alkB homolog (ALKBH) family facilitate the removal of alkyl adducts such as 1-methyladenine and 3-methylcytosine from single-stranded DNA in both *Escherichia coli* and humans (Duncan et al., 2002; Mohan et al., 2018; Nigam et al., 2018). In the absence of any repair mechanisms, these adducts impede DNA replication and induce cellular toxicity (Boiteux & Laval, 1982). The ability of R-2-hydroxyglutarate (R-2-HG) to inhibit AlkB activity has been exploited to target the mIDH-positive tumours with DNA alkylating agents (Chen et al., 2017; Wang et al., 2015). Recent research work suggested that R-2-HG exhibits anti-tumour effects by inhibiting a specific target, a member of the AlkB family of dioxygenases called fat mass and obesity-associated protein (FTO) (Su et al., 2018a). FTO has been recognized as the first mRNA N^6-methyladenosine (m6A) demethylase (Bartosovic et al., 2017; Jia et al., 2011). Inhibition of FTO by R-2-HG leads to decreased stability

of Myc mRNA, thereby inhibiting cancer cell proliferation. Due to this functionality of R-2-HG, mIDH-positive tumours may have a better prognosis than wild-type IDH tumours.

DNA replication, Replicative Stress, and Stress Response

DNA replication is a fundamental cellular process that involves the accurate duplication of the genetic material (Alberts et al., 2002). It takes place during the synthesis phase (S phase) of the cell cycle and requires the coordinated action of multiple proteins to ensure successful completion before cell division (Hustedt et al., 2013; Nedelcheva-Veleva et al., 2006). DNA replication is initiated at a conserved region of the genome, called the Origin site (ORI). These sites maintain stable interactions with a cluster of proteins collectively referred to as the Origin Recognition Complex (ORC). As the cell cycle progresses and kinase activity shifts, pre-replicative complexes (pre-RCs) form (Gilbert, 2002). This assembly is facilitated by the involvement of Cdc6 (cell division cycle 6) and Cdt1 (chromatin licensing and DNA replication factor 1), which assist in recruiting the MCM2-7 (mini-chromosome maintenance) helicase complex to ORC sites. This critical process is named as origin licensing (Fragkos et al., 2015).

Even though pre-RCs and other recruited factors are loaded onto the ORC, they remain dormant until signaled by checkpoint kinases that oversee the progression of the cell cycle. As the transition from the G1 phase to the S phase takes place, Cyclin-dependent kinase (CDK) and Dbf4-dependent kinase (DDK) are activated (Figure 5A) (Gómez-Escoda & Jenny Wu, 2017; Heller et al., 2011; N. Li et al., 2023). They phosphorylate the MCM complex, RECQ-like helicase 4, and TopBP1, fostering their interactions. This, in turn, facilitates the helicase activation by recruiting Cdc45 and the GINS (go-ichi-ni-san) complex to MCM, identified as CMG helicase (Pasero & Gasser, 1998; Stenlund, 2003). Furthermore, DNA polymerases are recruited to the CMG helicase prior to its DNA unwinding activity. This collective assembly of proteins constitutes a replisome and leads to the initiation of DNA replication or origin firing (Yeeles et al., 2015).

The launch of DNA replication hinges on the MCM helicase complex binding to the DNA and utilizing ATP hydrolysis to meticulously separate the DNA strands (Chong et al., 2000; Shechter et al., 2004). This unwinding process leads to the formation of a replication fork, and single-stranded segments are supported by single-stranded binding proteins (SSBs) or replication protein A (RPA) (Bhat et al., 2015; Nagata et al., 2019). Additionally, the supercoiling of DNA is addressed by topoisomerase action (Pommier et al., 2016). Within the heart of the replication fork, pivotal players such as the DNA polymerase α/RNA primase complex, DNA polymerase ε and δ, a sliding DNA clamp termed PCNA, and a clamp loader known as RFC collaborate (Adelman et

al., 2010; Schrecker et al., 2022). This orchestration of activities culminates in the synthesis of new DNA on both the leading and lagging strands (Figure 5B) (Cooper, 2000).

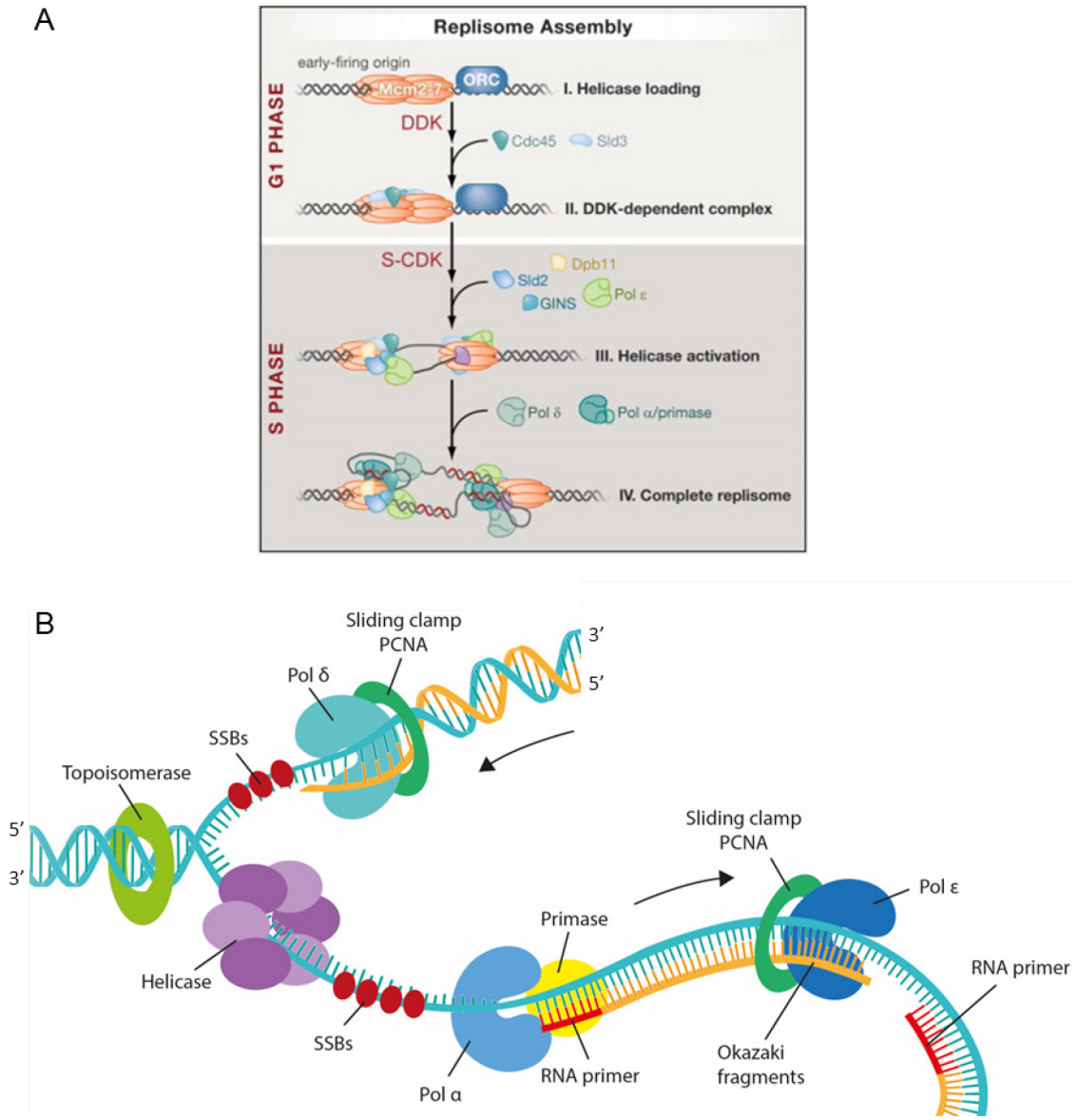

Figure 5 – The process of DNA replication in eukaryotes.

A) Series of protein recruitment and complex activation forming replisome assembly (Heller et al., 2011) prior to the initiation of DNA Replication. **B)** A representation of replisome machinery during the elongation of DNA replication (Image by LabXchange)

The stability of the genome can be compromised by various processes associated with DNA, including DNA replication. The resulting genome instability is considered as a hallmark of cancer

(Ferguson et al., 2015; Fugger et al., 2009; Negrini et al., 2010). Genome instability fuels cancer evolution and therapeutic resistance which is a major roadblock to finding universal treatment solution. The term 'DNA replicative stress' refers to a significant increase in replication forks (RF) that are compromised, either due to slow progression or stalling. During this replication stress, activities of the DNA polymerase and the CMG helicase become uncoupled, potentially exposing single-stranded DNA (ssDNA) which is highly susceptible to nucleases (Klein, 2020; Lemay et al., 2022; Sabatinos & Forsburg, 2015).

Consequently, the initial step in the Replicative Stress Response (RSR) mechanism involves the accumulation of RPA at the exposed ssDNA. This accumulation triggers the activation and binding of checkpoint kinases ATR (ataxia telangiectasia-mutated and Rad3-related) and ATRIP (ATR Interacting Protein) (Byun et al., 2005; Ré mi Buisson et al., 2015). When the ATR kinase interacts with RPA, downstream effectors such as H2AX and Chk1 (specifically serine residues 317 and 345) proteins, as well as RPA (serine residue 33) undergo phosphorylation. Despite its unclear mechanism, ATR signalling eventually leads to a delay in the firing of replication origins and a cell cycle arrest (Beggs & Yang, 2019; Brown & Baltimore, 2003; Gralewska et al., 2020; Técher & Pasero, 2021).

Compromised DNA replication in IDH-mutant cancer

Replicative stress can stem from numerous factors, yet it remains largely uncertain whether IDH mutations or the altered metabolism induced by R-2-HG play a pivotal role in driving replicative stress in IDH-mutant tumorigenesis. DNA replication is protected by two of the major tumor suppressor genes, ATRX and TP53 (Aguilera & López-Contreras, 2023; Klusmann et al., 2016). The ATRX protein acts as a chromatin remodeler averting the formation of complex DNA structures in heterochromatin during replication (Teng et al., 2021). Additionally, there is evidence demonstrating that ATRX interacts with the MRN (Mre11, Rad50 and Nbs1) complex enabling replication fork stabilization, thereby preventing replication stress/genome instability (Clynes et al., 2014). Similarly, TP53, a transcription factor, has been extensively investigated for its role in stabilizing the 'chicken foot' structures (RF reversal) that arise during replication stress (Klusmann et al., 2016; Subramanian & Griffith, 2005).

It is interesting to observe that, as per cBioPortal data, there is a significant co-occurrence of ATRX and TP53 mutations in IDH1-mutant samples among the brain/CNS cancer studies (Table 3). Moreover, mIDH-positive astrocytoma with ATRX mutations were distinguished by an alternative lengthening of telomeres (ALT) phenotype (Ferreira et al., 2020). This phenotype, resulting from telomere replication defects, played a role in enabling the immortalization of cancer cells. In a recent investigation, cells with IDH mutations exhibited slow RF progression in the heterochromatin region. Nevertheless, the study did not elucidate the underlying mechanism responsible for this observation (Schvartzman et al., 2022). Provided the indispensable functions of ATRX and TP53 in DNA replication, IDH-mutant cells are prone to accumulating replication stress/genome instability, thereby fostering cancer heterogeneity. A precise manner by which IDH mutations or the production of R-2-HG impacting DNA replication has yet to be determined. Multiple viable mechanisms could potentially lead to replicative stress in IDH-mutant tumors, including direct inhibition of histone KDM activity by R-2-HG or indirect constraints on histone availability. The following details the possible explanation.

Table 3 - Mutual exclusivity analysis between IDH1/2 and ATRX, TP53 with CNS/Brain studies using cBioPortal last accessed on 16 August 2023. The frequent mutations are as follows: IDH1 R132H, IDH2 R172K, TP53 Y220C and ATRX truncation.

A	B	Neither	A Not B	B Not A	Both	p-Value	q-Value	Tendency
TP53	ATRX	3446	890	107	934	<0.001	<0.001	Co-occurrence
ATRX	**IDH1**	**3497**	**164**	**839**	**877**	**<0.001**	**<0.001**	**Co-occurrence**
TP53	**IDH1**	**2907**	**754**	**646**	**1070**	**<0.001**	**<0.001**	**Co-occurrence**
IDH2	IDH1	3582	79	1705	11	<0.001	<0.001	Mutual exclusivity
IDH2	ATRX	4272	64	1015	26	0.03	0.036	Co-occurrence
IDH2	TP53	3488	65	1799	25	0.261	0.261	Mutual exclusivity

Indirect Mechanism – Disturbance in histone supply

Both histone depletion and accumulation have been shown to impede DNA replication (Groth et al., 2007a; Kim et al., 2021; Mejlvang et al., 2014). The histone chaperone CAF1 plays a critical role in regulating the availability of histones and the assembly of nucleosomes around the replication fork, as established by Tyler et al., 1999. In a proximity labelling study, CAF1 and another histone chaperone, NAP1, were identified as interactors of KDM5-family proteins (Yheskel et al., 2023). Additionally, knocking down KDM3B led to elevated levels of the histone chaperone NASP (Nuclear Autoantigenic Sperm Protein), resulting in an accumulation of free H3-H4 pool and compromising the progression of the S-phase. (Richardson et al., 2006; Saavedra et al., 2020). These studies suggest that specific KDM proteins may possess gene regulatory functions that go beyond their demethylase activity. These functions could also involve interactions with histone chaperones like CAF1, NAP1, and NASP, consequently limiting the process of DNA replication.

Notably, the depletion of a histone mRNA processing factor SLBP1 (stem-loop-binding protein) has been linked to slow down of replication fork progression. (Mejlvang et al., 2014). Moreover, the methylation on histone mRNA may be modulated through the known inhibitory impact of R-2-HG on m6A (N6-methyladenosine) demethylases like FTO and ALKBH5 (Joberty et al., 2016; Su et al., 2018). Consequently, this modification could regulate both the signaling of histone mRNA degradation and its overall abundance. (Shi et al., 2017). Nonetheless, it is important to note that thus far, no demethylase has been identified as a regulator of histone mRNA methylation. In conclusion, aside from the influence of histone chaperones, the regulation of histone mRNA processing by R-2-HG has the potential to slowdown DNA replication.

Direct Mechanism – Alteration in histone KDM activity

Histone modifications play a crucial role in various aspects of DNA replication and RSR. Several studies have investigated the impact of KDM activity on histone tails in these processes, and few key findings are summarized in Table 4. The activity of KDM4D, through demethylation of H3K9me, was observed to regulate the formation of pre-replicative complexes (pre-RCs) required for the initiation in DNA replication (Wu et al., 2017). When the levels of KDM2B, which demethylates H3K79me, are low, it led to a defect in PCNA dissociation during completion of DNA replication, likely due to its affinity with H3K79me (Kang et al., 2020). KDM4A and KDM4B directly interacted with MCM subunits and DNA polymerase, facilitating DNA replication (Mishra et al., 2018). Furthermore, overexpression of KDM4A and KDM4B led to their coimmunoprecipitation with replisome components MCM 3 and 4, further supporting their role in DNA replication (unpublished data from Mallette's lab). Intriguingly, AlkB homolog 2 (ALKBH2) colocalized as well as interacted with PCNA (at replication foci) which acts as a sliding clamp in the replisome (Aas et al., 2003; Gilljam et al., 2009). Through an iPOND interactome analysis, PHF2, a specific lysine-specific demethylase, was identified as a telomere replication factor (Lin et al., 2021). In addition, a KDM4A knockdown has been found to increase the proportion of chromosomes with telomere defects possibly due to telomere replicative stress (unpublished data from Mallette's lab). Currently, there is a growing body of research that links the epigenetic markers modulated by α-KG-dependent dioxygenases to DNA replication. In the near future, we anticipate that the mechanisms driving this relationship will be revealed in cancers caused by IDH mutations.

Table 4 – Role of KDM enzymes in DNA replication, RSR and DNA damage response.

JmjC-domain-containing KDMs	Substrate specificity	Functional Significance
KDM2A, KDM2B	H3K36me2/me1, H3K4me3	- PCNA dissociation in DNA replication termination (Kang et al., 2020) - Recruitment of 53BP1 on DNA breaks (Bueno et al., 2018)
KDM3A/JMJD1A, KDM3B/JMJD1B	H3K9me2/me1	- Restrained DNA damage response in senescence and promote heterochromatin reorganization (Huang et al., 2019) - DNA Damage Response (DDR) gene regulation via c-Myc (Fan et al., 2020) - Regulated protein levels of histone chaperone NASP (Saavedra et al., 2020)
KDM4A/JMJD2A, KDM4B/JMJD2B, KDM4C/JMJD2C, KDM4D/JMJD2D, KDM4E/JMJD2E	H3K9me3/me2/me1 + H3K36me3/me2	- p53-dependent regulation of DNA damage response proteins p21 and PIG3 (Castellini et al., 2017) - ALT pathway activation in ATRX-mutant glioblastomas (Udugama et al., 2021) - DNA replication pre-initiation complex (Wu et al., 2017) - Disruption of HDR (Sulkowski et al., 2020)
KDM5A, KDM5B, KDM5C, KDM5D	H3K4me3/me2	- Replicative stress contributed to HU tolerance (Gaillard et al., 2021) - Interaction with CAF1 and NAP1 (Yheskel et al., 2023)
KDM6A/UTX, KDM6B/JMJD3	H3K27me3/me2	- Regulate DDR transcriptional activation (Boila et al., 2023) - Formation of nuclear condensates (Vicioso-Mantis et al., 2022)
KDM7C/PHF2	H3K9me2/me1 + H3K27me2/me1	- Regulation of 53BP1 and BRCA1 foci on DNA damage site (Alonso-De Vega et al., 2020; Pappa et al., 2019)
KDM8/JMJD5	H3K36me2	- Monomethylated H3 N-tail proteolytic cleavage during DNA damage response (Shen et al., 2017) - Pathogenic variants caused DNA replication stress (Fletcher et al., 2023)

Integrated Stress Response

The integrated stress response (ISR) is a signalling pathway that becomes activated in response to various external or internal stress stimuli and is primarily sensed by the endoplasmic reticulum (ER). The activation of the PERK/EIF2AK3 kinase pathway can be triggered by multiple stressors including the accumulation of misfolded proteins, disruption of calcium ion (Ca^{2+}) homeostasis, hypoxia, and oxidative stress (Rouschop et al., 2013). Additionally, the PKR/EIF2AK2, HRI/EIF2AK1, and GCN2/EIF2K4 modes of ISR signalling are respectively activated by stimuli such as double-stranded RNA, heme deficiency, and nutrient deprivation. In response to stress-induced activation, these kinases phosphorylate eIF2α (eukaryotic translation initiation factor 2 alpha) on serine residue 51. eIF2α is a part of the eIF2-GTP-tRNA(i)Met ternary complex (TC) that is required for initiation of protein translation (Baird & Wek, 2012). Due to the inhibition of the GEF (guanine nucleotide exchange factor) recycling activity in TC, the eIF2α phosphorylation is marked by a reduction in global protein synthesis (Figure 6).

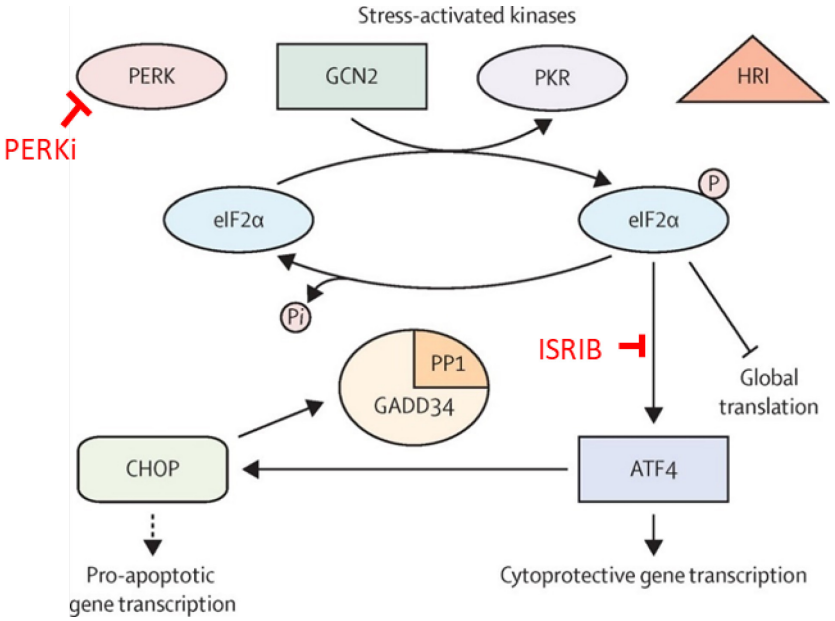

Figure 6 – Schematic of ISR signalling pathway (Way & Popko, 2016). PERKi (GSK2606414) and ISRIB are commonly used inhibitors for blocking ISR signalling.

The activation of the integrated stress response (ISR) pathway leads to the upregulation of Activating transcription factor 4 (ATF4) at the translational level. ATF4 is a transcription factor that contains a basic-leucine zipper (bZIP) domain, critical for its DNA binding ability (Podust et

al., 2001). This bZIP domain also acts as a regulatory element, requiring heterodimerization with partner proteins containing a bZIP domain for full functionality. The expression level of the ATF4 protein is a key determinant of its transcriptional activity (Podust et al., 2001). Despite the presence of abundant ATF4 mRNA, its functionality as a transcription factor relies on increased translation in response to stress stimuli.

Upon upregulation, ATF4 translocate into the nucleus and acts as a transcription factor (Harding et al., 2003). In response to stress, ATF4 modulates several genes involved in survival, senescence, autophagy, and apoptosis (Frank et al., 2010; J. Han et al., 2013; Hiramatsu et al., 2014; Matsumoto et al., 2013; Wortel et al., 2017). In addition, ATF4 also initiates a negative feedback mechanism by upregulating the expression of CCAAT-enhancer-binding protein homologous protein (CHOP) (Márton et al., 2022; Shan et al., 2009). The cooperative action of ATF4 and CHOP as activators induces the expression of growth arrest and DNA-damaged protein 34 (GADD34) and protein phosphatase 1 (PP1), which forms a complex that removes eIF2α phosphorylation thereby recovering global protein synthesis (Figure 6) (C. L. Liu et al., 2014; Rojas et al., 2015).

ISR signalling is considered to be a canonical pathway of upregulating ATF4. In some cases, however, the upregulation of ATF4 occurs independently of eIF2α phosphorylation (Wolzak et al., 2022). For instance, the mechanistic target of rapamycin complex (mTORC) signalling has been implicated in the upregulation of ATF4 protein by stabilizing its mRNA and enhancing translation (Y. Park et al., 2017; Sulkowski et al., 2020; Tabata et al., 2023; Tameire et al., 2019; Torrence et al., 2021). Additionally, KDM4C directly regulated the level of ATF4 mRNA and protein, and the interaction between KDM4C and ATF4 as activators governed amino acid metabolism (E. Zhao et al., 2016).

ISR activation in IDH-mutant cancer

Activation of ISR has been extensively investigated in the development of tumours (Ghaddar et al., 2021). However, limited research has been conducted on its role in cancer with mutations in the IDH1/2 genes. In an early study, it was discovered that the inhibitory role of R-2-HG on the enzyme called prolyl hydroxylase (PHD) triggered endoplasmic reticulum (ER) stress in a mouse knock-in model with the IDH1 R132H mutation (Sasaki et al., 2012). Inhibiting the PHD enzyme resulted in the stabilization of hypoxia-inducible factor-1 alpha (HIF-1α), which influenced glucose

metabolism and cell cycle progression, potentially facilitating the development of cancer (Aprelikova et al., 2004; Hu et al., 2022; Selak et al., 2005; Xu et al., 2011).

In mouse embryonic fibroblasts (MEFs), R-2-HG activated the mTORC signalling pathway which is associated with increased expression of ATF4 (Carbonneau et al., 2016; Torrence et al., 2021). Additional supporting evidence is found in the transcriptome analysis conducted on A172 cells, which are patient-derived glioblastoma cells overexpressing the IDH1 R132H mutation. When compared to the wildtype counterpart, these cells bearing the IDH1 mutation exhibited a distinct signaling pattern indicative of hypoxia and the unfolded protein response (UPR). Importantly, this distinctive pattern was reversed upon treatment with GSK864, an inhibitor of the IDH1-mutant enzyme (Kayabolen et al., 2020). Furthermore, these IDH1-mutant cells showed increased ATF4 levels in response to the combined treatment of histone demethylase 6A/B (KDM6A/B) and histone deacetylase (HDAC) inhibitors. The relationship between the inhibition of histone methylase and activation of stress pathways strongly implies that the intrinsic accumulation of R-2-HG potentially undermines the functionality of epigenetic modifiers, thus triggering cellular stress.

Interestingly, inducing ER stress inhibited DNA synthesis through activation of the PERK signalling pathway (Cabrera et al., 2016). In support of this notion, a study suggested that impaired RF progression by ISR occurred due to increased DNA:RNA hybrids and limited histone availability (Choo et al., 2020). Overall, it can be argued that IDH mutations associated with the accumulation of R-2-HG, either directly or indirectly through its antagonistic effects, are likely to act as a stressor which further impede cellular functioning.

Rationale and Hypothesis

IDH1/2 mutations are prevalent in gliomas and glioblastomas with a characteristic accumulation of R-2-HG. Interestingly, along with IDH1 mutations, there is a frequent co-occurrence of mutations in the tumour suppressor genes ATRX and TP53. IDH1 mutations occur early in tumour development as reported by Watanabe et al., 2009. It is, therefore, plausible to consider that mutations in ATRX and TP53 arise as a consequence of genomic instability following mutations in IDH1. Furthermore, the pathologies related to IDH mutations are characterized by a deficiency in HR repair, known as 'BRCAness', which is considered to be a source of replicative stress (Sulkowski et al., 2017). The accumulation of R-2-HG is also increasingly recognized as a cause of cellular stress that can have a detrimental effect on DNA replication.

Therefore, we hypothesized that the accumulation of R-2-HG impairs the DNA replication process in cells with IDH1/2 mutations possibly by activating Integrated Stress Response. In our efforts to examine our hypothesis, we primarily employed normal human astrocytes (NHA), as they are the primary source of origin for glioma and glioblastoma development. Nevertheless, to ensure the robustness of our findings, we validated these outcomes across a spectrum of other normal and cancer cell lines, including U2OS, HeLa, MEF, and HT1080 cells. Following are the specific aims addressed in this project.

1. To study replication fork dynamics and S-phase progression upon exogenous treatment of octyl-R-2-HG (cell permeable)
2. To examine the expression of protein markers denoting ISR activation as well as whether there is a rescue effect on DNA replication by blocking ISR signalling.
3. To investigate whether results from exogenous octyl-R-2-HG treatment can be replicated in an inducible system of IDH1/2 mutant gene overexpression

Chapter 2 – Materials and Methods

Cell Culture and Medium

Normal Human Astrocytes immortalized by hTERT (NHA-hTERT) were kindly provided by Dr. Nada Jabado. HT1080 fibrosarcoma with native IDH1 R132C mutation (G. Jin et al., 2012), HeLa, HEK293T, and U2OS cell lines were purchased from American Type Culture Collection (ATCC). *tp53*$^{-/-}$ MEF were produced from mouse embryos (Mallette et al., 2010). All the cell lines were cultured in Dulbecco's Modified Eagle Medium (DMEM 1X Gibco / Thermo Fisher) supplemented with 10% Fetal Bovine Serum (FBS, Thermo Fisher 12483020), 2mM L-Glutamine (Bioshop GLU102), 120µg/mL Penicillin G Sodium Salt (Bioshop PEN333.500) and 200µg/mL Streptomycin Sulfate (USP GRADE Bioshop STP101.500). This is referred to as a 'complete medium'. Cell lines were cultured at 37ºC under 5% CO_2 in a humidified atmosphere.

For harvesting cells in 10mL culture and 10cm dish, the complete medium was aspirated, and cells were washed with 10mL 1X PBS (Table 5). After removing PBS, cells were treated with 1mL 0.5% Trypsin-EDTA, phenol red (Wisent 325-043-CL) for 5 minutes at 37ºC and 9mL of complete medium was added for quenching the trypsin activity. For seeding, cells were counted using a hemocytometer under an inverted phase contrast microscope (Olympus Model CKX31SF). NHA and MEF cells were kept in culture for a month i.e., 10-12 passages after thawing, whereas HeLa and U2OS cells were kept in culture for up to three months. For storage, cells were grown to 70-80% confluency, harvested in a 50mL tube, and centrifuged at 1500rpm for 5 minutes at room temperature. The pellet was resuspended in freezing medium (50% FBS, 40% DMEM, and 10% DMSO (Sigma Aldrich D8418)). Approximately, 3-4 million cells were aliquoted per vial and stored at -80ºC for 24 hours and afterwards in liquid nitrogen. For thawing cells, the frozen vial was thawed briefly in a 37ºC water bath, transferred into a 50mL tube and 9mL complete medium was added in a drop-by-drop fashion. Cells were centrifuged at 1500rpm for 5 minutes at room temperature and the medium was aspirated. This step removed the medium containing DMSO. The cell pellet was dissolved in complete medium and grown at 37ºC as previously described.

Table 5 – Composition of 1X PBS

1X PBS	Final concentration
Sodium chloride (NaCl, Bioshop SOD002.5)	0.137M
Potassium chloride (KCl, Bioshop POC308.500)	2.7mM
Sodium phosphate, Dibasic (Na_2HPO_4, EMD Millipore 8210)	10mM
Potassium dihydrogen phosphate (KH_2PO_4, Bioshop PPM302.500)	1.8mM
Distilled water	To make up the final volume and afterwards, autoclaved the solution.

Metabolite, Genotoxic, and ER Stress Treatment

The metabolites 1-octyl-*R*-2-hydroxyglutarate (R-2-HG) and 1-octyl-*S*-2-hydroxyglutarate (S-2-HG) were synthesized as described (Carbonneau et al., 2016) at the Medicinal Chemistry Platform, CHU de Québec-Université Laval. 1-Octyl-2-ketoglutarate (α-KG) was obtained from Sigma-Aldrich (SML2205). Metabolites were suspended in DMSO (Sigma D2650) and a stock concentration of 400mM octyl-R-2-HG, octyl-S-2-HG, and 500mM octyl-α-KG was maintained to ensure that the working concentration of DMSO in culture remains less than or equal to 1%.

Hydroxyurea (HU, Bioshop HYD023) was dissolved in complete medium at 200mM concentration and used as a positive control for genotoxic stress and dissolved in a complete medium. UV irradiation was performed on cell monolayers as described in Lemay et al., 2022. VE-821 or ATRi (MedChemExpress HY-14731) and MK-8776 or CHK1i (MedChemExpress HY-15532) were used as inhibitors for replicative stress response and suspended in DMSO.

Dithiothreitol (Bioshop DTT002) and Thapsigargin (Bioshop THA101), used as ISR activators, were dissolved in distilled water and DMSO, respectively. Integrated Stress Response Inhibitor (ISRIB, Sigma-Aldrich SML0843) and PERK Inhibitor I or PERKi (Sigma-Aldrich 516535), used as ISR inhibitors, were dissolved in DMSO. Multiple freeze-thawing was avoided for all the compounds mentioned above. All the treatments in the experiment contained an equal amount of DMSO adjusted to the highest DMSO-containing compound combinations.

DNA Fibre Assay

The progression of the replication fork was monitored using a DNA fibre assay. 1 million NHA were seeded in a 6 cm dish 24 hours before the experiment. To begin the experiment, cells were washed twice with 1X PBS. Cells were then sequentially labelled with 2 thymidine analogs,

30μM 5-chloro-2′-deoxyuridine (CldU, Sigma-Aldrich C6891) and 250μM 5-iodo-2′-deoxyuridine (IdU, Sigma-Aldrich I7125) for 30 and 60 minutes, respectively. After CldU labelling, the medium was removed, and cells were washed twice with 1X PBS. Cells were simultaneously labelled with IdU and treated with DMSO or 4mM octyl-R-2-HG. Cells were harvested as described previously in a 15mL tube precooled on ice. Cells were pelleted at 1500rpm for 3 minutes at 4°C, washed with 1X PBS, and resuspended in 250μL of 1X PBS. 2μL of cell suspension was placed on a microscopic slide, and air dried for 5 minutes, 7μL of Lysis Solution (50mM EDTA (Bioshop EDT003), 0.5% SDS (Bioshop SDS999) in 200mM Tris pH 7.5) was added to the drop and mixed gently, followed by air drying for 3 minutes. The slide was tilted to roll down the drop on the slide. Once the drop reached the bottom of the slide, the slide was placed horizontally and allowed to dry. Slides were fixed with 3:1 methanol: acetic acid (pre-chilled at -20°C) for 10 minutes in a Coplin jar and then washed once in distilled water. Slides were denatured with 2.5M HCl for 80 minutes in a Coplin jar and then washed three times with 1X PBS.

From here, slides were incubated in a humid chamber. Slides were blocked in 200μL of blocking solution (5% Bovine Serum Albumin (BSA, Fischer Scientific L-15899) in 1X PBS) for 90 minutes and then washed three times by immersing for 5 minutes in PBS-T (1X PBS with 0.05% Tween 20 (Sigma-Aldrich P1379)) and once with 1X PBS in a Coplin jar. CldU and IdU were probed by incubating slides in 50μL of primary antibody solution (1:400 anti-BrdU (cross-reacts with CldU, Abcam ab6326, rat) and 1:25 anti-BrdU (cross-reacts with IdU, BD Biosciences 347580, mouse) mixed in blocking solution) for 90 minutes. Slides were washed in PBS-T and PBS as described previously. Slides were incubated in 50μL of secondary antibody solution (1:100 anti-rat Alexa594 (Life Technologies A11007) and 1:100 anti-mouse Alexa488 (Life Technologies A11029) mixed in blocking solution) for 60 minutes followed by washing. Slides were mounted using a 50 x 22mm coverslip. Images were taken at 60x magnification using the DeltaVision Elite system (GE Healthcare).

DNA Fibre Analysis

DNA Fiber images from DMSO and octyl-R-2-HG treatment were pooled, and the file name was randomized using the File Name Encryptor under the Blind Analysis tool of FIJI plugins. The tract length of the two analogs was measured using FIJI (Schindelin et al., 2012). Due to the short length and irregularities of DNA fibres obtained by this assay, the quantification was limited to unidirectional fibres. A minimum of 100 fibres were counted for each condition and experiment. Graph plotting and statistical analysis were performed using GraphPad Prism 9.

Flow Cytometry and Cell Sorting

DNA replication progression in the cell cycle was assessed by the amount of 5-Ethynyl-2'-deoxyuridine (EdU, Abcam ab146186) incorporated into chromatin. Chromatin bound γH2AX and RPA70 were monitored as markers of Replicative Stress Response activation. Replisome units such as PCNA and MCM4 proteins were used to quantify the frequency of replication fork initiation or origin firing. As an ISR activation marker, ATF4 was quantified on chromatin for all experiments, except for NHA overexpressing wildtype IDH1/2 and mutant cell lines upon induction where whole-cell ATF4 protein levels were quantified. 1 million cells were seeded in a 6 cm dish 16-24 hours before the experiment. For all EdU incorporation experiments described in the figures, cells were labelled with a 10μM EdU for 30 minutes before the treatment completion. Afterward, cells were harvested in a pre-chilled 15mL tube, centrifuged at 1500rpm for 3 minutes at 4ºC, and washed with chilled 1X PBS. The next step, i.e., either partial permeabilization or fixation was carried out depending on the requirement of chromatin-bound or total-cell protein quantification.

For quantifying chromatin-bound protein, non-chromatin-bound proteins were removed via partial permeabilization by resuspending the pellet in 100μL extraction buffer (0.2% Triton X-100 (EM Science 9410) in 1X PBS) for 10 minutes on ice, then 2mL 1X PBS-B (1 mg/mL BSA in 1X PBS) was added, following centrifugation at 1500rpm for 3 minutes. Cells were fixed by resuspending in 100μL fixation buffer (2% formaldehyde in 1X PBS) and incubating for 30 minutes at room temperature, then 0.5mL of 1X BD Perm/Wash buffer (BD Biosciences, 554723) was added before centrifugation at room temperature as before. For probing PCNA, an exceptional methanol fixation step was performed by incubating cells in a solution containing 500μL 1X PBS and 2mL methanol (pre-chilled at -20ºC) for 15 minutes at room temperature. Then cells were centrifuged and washed once with 1X BD Perm/Wash buffer. The cell pellet was either stored in a 100μL storage buffer (3% heat inactivated FBS, 0.09% sodium azide (Bioshop SAZ001.50) in 1X PBS) overnight or processed immediately for protein probing.

For quantifying total-cell protein, cells were initially fixed by resuspending in 2mL fixation buffer (4% formaldehyde (Sigma-Aldrich F1635) in 1X PBS) and incubating for 30 minutes at room temperature, then cells were washed once with 2mL cold 1X PBS. Cells were permeabilized by incubating in 2mL extraction buffer (0.1% Triton-X100 in 1X PBS) for 10 minutes on ice and then washed with cold 1X PBS. Cells were either stored in a 2mL storage

buffer (3% BSA, 0.09% sodium azide in 1X PBS) overnight or processed immediately for protein probing.

500,000 cells were probed for a maximum of two primary antibodies (from two different species) for each condition/treatment. Cells were resuspended in 50µL of 1:200 antibody (Table 6) mixed in 1X BD Perm/Wash buffer, incubated for 1 hour at room temperature, added 500µL of BD Perm/Wash buffer, and centrifuged. Cells were resuspended in 50µL of 1:200 Alexa fluor-conjugated secondary antibody (Table 6) mixed in 1X BD Perm/Wash buffer, incubated for 30 minutes at room temperature in the dark, 500µL of BD Perm/Wash buffer was added, and cells were centrifuged. Click chemistry was performed to probe for EdU by incubating cells in 50µL Click Reaction Mix (1:200 Alexa Fluor 647 Azide, triethylammonium Salt (Life Technologies A10277), 2mM copper (II) sulphate pentahydrate (Sigma-Aldrich C7631) and 10mM Sodium L-Ascorbate (Sigma-Aldrich A-7631) mixed in 1X PBS) for 30 minutes at room temperature in the dark, 500µL of BD Perm/Wash buffer was added and cells were centrifuged. Cells were stained with DAPI using 500µL analysis buffer (0.05% sodium azide, 250µg/mL RNase A (Bioshop RNA675), 0.5µg/mL DAPI (Thermo Scientific D1306) mixed in PBS-B) at 37ºC for 30 minutes or at 4ºC for 1-3 days. Fluorescent signal was acquired for 10,000 cells using BD LSRFortessa X20 cytometer (BD Biosciences) and the data were analyzed using FlowJo version 8.10.1 software.

NOTE: One of the experimental datasets was excluded from analysis in Figure 1 D and Figure 3 B due to consistently low-intensity values for all the probes.

Table 6 – List of primary and secondary antibodies used in flow cytometry and cell sorting.

Primary antibody	**Company**	**Catalog number**
Anti-phospho H2AX	EMD Millipore	JBW301
MCM4	Abcam	ab124836
PCNA	Abcam	ab70472
RPA70	Abcam	ab79398
ATF4	Cell Signalling	11815S
Anti-FLAG-M2	Sigma-Aldrich	F1804
Alexa Fluor-conjugated secondary antibody	Company	Catalog number
Alexa Fluor 488 anti-mouse IgG	Life Technologies	A11029
Alexa Fluor 594 anti-rabbit IgG	Life Technologies	A11012

Immunoblotting

Following the treatment in different experiments, the whole-cell protein was extracted by initially washing cells twice with 1X PBS and resuspending in 150µL lysis buffer (2% SDS dissolved in 25mM Tris pH 7.5 with protease and phosphatase inhibitors as listed in Table 7). Lysed cells were collected by a rubber policeman and heated at 95ºC for 5 minutes. Protein extracts were then sonicated twice at 20% amplitude for 20 seconds (Branson Digital Sonifier 450) and centrifuged at full speed for a minute at room temperature. Protein concentration was determined with Pierce BCA Protein Assay Kit (Thermo Scientific 23225) and the colorimetric reaction was measured on a BioTek EL800 spectrophotometer. An equal amount of all protein extracts were run on SDS-PAGE gel prepared as described by Lauber, 2013. Protein extracts were mixed with 1X dilution of 6X loading buffer (Table 8), ran in Mini-PROTEAN Electrophoresis apparatus (Bio-rad 1658004), and transferred overnight onto an Immuno-blot PVDF membrane (Bio-Rad 1620177) at 4ºC. The running and transfer buffer composition was summarized in Tables 9 and 10. Protein transfer was confirmed by Ponceau staining (EMD Millipore P3504). The membrane was blocked in blocking buffer (5% Milk in 1X TBS-T (Table-11)) for 60 minutes at room temperature and washed twice for 5 minutes in 1X TBS-T. The membrane was incubated in primary antibody solution (desired dilution of antibody (Table-12), 1% BSA, 0.02% sodium azide in 1X TBS-T) at room temperature overnight on a rocker, washed twice with 1X TBS-T for 10 minutes, and incubated in HRP-conjugated secondary antibody solution (dissolved in blocking buffer, Table 12) for 60 minutes at room temperature. The membrane was then washed thrice in 1X TBS-T for 10 minutes and once with 1X TBS. The blot was developed using Clarity Western Peroxide and Luminol/Enhancer Reagent (Bio-Rad 1705061) and Azure c600 imaging system (Azure Biosystems) was used to acquire images.

Table 7 – List of protease and phosphatase inhibitors used mixed in cell lysis buffer

Protease/phosphatase inhibitors	Working concentration	Company, catalog number
Aprotinin	1µg/mL	Bioshop, APR600
Leupeptin	1µg/mL	Bioshop, LEU001
Pepstatin	1µg/mL	Bioshop, PEP605
Phenylmethylsulphonyl fluoride (PMSF)	1mM	Bioshopb, PMS123
Sodium fluoride (NaF)	10mM	Sigma-Aldrich, S7920

Sodium Orthovanadate (Na_3VO_4)	1mM	Sigma-Aldrich, S6508
β-glycerophosphate, disodium salt, pentahydrate (BGP)	10mM	Bioshop, GYP001

Table 8 – Composition of 6X SDS loading buffer

6X SDS loading buffer	**10mL**	**Final concentration**
0.5M Tris-HCl pH 6.8 (Bioshop TRS002.1)	7mL	0.35mM
Glycerol 100% (Bioshop GLY002.1)	3mL	30%
SDS (Bioshop SDS999)	1g	10% w/v
Bromophenol Blue (EM Science BX1410-7)	Few grains	
1mL aliquots were stored in 1.5mL microcentrifuge tubes (FroggaBio LMCT1.7BG) at -20°C.		
2-Mercaptoethanol (Sigma-Aldrich M6250)	60µL/tube	

Table 9 – Composition of 10X Tris-glycine running buffer

10X Tris-glycine running buffer	**1L**	**Final concentration**
Tris base (Bioshop TRS001)	30.3g	0.25M
Glycine (Bioshop GLN002)	144.2g	1.92M
SDS 10%	100mL	1%
Double-distilled water	up to 1L	

Table 10 – Composition of 10X and 1X Transfer buffer

10X Transfer buffer	**1L**	**Final concentration**
Tris base	29g	0.25M
Glycine	145g	1.92M
Double-distilled water	up to 1L	
1X Transfer buffer	**1L**	**Final concentration**
10X Transfer buffer	100mL	1X
SDS 10%	5mL	0.5%
Methanol (ChapTek)	200mL	20%
Double-distilled water	up to 1L	

Table 11 – Composition of 10X TBS and 1X TBS-T buffer

10X Tris-buffered saline (TBS)	1L
Tris base	30g
Sodium chloride (NaCl)	8g
Potassium chloride (KCl)	2g
Double-distilled water	up to 1L, adjusted to pH 8 with HCl
1X TBS-T	1L
10X TBS	100mL
Tween 20	1mL
Double-distilled water	up to 1L

Table 12 – List of primary and secondary antibodies used in immunoblot experiments

Primary antibody	**Company, catalog number**	**Dilution**
Anti-FLAG-M2	Sigma-Aldrich, F1804	1:1000
ATF4	Cell Signalling, 11815S	1:1000
CHAF1A	Cell Signalling, 5480	1:1000
CHK1	Santa Cruz, sc-8408	1:1000
eIF2α	Cell Signalling, 2103S	1:1000
GAPDH	Santa Cruz, sc-365062	1:1000
GFP	Invitrogen, A-11122	1:1000
Lamin B1	Santa Cruz, sc-365214	1:500
PCNA	Abcam, ab70472	1:200
Phospho-H2AX (S 139)	EMD Millipore, JBW301	1:1000
Phospho-CHK1 (S 345)	Cell Signalling, 2348	1:1000
Phospho-eIF2α (S 51)	Cell Signalling, 9721S	1:1000
Phospho-RPA32 (S 33)	Bethyl (Cederlane), A300-246A	1:1000
Puromycin	EMD Millipore, MABE343	1:1000
RPA70	Abcam, ab79398	1:1000
Tubulin	Abcam, ab6161	1:1000
Secondary antibody	Company, catalog number	Dilution
Anti-mouse HRP-conjugated	Bio-Rad, 1705047	1:2000
Anti-rabbit HRP-conjugated	Santa Cruz, sc-2357	1:5000

Anti-rat HRP-conjugated	Santa Cruz, sc-2006	1:5000

Puromycilation Assay

Global protein synthesis was determined by treating cells with 10µg/mL puromycin (Gibco / Thermo Scientific A1113803) for 15 minutes before the treatment completion as labelled in the figures. Whole-cell protein extracts were obtained and an equal amount of proteins were analyzed using 10% SDS-PAGE as described in the section on Immunoblotting. Blot was probed with an anti-puromycin antibody detailed in Table 12.

Cellular Fractionation

Protein localization was monitored by cellular fractionation as described in (Kapur et al., 2022). 5 million cells were seeded in a 15cm dish 24 hours before the experiment. Cells were treated for an hour with DMSO, octyl-R-2-HG, or Hydroxyurea. All centrifugations and incubations were carried out at 4ºC and on ice. Cells were harvested and washed with cold 1X PBS and resuspended in 250µL 1X PBS. 5% cells (75µL), as Input mixed with 15µL 6X SDS loading buffer, kept aside. The rest of the sample was centrifuged and resuspended in 175µL buffer A (Table 13) with protease and phosphatase inhibitors (Table 7), incubated for 5 minutes on ice, and centrifuged at 1300xg for 4 minutes. The supernatant was collected as S1 (cytoplasm), pellets were washed once with buffer A, resuspended in 175µL buffer B (Table 14) with protease and phosphatase inhibitors (Table 7), incubated for 30 minutes on ice, and centrifuged at 1700xg. The supernatant was collected as S3 (soluble-nuclear), and pellets were resuspended in 122µL DNaseI digestion buffer (Table 15) per sample and incubated on ice for one hour, 53µL of DNaseI digestion buffer (without enzymes) was added to bring back to the same concentration as other steps and centrifuged at full speed. The supernatant was stored as S4, and chromatin pellets (P2) were resuspended in 87.5µL of 2X SDS loading buffer and DNaseI digestion buffer each. All the fractions were mixed with 6X SDS loading buffer (final 1X) and heated at 95ºC for 5 minutes. Immunoblotting was performed using 10% SDS-PAGE as described in the immunoblotting section.

Table 13 – Composition of Buffer A used in cellular fractionation

Buffer A	Final concentration
HEPES pH7.4 (Bioshop HEP005.1)	10mM
Potassium chloride (KCl)	10mM
Magnesium chloride ($MgCl_2$, Bioshop MAG520.500)	1.5mM

Sucrose (Sigma-Aldrich S0389)	0.34M
Glycerol 100%	10%
Dithiothreitol (DTT)	1mM
TritonX-100	0.1%
Double-distilled water	To make up the final volume

Table 14 - Composition of Buffer B used in cellular fractionation

Buffer B	**Final concentration**
Ethylenediaminetetraacetic acid (EDTA, Sigma-Aldrich E0270)	0.3mM
Egtazic acid (EGTA, Bioshop EGT101.25)	0.2mM
Double-distilled water	To make up the final volume

Table 15 – Composition of DNase I Digestion Buffer used in cellular fractionation

DNase I Digestion buffer	**Final concentration**
Tris-HCl pH7.6	0.3mM
Magnesium chloride ($MgCl_2$)	0.2mM
Calcium Chloride ($CaCl_2$, Sigma-Aldrich C-3881)	0.5mM
Double-distilled water	To make up the final volume
For each sample, the following concentration/amount of enzymes was added.	
RNase A	7-10µg
DNase I (New England Biolabs M0303, 2000 units/µL)	0.7µL

Real-Time quantitative PCR

The Real-Time quantitative PCR reaction was performed to quantify the fold change in mRNA levels. Total RNA was extracted with TRIzol Reagent (Life Technologies 15596026) method and RNA was dissolved in RNase-free water (Bioshop WAT222). RNA concentration was determined using an Infinite M200 PRO plate reader (Tecan). RNA degradation was checked by preparing a mix of 500 ng extracted RNA in 1X dilution of 6X RNA loading buffer (Table-16), heating at 65°C for 5 minutes and running on 3% agarose gel (Invitrogen 16500-500) with 0.3µg/mL ethidium bromide (EtBr, Bioshop ETB444.50) in 1X TAE buffer (Table 17). The agarose gel was visualized using AlphaImager Mini Imaging System and wavelength of 302 or 365nm. The images were captured using Alphaimager Software version 3.4.0.0.

Table 16 – Composition of 6X RNA loading buffer

6X RNA loading buffer	Final concentration
Formamide (Bioshop FOR001)	95%
SDS	0.05%
Bromophenol Blue	Few grains
TE buffer (10mM Tris-HCl pH8, 1mM EDTA mixed in double-distilled water)	To make up the final volume

Table 17 – Composition of 50X TAE buffer

50X TAE buffer	1L	Final concentration
Tris base	242g	40mM
Glacial Acetic Acid (Bioshop ACE333)	57.1mL	5.7%
Ethylenediaminetetraacetic Acid, Disodium Salt, Dihydrate ($Na_2EDTA{\cdot}2H_2O$, Bioshop EDT001.500)	97.2g	2mM
Double-distilled water	up to 1L	

Reverse transcription (RT) was performed using M-MuLV Reverse Transcriptase and buffer (NEB M0253), random primers (Invitrogen 48190011), and dNTPs (dTTP (Biobasic D0046T), dATP (Bioshop NUC003A), dGTP (Bioshop NUC003G), dCTP (Bioshop NUC003C)) to obtain complementary DNA (cDNA) corresponding to the total RNA. Initially, either 1µg of RNA or RNase-free water (RT-negative control) was mixed with 2µL of random primers to a total volume of 10µL in RNase-free 0.2mL PCR tubes (Sarstedt 72.737.002) and incubated at 65^{o}C for 10 minutes. Then, the components were added in the given manner (Table 18) to both the tubes (RNA and RT-negative), incubated at 37^{o}C for an hour, stored at -20^{o}C, or kept on ice, and proceeded for qPCR preparation. It was assumed that the RT reaction was 100% efficient i.e., 1µg of RNA yielded 1µg of cDNA (or 50ng/µL). Upon completion, the RT reaction was diluted to 1 ng/µL with RNase-free water for all qPCR reactions.

Table 18 – Composition of Reverse Transcription Reaction

Components	For 20µL RT reaction	Final concentration
10X M-MuLV buffer	2µL	1X
5mM dNTPs	2µL	0.5mM
M-MuLV Reverse transcriptase	0.75µL	150 Units

Water (RNase-free)	5.25µL	

For quantitative Real-Time PCR, all the primers (Table 19) were synthesized from Invitrogen and dissolved in RNase-free water. The amplification efficiency of primers was determined using cDNA extracted from NHA without any treatment. The cycle threshold or C_t value, obtained from qPCR reactions, was plotted against at least five cDNA dilutions to calculate the slope. Subsequently, the primer efficiency was computed using the qPCR Efficiency Calculator, employing the derived slope (Thermo Fisher Scientific, https://www.thermofisher.com/ca/en/home/brands/thermo-scientific/molecular-biology/molecular-biology-learning-center/molecular-biology-resource-library/thermo-scientific-web-tools/qpcr-efficiency-calculator.html, last accessed on 15 May 2023). The efficiency is generally calculated using the formula $Efficiency\ (\%) = \left(10^{\frac{-1}{Slope}} - 1\right) \times 100$. The primers with amplification efficiency ranging from 90-110% were selected for the experiments.

The qPCR reaction was performed using 2X SYBR Green qPCR Master Mix (Bimake B21203), forward and reverse primer mix, and cDNA template. These components were mixed as shown in Table 20, the reactions were arranged in a 96-well PCR plate, centrifuged for 30 seconds at room temperature, and covered with PCR clear adhesive plate seals (Santa Cruz 205896). For each primer, two reaction mixes were prepared where the cDNA template was replaced with RNase-free water and RT-negative reaction mix as qPCR-negative and RT-negative controls, respectively, to rule out non-specific amplification or contamination. The reactions were carried out in 7500 Real-Time PCR device (Applied Biosystems, Thermo Fischer) using the two-step run method as described in the Bimake qPCR Master Mix user guide. All the reactions were performed in triplicates. Expression fold change of mRNA was calculated using $2^{-\Delta\Delta Ct}$ formula after normalizing to HPRT gene. Graph plotting was obtained using GraphPad Prism 9.

Table 19 – List of qPCR primers

Gene (Reference)	**Forward primer (5' → 3')**	**Reverse primer (5' → 3')**	**Product size (base pair)**	**Primer efficiency (%)**
ATF4 (Vasudevan et al., 2020)	GGAGATAGGAAGCCAGACTACA	GGCTCATACAGATGCCACTATC	103	109

CHOP (Çelik et al., 2016)	CAAGAGGTCCTGTCTTCAGATG	GGGTCAAGAGTGGTGAAGATT	95	104
HPRT (Lemay et al., 2022)	CCCTGGCGTCGTGATTAGTG	TCGAGCAAGACGTTCAGTCC	139	107

Table 20 – Composition of qPCR Reaction

Components	For 10µL qPCR reaction	Final concentration
2X Bimake Master mix + Rox dye	5µL	1X
2.5µM Forward & Reverse primer mix	2µL	0.5µM
cDNA (1ng/µL)	3µL	3ng

Cell Proliferation Assay by Incucyte

Cell proliferation was determined by time-course cell imaging (phase contrast) using Incucyte® Live-Cell Analysis System (Sartorius). For cell proliferation experiments related to metabolite treatment, 10,000 cells (~20% confluency) were seeded in a 12-well plate (Sarstedt 83.3921) 24 hours before the treatment. The plate medium was replaced with fresh medium containing either DMSO or metabolite with or without ISRIB, placed into the device and a schedule was initiated to acquire at least 9 images / well or condition every four hours for 6-7 days. The device was operating inside an incubator with growth settings as described previously. For cell proliferation assays related to doxycycline-induced GFP / IDH overexpression NHA cell lines, 2,500-5,000 cells were seeded in a 24-well plate (Sarstedt 83.3922). 1µg/mL doxycycline hyclate (Bioshop DOX444) with or without ISRIB was added while seeding. The plate was placed in Incucyte, and the acquisition schedule was started 24 hours after the seeding step.

The images were initially analyzed using the Basic Analyzer of the Incucyte system. Using AI-based cell segmentation (Figure 7), a minimum area of 350 to 400 μm^2 was selected (Figure 8) This selection eliminated the background noise and cellular debris. The completion of this analysis resulted in confluence percent, representing the percentage of image area occupied by cells (using average cell area). The following analysis as well as the statistical analysis were performed using GraphPad Prism 9. To obtain normalized confluence percent, first, a baseline correction was performed by subtracting the confluence percent at the first time point from the confluence percent at each subsequent time point. Baseline-corrected confluence percent were

normalized in such a way that 0% is defined as 0% confluence percent and 100% is defined as the maximum confluence percent of control (DMSO) for metabolite treatment experiments. When normalizing NHA transduced cell lines, 100% was defined as the maximum confluence of respective confluence percent of the cell without doxycycline induction.

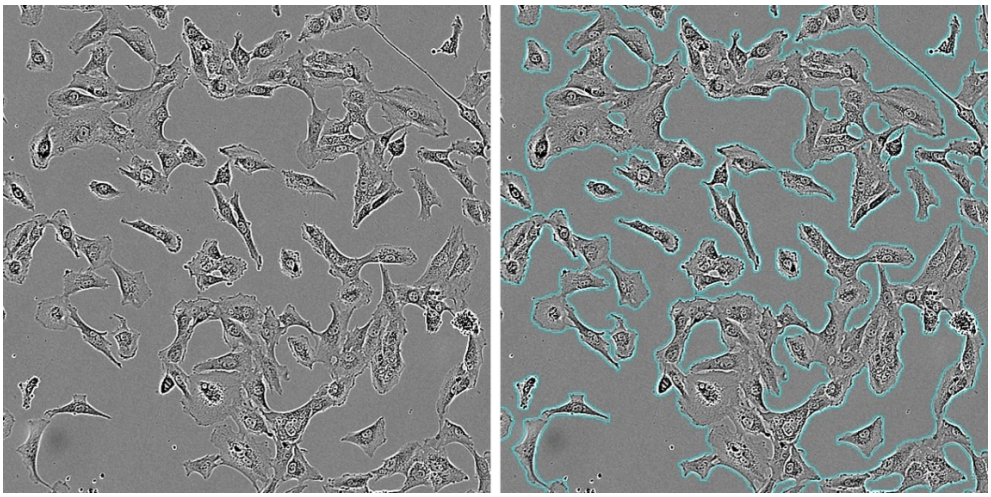

Figure 7 – Images representing before and after application of AI-based Cell Segmentation on NHA cells.

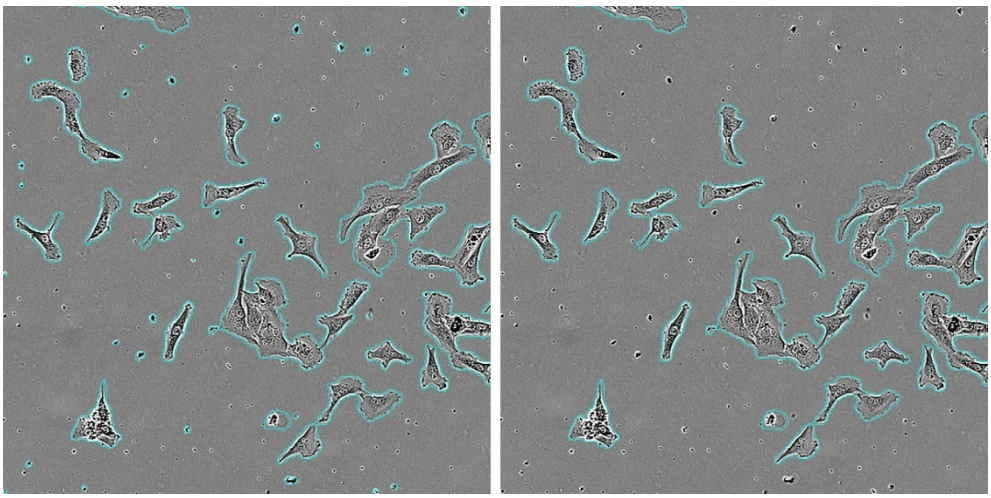

Figure 8 – Images representing before and after application of 400 μm^2 area filter during analysis. This filter eliminated the segmentation of debris.

Transduction and Selection

Inducible IDH wildtype and mutant overexpressed NHA cell lines were obtained via lentiviral transduction of plasmids listed in Table 21. Restriction digestion was performed to confirm the presence of the gene of interest in plasmids. To generate lentiviral particles, 500,000 HEK293T cells (70-90% confluency) were seeded 24 hours before transfection. The transfection mix was

prepared using 3rd generation lentiviral packaging plasmids (Table 21), expression plasmids, lipofectamine (Life Technologies 11668500) and OptiMEM (Life Technologies 11058021) as described in Table 22. Tubes were incubated for 5 minutes at room temperature then, mixed and incubated for 30 minutes, added to the cells and made up the volume to 10mL with a complete medium. The next day, the media was changed to a 6.5mL complete medium eliminating the transfection mix. The next day, the supernatant (media) was collected using a syringe and filtered through a 0.45µm filter, stored at 4ºC and 6.5mL complete medium was added to the culture. The next day, the previous step of collecting supernatant was repeated, the viral suspension was pooled (~12mL), aliquoted and stored at -80ºC.

Table 21 – List of lentiviral expression and packaging plasmids used for generating NHA cell lines

Lentiviral expression plasmids	**Reference**
pSLIK-GFP	Addgene 66844
pSLIK-IDH1-FLAG	Addgene 66802
pSLIK-IDH1-R132H-FLAG	Addgene 66803
pSLIK-IDH2-FLAG	Addgene 66806
pSLIK-IDH2-R172K-FLAG	Addgene 66807
Lentiviral packaging plasmids	**Reference**
pMDLg/pRRE	Addgene 12251
pRSV-Rev	Addgene 12253
pMD2.G	Addgene 12259

Table 22 – Composition of transfection mix for generating lentiviral particles

Transfection Mix – TUBE 1	**Volume**
pMDLg/pRRE	3.6µg
pRSV-Rev	2.38µg
pMD2.G	1.2µg
Lentiviral expression plasmid	4.8µg
OptiMEM	Makeup volume to 750µL
Transfection Mix – TUBE 2	Volume
Lipofectamine	30µL

OptiMEM	720µL

Viral titration was performed in HeLa cells by seeding 4000 cells/well in a 96-well plate (volume of 75µL) and cells were grown in DMEM supplemented with 10% Calf Bovine Serum (CBS, HyClone SH3007303HI). Cells were seeded in quadruplicates for each virus and its two dilutions as well as for killing and proliferative controls. The next day, two dilution mixes for each virus were prepared as mentioned in Table 23 and 8µL of each dilution mix was pipetted to the respective wells. Wells with HeLa cells designated as killing and proliferative controls were untouched. After two days, the medium was replaced with a fresh complete medium containing 300µg/mL hygromycin (InvivoGen HGG-41-02) for the wells except for proliferative controls where fresh complete medium without hygromycin was added. After two days, the previous step was repeated. After the next two days, crystal violet (Bioshop CRY422) staining was performed. The medium was aspirated, cells were washed with 1X PBS and 50µL of crystal violet stain (1.25 - 25% w/v crystal violet dissolved in 95% v/v ethanol) was added. Cells were incubated for 10 minutes at room temperature. The stain was aspirated, and cells were washed twice with double-distilled water. Plague Forming Unit or PFU/mL was estimated by counting the number of colonies per well using a hemocytometer.

Table 23 – Dilution strategy used for the viral titration experiment

Components	**1:40**	**1:1000**
Viral suspension	2.5µL	4 µL of 1:40 dilution mix
Complete medium	95.3µL	93.8µL
6 mg/mL Polybrene (Sigma-Aldrich H9268)	1.4µL	1.4µL

A multiplicity of infection (MOI) of 0.3 was utilized for generating all the NHA cell lines. Initially, NHA cells were seeded in a complete medium. The next day, the medium was replaced with 10mL complete medium containing lentiviral particles. After 16 hours, the medium was replaced with 10mL fresh complete medium. After 24 hours, the medium was replaced with a fresh medium with 300µg/mL hygromycin for the selection of transduced cells. Cells were then grown till reaching 90-100% confluency in the presence of hygromycin and the medium was replaced every two days. Afterwards, cells were expanded to 3-5 passages and frozen as described in the cell culture section. All the experiments shown in the study were performed in the presence of 100µg/mL hygromycin and cells were kept in culture for 1-1.5 months (7-8

passages). For validating the overexpression, 1 million cells were induced for respective expression with 1µg/mL doxycycline hyclate for 24 hours. Whole-cell GFP and FLAG levels were quantified using immunoblotting as well as flow cytometry.

Chapter 3 – Results

Octyl-R/S-2-HG accumulation slows RF progression without elevating replicative stress response markers

As a model system for low-grade gliomas, we used NHA immortalized by hTERT overexpression. To mimic the R-2-HG oncometabolite cellular accumulation, we treated asynchronous cells with cell-permeable octyl-R-2-HG in a concentration range of 0.5 - 4mM relevant to IDH mutant cancers (Ježek, 2020). By utilizing two widely used approaches, namely DNA fibre (Halliwell et al., 2020) and EdU incorporation assay (Flomerfelt & Gress, 2016), we sought to characterize DNA RF dynamics and cell proliferation. DNA fibre assay involves labelling actively replicating DNA strands with nucleotide analog CldU followed by IdU, which are then visualized using specific antibodies or fluorescent dyes. NHA were simultaneously treated with IdU and DMSO or octyl-R-2-HG. After 4mM octyl-R-2-HG treatment for one hour, DNA fibre assays showed a decrease in the ratio of IdU to CldU tract length, indicating that cellular uptake of octyl-R-2-HG slowed the rate of RF progression (Figure 9A) and in a dose-dependent manner (Figure 10B). This observation was consistent with a lowered DNA synthesis as observed by reduced EdU incorporation (Figure 9B and D). The rate of nucleotide analog incorporation in replicating DNA could also be affected by lower replication initiation or reduced origin firing. The chromatin bound PCNA, directly correlating with the origin firing or frequency of RF, was quantified to exclude this possibility. As a result of octyl-R-2-HG accumulation, chromatin-bound PCNA was reduced during the early stage of the S phase, as measured by flow cytometry (Figure 10F). However, in the immunoblot analysis, the PCNA level in the chromatin fraction (P2) remained unaffected (Figure 11C). Therefore, despite an existing trend, further research is necessary to determine the statistical significance of decreased PCNA loading or RF frequency upon octyl-R-2-HG treatment.

The slowing of RF progression generally activates the replication stress response (RSR) (Técher & Pasero, 2021b; Zeman & Cimprich, 2013). To investigate whether octyl-R-2-HG-dependent fork progression defects activates a replication stress response, we assessed the levels of the ssDNA-bound RPA70, as well as phosphorylated forms of RPA32 (S33), H2AX (S139) and CHK1 (S345) proteins. In comparison with the negative control, DMSO, there was no significant increase in the levels of these markers on chromatin (Figure 9B and D). The phosphorylation state of CHK1 and

RPA32 indicated similarly that octyl-R-2-HG did not activate the RSR (Figure 9C). In contrast, hydroxyurea, a replicative stress-inducing genotoxic agent used as a positive control induced elevated levels of all the above markers. To maintain fork stability and regulate cell cycle progression, RSR activates checkpoint kinases ATR and CHK1. Hence, we monitored the effects of ATR and CHK1 inhibitor, preventing the catalytic phosphorylation of CHK1 serine residue 296 and CHK1 autophosphorylation activity at serine residue 345, respectively, in octyl-R-2-HG treated cells. The inhibition of neither ATR nor CHK1 kinase aggravated the EdU incorporation defect upon octyl-R-2-HG treatment indicating that the impairment in fork progression occurs independent of these cell-cycle checkpoint proteins (Figure 9E). This oncometabolite-associated defect on DNA replication was also reproduced in other normal and cancer-related cell lines such as MEF, U2OS, HeLa (Figure 10A, C, D and E), and remarkably in HT1080, a fibrosarcoma cell line with somatic heterozygous $IDH1^{R132C}$ mutation (Figure 10G). It is interesting to note that the enantiomer of R-2-HG, namely octyl-S-2-HG, also lowered DNA synthesis within one hour without increasing the RPA levels on chromatin (Figure 9F).

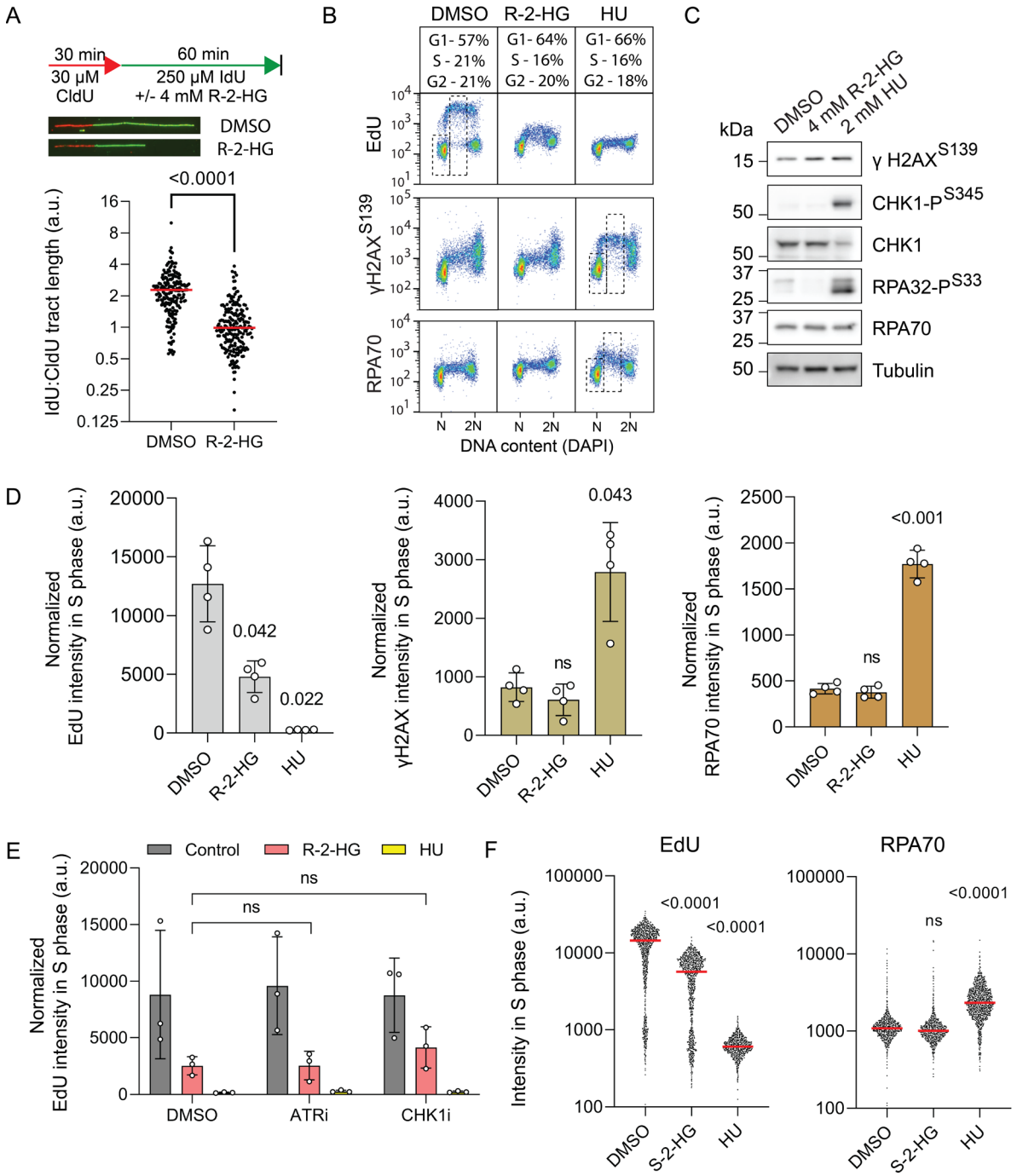

Figure 9 – Octyl-R/S-2-HG uniquely modulates the replication fork progression in NHA cells.

A) An experimental scheme of DNA fibre assay and exemplary fibre images are shown on top. DNA fibre analysis from cells that were treated with 4mM octyl-R-2-HG and an equivalent amount of DMSO for an hour is shown at the bottom. Using unidirectional forks (N=200), the ratio of IdU to CldU tract length was calculated from one experiment. **B)** Dot plot representation of chromatin-associated EdU, γH2AX and RPA70 quantified by immunofluorescence flow cytometry and plotted against DNA content (DAPI stain). Cells were treated with DMSO, 4mM octyl-R-2-HG and 2mM HU for an hour. 10µM EdU was added 30 minutes before the treatment completion. HU

was used as a positive control for reduced DNA replication and increased RPA70 on chromatin. Percent cells in the cell cycle were estimated by fitting the Watson (pragmatic) model in the DAPI signal by FlowJo software. The dashed lines represent the G1, and S phase gating for the analysis in (D). **C)** Immunoblot analyses of replication stress response markers from whole-cell protein extracts following treatments described in (B). **D)** Mean with SD of normalized chromatin-associated EdU, γH2AX and RPA70 intensity in the S phase following treatments in (B). The normalized intensity in the S phase is defined by subtracting the median of the G1 gate from the median of the S gate (gating represented in B). The data was plotted from four independent experiments. **E)** Mean with SD of chromatin-associated EdU intensity in S phase following treatments in (B) with or without 10μM ATR or CHK1 inhibitor. Cells were pre-treated with the inhibitors for an hour. The median data was plotted from three independent experiments. **F)** Chromatin-associated EdU, and RPA70 intensity in the S phase following DMSO, 4mM octyl-S-2-HG and 2mM HU treatment for an hour from one experiment. The intensity in the S phase is obtained from individual cells in the S phase gating without G1 median subtraction. **(D, E**) The adjusted p-values were obtained from multiple unpaired t-tests using the Holm-Šídák method. **(A, F)** The red line represents the median, and the p-value was obtained from the unpaired t-tests. The definition of statistical significance is $p < 0.05$

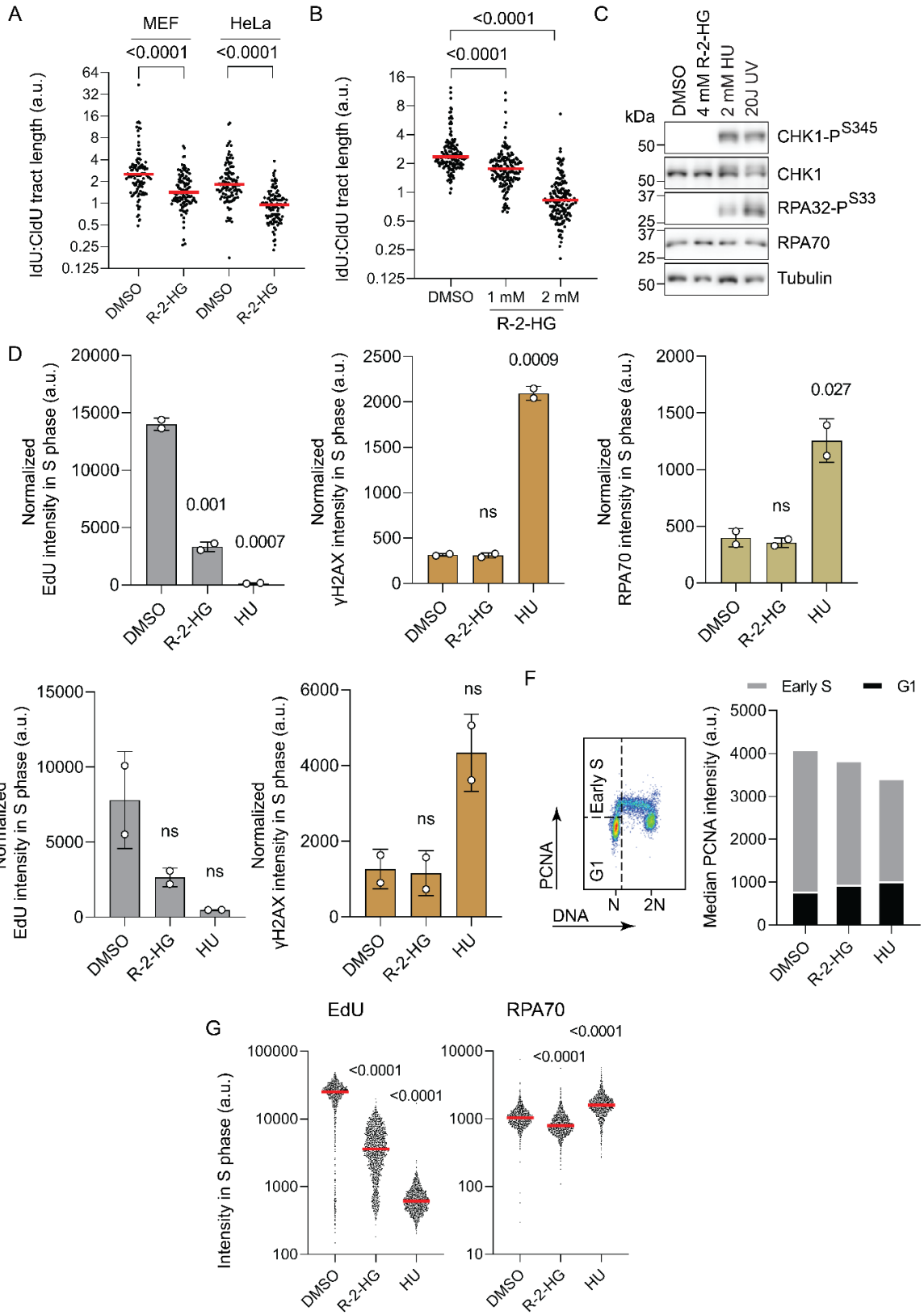
A
MEF
HeLa
<0.0001
<0.0001
IdU:CldU tract length (a.u.)
64
32
16
8
4
2
1
0.5
0.25
0.125
DMSO
R-2-HG
DMSO
R-2-HG
B
<0.0001
<0.0001
IdU:CldU tract length (a.u.)
16
8
4
2
1
0.5
0.25
0.125
DMSO
1 mM
2 mM
R-2-HG
C
DMSO
4 mM R-2-HG
2 mM HU
20J UV
kDa
50
CHK1-P S345
50
CHK1
37
25
RPA32-P S33
37
25
RPA70
50
Tubulin
D
Normalized EdU intensity in S phase (a.u.)
20000
15000
10000
5000
0
0.001
0.0007
DMSO
R-2-HG
HU
Normalized γH2AX intensity in S phase (a.u.)
2500
2000
1500
1000
500
0
0.0009
ns
DMSO
R-2-HG
HU
Normalized RPA70 intensity in S phase (a.u.)
2000
1500
1000
500
0
0.027
ns
DMSO
R-2-HG
HU
E
Normalized EdU intensity in S phase (a.u.)
15000
10000
5000
0
ns
ns
DMSO
R-2-HG
HU
Normalized γH2AX intensity in S phase (a.u.)
6000
4000
2000
0
ns
ns
DMSO
R-2-HG
HU
F
PCNA
DNA
Early S
G1
N
2N
Early S
G1
Median PCNA intensity (a.u.)
5000
4000
3000
2000
1000
0
DMSO
R-2-HG
HU
G
EdU
RPA70
Intensity in S phase (a.u.)
100000
10000
1000
100
<0.0001
<0.0001
10000
1000
100
10
<0.0001
<0.0001
DMSO
R-2-HG
HU
DMSO
R-2-HG
HU

Figure 10 – Octyl-R-2-HG uniquely modulates replication fork progression in normal and cancer cell lines.

A) DNA fibre analyses of HeLa and MEF cells treated with 4mM octyl-R-2-HG and an equivalent amount of DMSO for an hour (N=110). **B)** DNA fibre analysis of HeLa cells treated with octyl-R-2-HG in a dose-dependent manner for an hour (N=158). **(A, B)** The unidirectional forks were analyzed from one experiment. **C)** Immunoblot analyses of replication stress response markers from U2OS whole-cell protein extracts after an hour of treatments as labelled. **(D, E)** Mean with SD of chromatin-associated normalized EdU, γH2AX and RPA70 intensity in the S phase from U2OS (D) and MEF cells (E) after treating with DMSO, 4mM octyl-R-2-HG and 2mM HU for an hour. The data was plotted from two independent experiments. The adjusted p-values were obtained from multiple unpaired t-tests via the Holm-Šídák method. **F)** The G1 and Early S phase gating schematic is shown on the left. The median intensity of chromatin-bound PCNA in G1 and early S phase was plotted from one experiment. **G)** Chromatin-associated EdU, and RPA70 intensity in the S phase from HT1080 fibrosarcoma cell line with heterozygous $IDH1^{R132C}$ mutation following treatments as described in (E). The data was plotted from one experiment. **(A, B, G)** The red line represents the median, and the p-value was obtained from the unpaired t-tests. The definition of statistical significance is $p < 0.05$.

Octyl-R/S-2-HG activates ISR

Slowed fork progression is a form of replication stress that triggers the activation of the replication stress response (Bellelli & Boulton, 2021). In contrast, Mejlvang et al. (2014) reported that histone depletion after knocking down the SLBP protein, which is crucial for processing histone pre-mRNA, resulted in a reduced ratio of IdU to CldU tract length without affecting RPA or H2AX phosphorylation. In addition, Choo et al. (2020) reported a similar fork defect caused by activation of the integrated stress response (ISR) without any change in H2AX or CHK1 phosphorylation levels. In this study, ISR has been linked to the fork progression defect by blocking global translation, thereby limiting histone synthesis, which is in agreement with the previous mentioned study. Consistent to this, the activation of ISR kinase PERK was associated with impaired DNA replication (Cabrera et al., 2017). Another noteworthy study demonstrated that the introduction of the IDH1 R132H mutation in mice led to ER-associated unfolded protein response (UPR) activation (Sasaki et al., 2012) thereby establishing a preliminary notion that mIDH-derived R-2-HG influence DNA replication via ISR activation.

Based on these data, we investigated whether the exogenous treatment of octyl-R/S-2-HG regulates ISR. We measured levels of ATF4 and eIF2α phosphorylation, which are typically upregulated upon ISR activation. Thapsigargin (Tg) and dithiothreitol (DTT) were used as positive controls for ER-stress-induced ISR activation. Compared to the control (DMSO) in both NHA (Figure 11A) and U2OS cells (Figure 12A), an increase in ATF4 protein levels was observed after exposure to octyl-R-2-HG for one hour. However, the eIF2α phosphorylation level was unaffected in NHA and slightly increased in U2OS cells. ATF4 was also localized in the chromatin fraction which is in line with supporting its activity as a transcription factor upon ISR activation in response to oncometabolite treatment (Figure 11C). In response to ISR activation, stress-induced transcription factors including CHOP (also known as DDIT3) exhibit transcriptional upregulation, whereas ATF4 displays translational upregulation (Pakos-Zebrucka et al., 2016). To confirm this, we assessed the mRNA levels of CHOP and ATF4 following oncometabolite treatment for one hour. This data revealed two-fold increase in CHOP and no changes in ATF4 mRNA levels as expected (Figure 11D).

The ISR signalling cascade, that results in eIF2α phosphorylation, eventually blocks global protein synthesis (Costa-Mattioli & Walter, 2020). Short-term treatment with puromycin, an antibiotic

inhibiting translation after its integration in the peptide chain and thus labelling the peptide, was used to assess translation rates. Following exposure to octyl-R/S-2-HG for an hour, the intensity of puromycin was markedly reduced relative to the vehicle control in NHA (Figure 11A and B) as well as in U2OS cells (Figure 12A and B). Integrated Stress Response Inhibitor (ISRIB), a well-established small compound which binds to the eIF2α complex and prevents downstream ISR signalling without affecting eIF2α phosphorylation was used as a rescue approach (Sidrauski et al., 2015; Zyryanova et al., 2021). Addition of 1 μM ISRIB with 4mM octyl-R/S-2-HG lowered ATF4 levels to similar levels as DMSO and partially reverted the rate of protein synthesis, as demonstrated by an increase in puromycin intensity in NHA (Figure 11A and B) and U2OS cells (Figure 12A and B). These results confirm the activation of ISR signalling by the cellular uptake of octyl-R/S-2-HG in normal and cancerous cell lines.

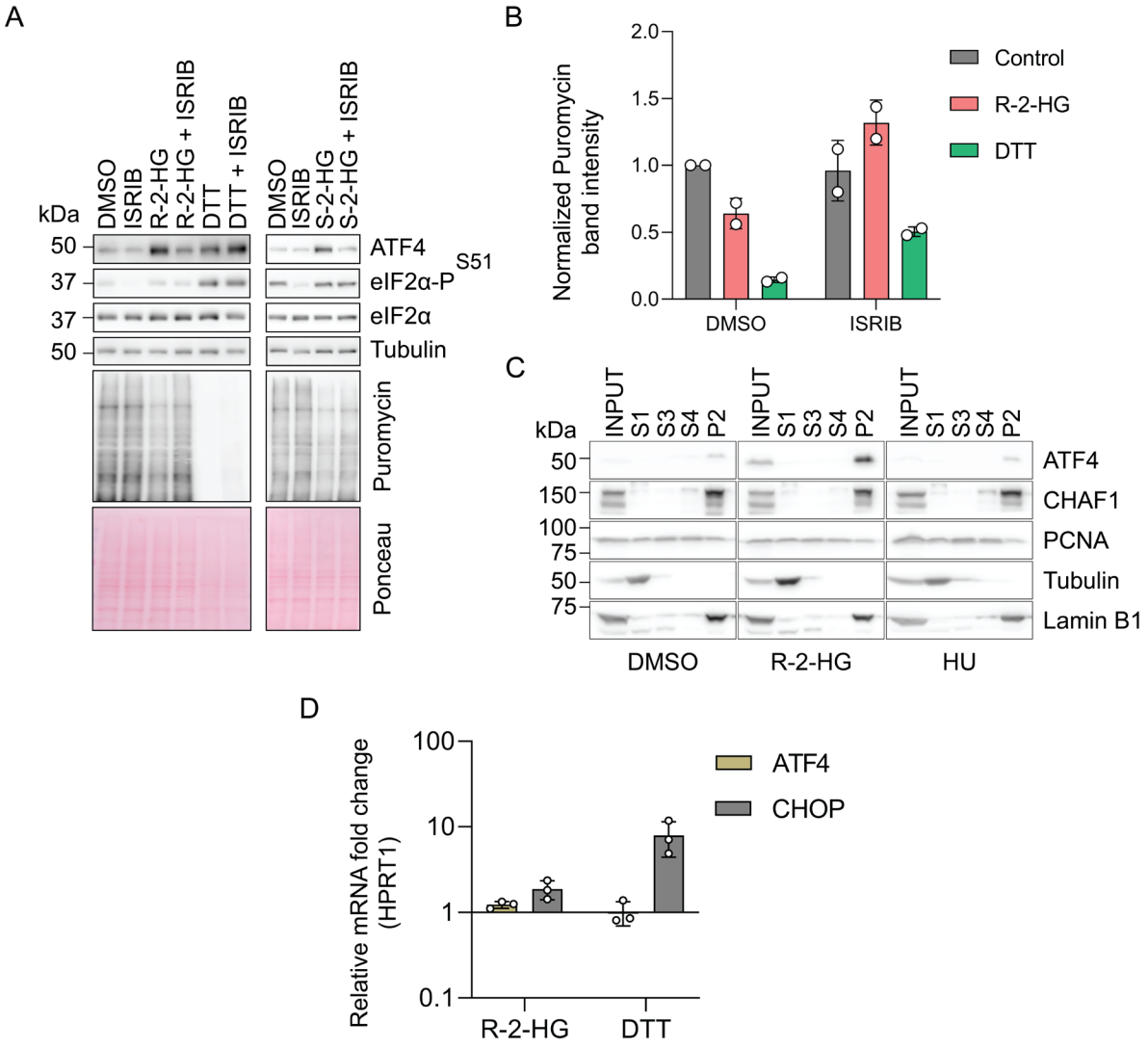

Figure 11 – Octyl-R/S-2-HG activates ISR signalling in NHA.

A) Immunoblot analysis of ISR activation markers from whole-cell protein extracts following DMSO, 1µM ISRIB, 4mM octyl-R/S-2-HG with or without ISRIB for an hour. 10µg/mL puromycin was added 15 minutes before treatment completion and ponceau staining acted as a loading control. **B)** Normalized band intensity quantified from immunoblots probing for puromycin as shown in (A). Each sample was normalized to DMSO, and the graphical plot was obtained from two independent experiments. For each experiment, average band intensities were calculated from technical (loading) replicates. **C)** Immunoblot analysis of cellular fractionation following treatment as shown in Figure 1B. S1 – cytoplasm, S3 – free-nuclear and P2 – chromatin-associated fractions. **D)** RT-qPCR analysis of mRNA levels following octyl-R-2-HG and 1mM DTT treatment for one hour and six hours, respectively. Technical triplicates were plotted from one experiment.

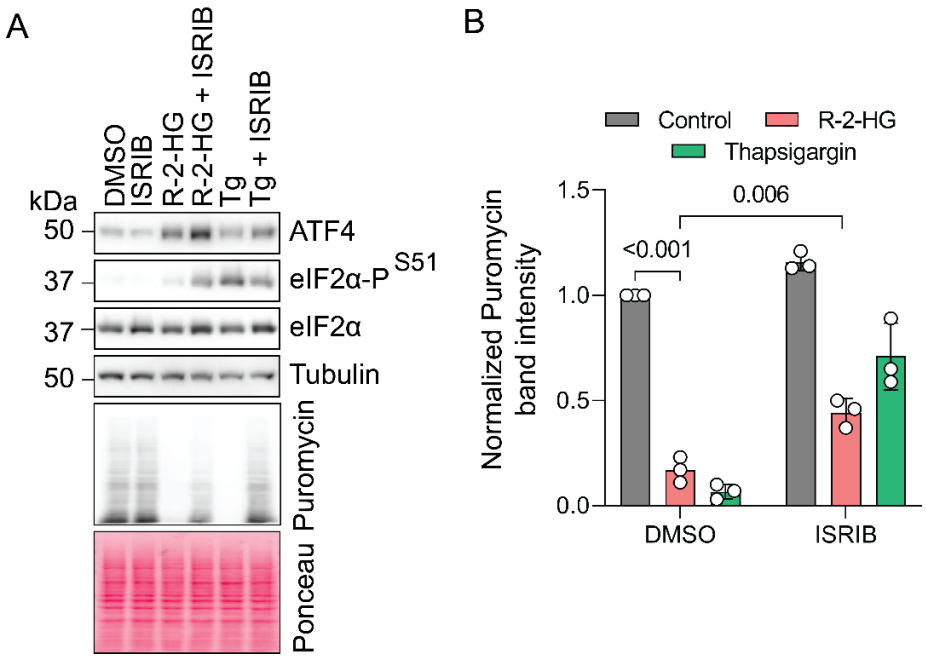

Figure 12 – Octyl-R-2-HG activates ISR signalling in U2OS cells.

A) Immunoblot analysis of ISR activation markers from whole-cell protein extracts following one-hour treatment as labelled in the figure. **B)** Normalized band intensity quantified using puromycin immunoblots shown in (A) from three independent experiments. For each experiment, average band intensities were calculated from loading replicates. The adjusted p-values were obtained from multiple unpaired t-tests using the Holm-Šídák method. The definition of statistical significance is $p < 0.05$.

Inhibition of ISR signalling partially rescues octyl-R/S-2-HG dependent RF progression defects

ISR signals the shutdown of protein synthesis in response to various internal and external stress stimuli, which impacts RF progression (Choo et al., 2020b). Having established that the oncometabolite regulates ISR, we explored whether blocking ISR activity triggered by the octyl-R-2-HG treatment could restore RF progression. Interestingly, the fork progression defect caused upon one hour of treatment with octyl-R-2-HG was rescued by ISRIB in NHA (Figure 13A) as well as in HEK293T cells (Figure 14A). Likewise, EdU incorporation was rescued when ISR signalling was blocked in NHA (Figure 13B) and U2OS cells (Figure 14C) upon octyl-R-2-HG treatment. A similar trend was seen in MEF cells (Figure 14B). The enantiomer octyl-S-2-HG also reduced the EdU incorporation in NHA (Figure 13C). The effectiveness of ISRIB was demonstrated by exposing cells to either DTT or Tg, with or without ISRIB treatment, and confirming that DNA synthesis was restored with ISRIB treatment in all experiments (Figure 13B, C and Figure 14C, D). PERK/EIF2AK3 is a kinase of the ISR signalling pathway that is activated by UPR (Read & Schröder, 2021). So, we utilised an inhibitor (PERKi) which binds to PERK and inhibits its catalytic phosphorylation activity on eIF2α at serine residue 51 to rule out whether octyl-R-2-HG impairs fork progression via the PERK axis of the ISR pathway. Our results showed that PERK inhibition did not significantly rescue the EdU incorporation upon octyl-R-2-HG treatment in cells for one hour when compared to ISRIB. In addition, pre-treatment of cells with the inhibitors for one hour did not improve the rescue in EdU incorporation levels (Figure 14D). At this point, the contribution of other ISR kinases in RF progression defect remain uncharacterized.

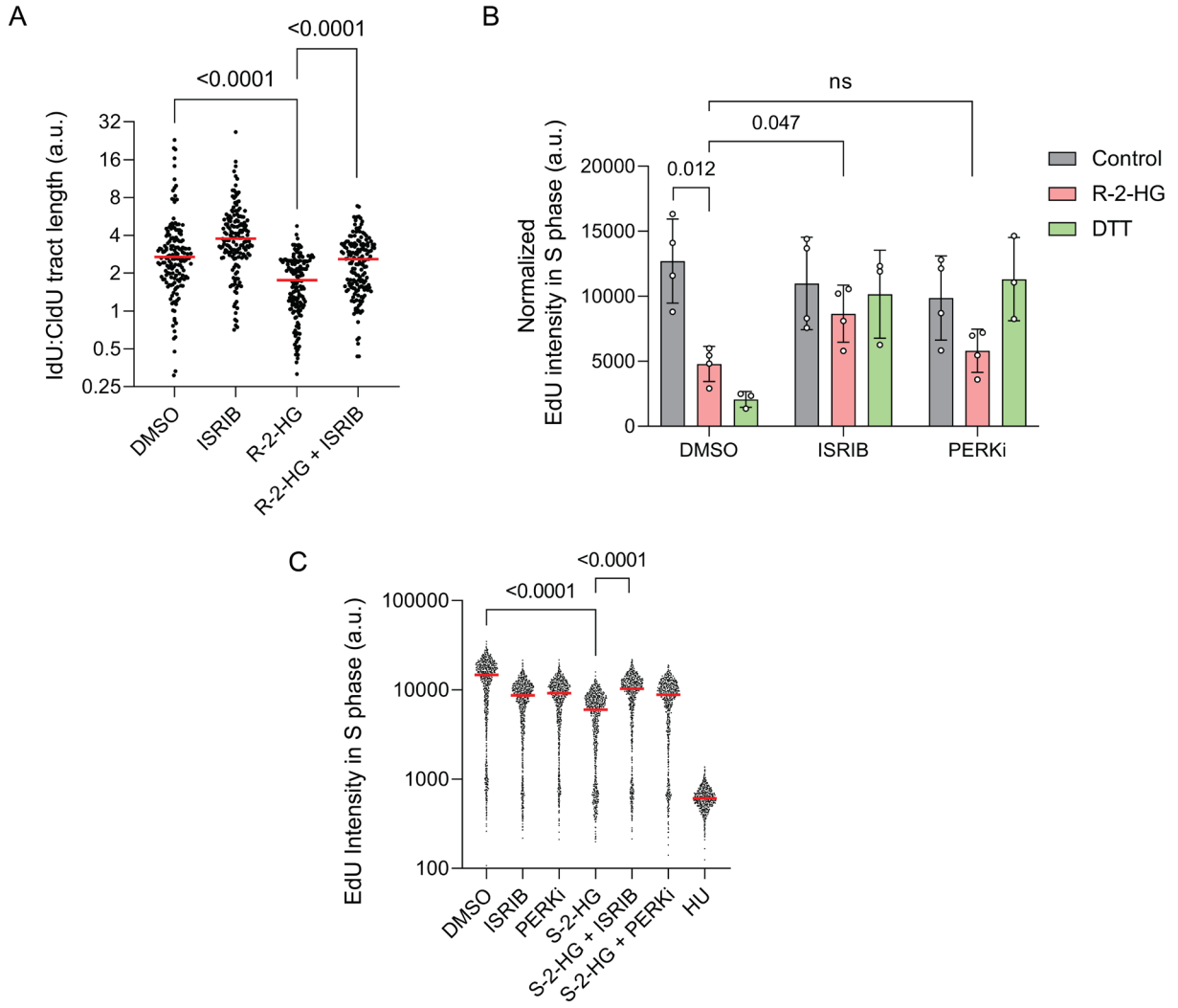

Figure 13 – Blocking ISR partially rescues the replication fork progression defect caused by octyl-R/S-2-HG in NHA.

A) DNA fibre analysis of cells treated with DMSO, 1µM ISRIB, and 4mM octyl-R-2-HG with or without ISRIB for an hour from a single experiment (N=160). **B)** Mean with SD of normalized chromatin-associated EdU intensity in the S phase following treatment described in (A) in addition to 1mM DTT together with and without 1µM ISRIB or 0.5µM PERKi. DTT is used as a positive control for ER-stress-induced ISR signalling. The data for octyl-R-2-HG with or without ISRIB and PERKi were plotted from four independent experiments. Data from three independent experiments were plotted for DTT with or without ISRIB and PERKi. The adjusted p-values were obtained from multiple unpaired t-tests using the Holm-Šídák method. **C)** Chromatin-associated EdU intensity in the S phase following treatment as labelled for an hour from a single experiment. **B, C)** The red line represents the median, and the p-value was determined based on unpaired t-tests. The definition of statistical significance is $p < 0.05$.

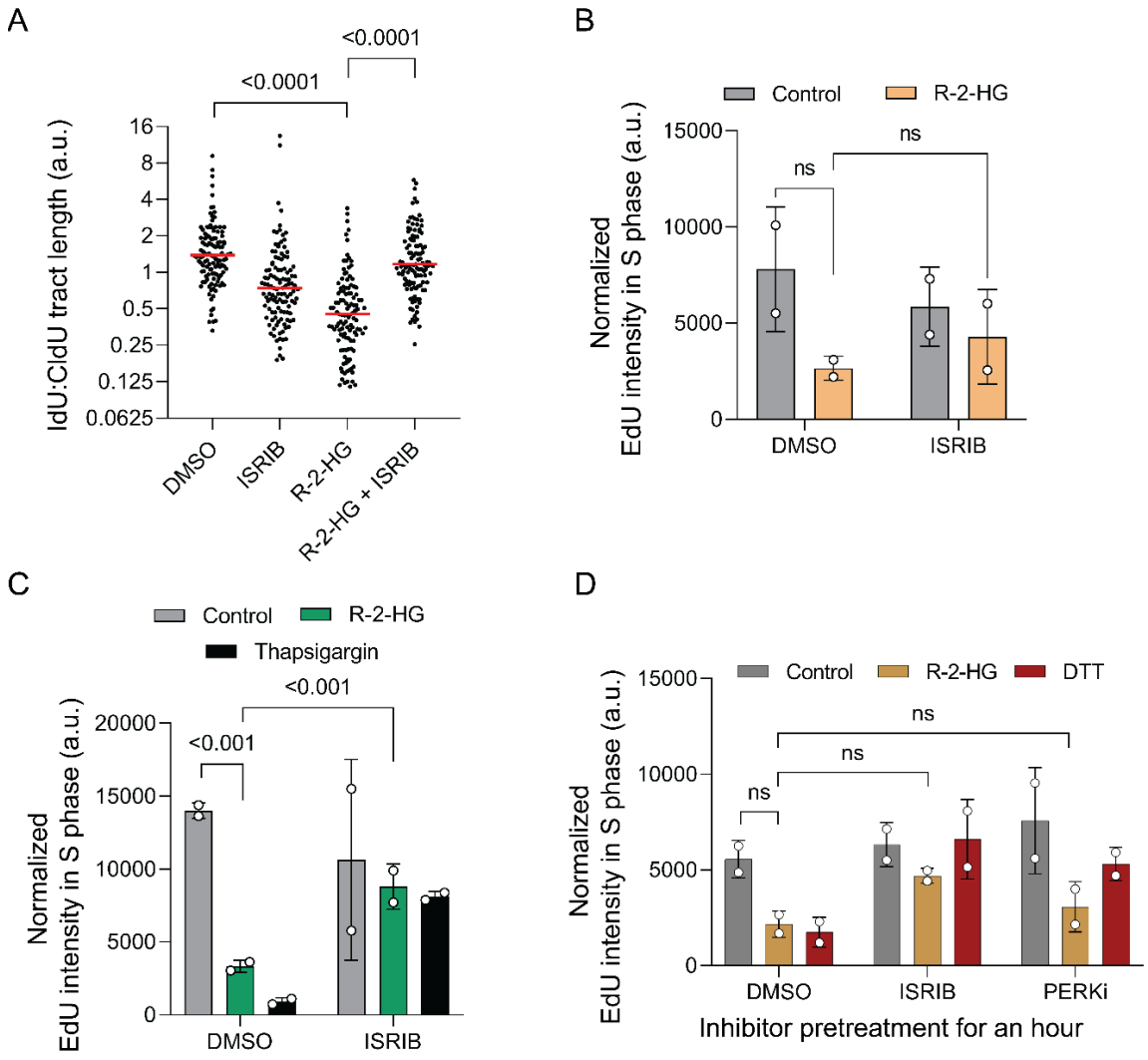

Figure 14 – Blocking ISR partially rescues the replication fork progression caused by octyl-R-2-HG in normal and cancer cell lines.

A) DNA fibre analysis of HEK293T cells treated with DMSO, 1 µM ISRIB, and 4 mM octyl-R-2-HG with or without ISRIB for an hour from a single experiment (N=117). The red line represents the median, and the p-value was determined using unpaired t-tests. **(B, C, D)** Mean with SD of normalized chromatin-associated EdU intensity in the S phase from MEF (B), U2OS (C) and NHA cells (D) following treatment as shown in (A). The data was plotted from two independent experiments. 2 µM thapsigargin (Tg) was used as a positive control for ER-stress-induced ISR signalling in (C). Cells were pre-treated with either 1 µM ISRIB or 0.5 µM PERKi for one hour in (D). The adjusted p-values were obtained from multiple unpaired t-tests using the Holm-Šídák method. The definition of statistical significance is $p < 0.05$.

pH changes in the extracellular medium by octyl-R-2-HG did not affect the DNA replication process

We noticed a change in the medium colour upon addition of 4 mM octyl-R-2-HG, consistent with pH changes associated with similar metabolites (Singh et al., 2013; B. Yang et al., 2023). A pH measurement in a cell-free medium revealed acidification of the medium (from pH 7.8 to 7.5) after mixing in the oncometabolite (Figure 15A). To determine whether this pH change contributes to the DNA synthesis defect caused by octyl-R-2-HG, NHA cells were grown in complete medium in which the pH was adjusted from pH 7.8, which is the medium's normal pH, to pH 7.5 and 7 using sulfuric acid (H_2SO_4). The pH-adjusted media did not influence EdU incorporation (Figure 15B) or increase chromatin-bound ATF4 levels (Figure 15C). This suggests that pH changes caused by octyl-R-2-HG mixing do not contribute to the effect of this oncometabolite on RF progression or stress-induced elevation of chromatin-bound ATF4 protein.

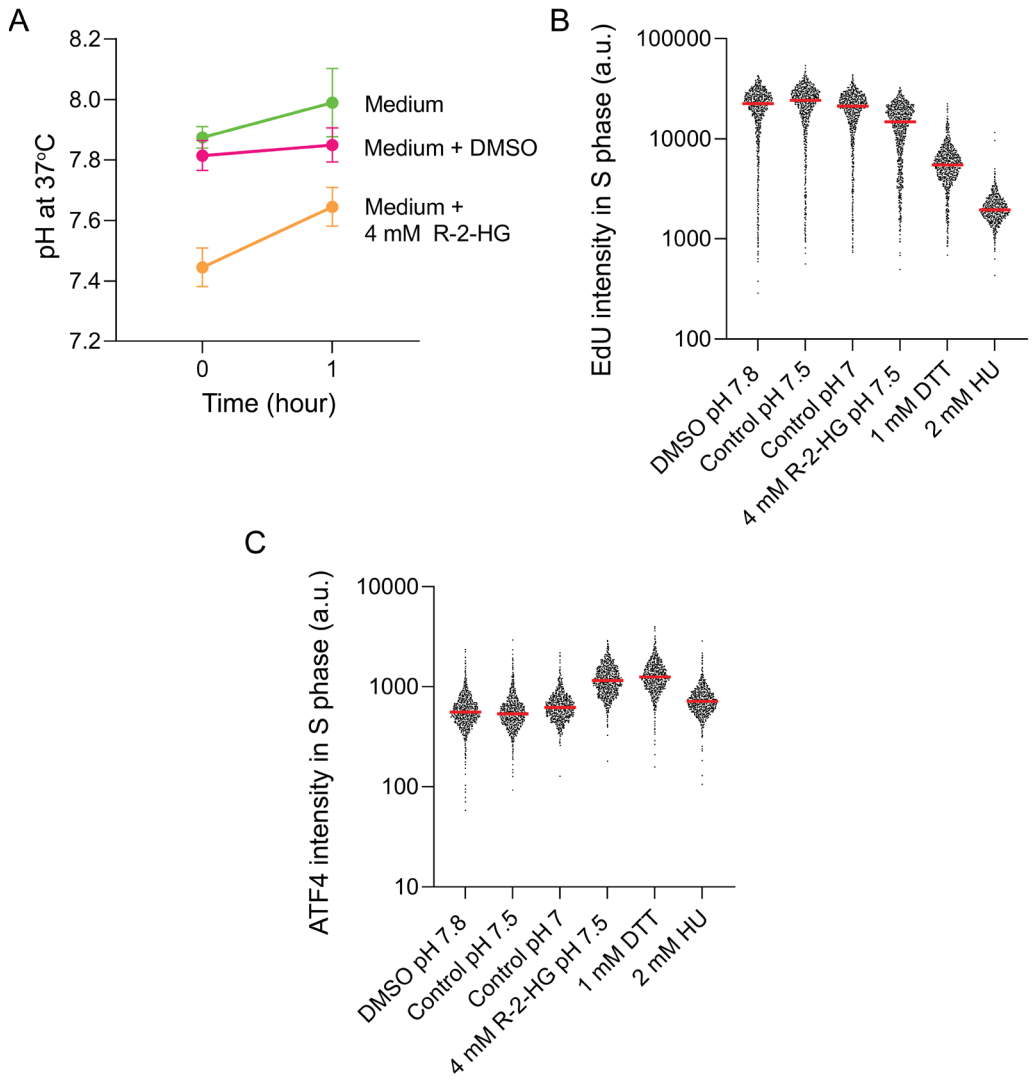

Figure 15 – Octyl-R-2-HG acidifies the growth medium which does not contribute to the replication fork progression defect in NHA.

A) pH measurement of complete medium alone, mixed with DMSO and 4mM octyl-R-2-HG at 37°C. Timepoint 0 hour on the X axis, represents pH measurement right after mixing the compounds. These mediums were then incubated without cells for an hour and the pH measurement was repeated. The graph was plotted from two independent experiments. **(B, C)** Chromatin-associated EdU (B) and ATF4 (C) intensity in the S phase of cells treated as labelled for an hour. A pH value indicates the pH after mixing compounds in a given condition. Control pH 7 and 7.5 treatments were with complete medium, and their pH was adjusted using H_2SO_4. The red line represents the medium value.

Octyl-α-ketoglutarate shows similar ISR-mediated defect in DNA replication

To demonstrate the specificity of the R-2-HG/ISR axis modulating the DNA replication, we evaluated the effect of physiologically normal and cell-permeable metabolite octyl-α-ketoglutarate (octyl-α-KG) on DNA synthesis. Overexpression of α-KG-dependent histone demethylases has been shown to promote DNA replication initiation and PCNA dissociation during termination (Gerace & Moazed, 2010; Rondinelli et al., 2015). Based on these studies, we speculated that the accumulation of octyl-α-KG inside cells accelerates the DNA replication process while being unsure about its impact of ISR activation. However, ISR may be activated by the accumulation of octyl moiety during the processing of octyl reagents inside the cells (Parker et al., 2021).

NHA cells were not viable when treated with an equal amount of octyl-α-KG as 4mM octyl-R-2-HG used previously in our studies (Figure 18A), so we experimented with a lower concentration ranging from 0.5 – 2mM, typically present in cultured cells (Metabolomics Workbench DOI: 10.21228/M83C78) and recommended as growth supplement (B. Yang et al., 2023). Intriguingly, flow cytometry analysis of EdU incorporation revealed a decrease in DNA synthesis or S-phase progression, slightly elevated H2AX phosphorylation and an increase in chromatin-bound ATF4, all in a dose-dependent manner upon one-hour octyl-α-KG treatment (Figure 16A, B and C). Moreover, consistent with octyl-R-2-HG, blocking ISR signalling with ISRIB partially rescued DNA synthesis (Figure 16D). Taken together, the results suggest that octyl-α-KG impaired the DNA replication process via the ISR pathway, however, a dose-dependent elevation of H2AX phosphorylation indicated the activation of the replication stress response. When octyl-α-KG treatment was combined with ISRIB, ATF4 levels were found comparable to those of cells with DTT (Figure-16E), indicating that either the experimental timeline is insufficient to observe a rescue in ATF4 levels or ATF4 translation is upregulated via ISR-related eIF2α phosphorylation-independent pathways. At this point it is unclear whether ISR activation was specific to the oncometabolite R-2-HG.

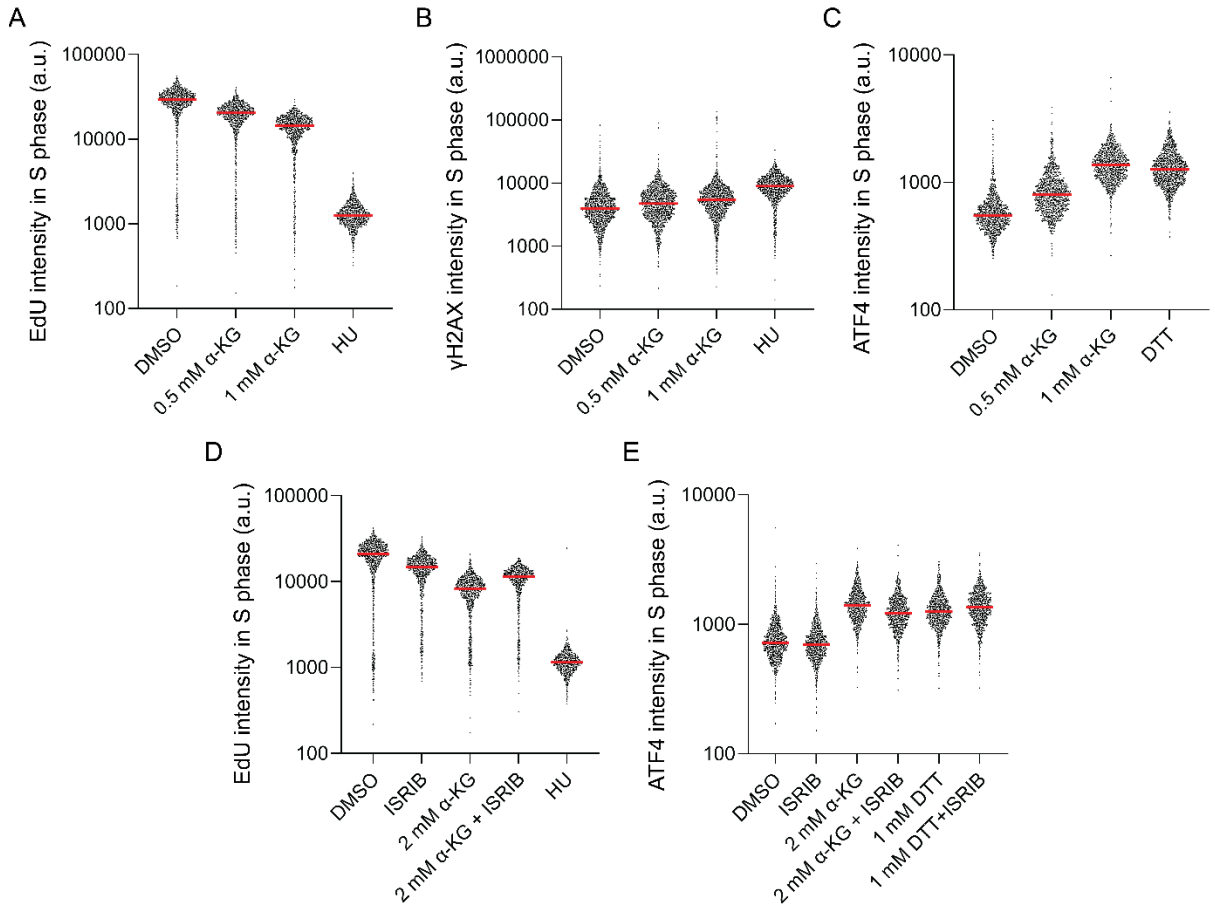

Figure 16 – Octyl-α-KG impairs DNA replication and activates a replicative stress response in a dose-dependent manner.

Chromatin-associated EdU **(A, D)**, γH2AX **(B)** and ATF4 **(C, E)** intensity in the S phase following treatment with DMSO, different concentrations of octyl-α-KG, 2mM HU, and 1mM DTT. Both octyl- α-KG and DTT were also treated in combination with 1μM ISRIB for an hour. The red line represents the median value.

Long-term treatment of octyl-R-2-HG impairs NHA cell growth and blocking ISR rescues the growth defect

To further question the R-2-HG/ISR axis specificity, we conducted a growth assay with octyl-α-KG, octyl-R-2-HG and octyl-S-2-HG. We also observed the effect of blocking ISR signalling for 6 days with these metabolites. Among all three metabolites, NHA cells were extremely sensitive to octyl-S-2-HG, as evidenced by the decline in proliferation after 2-3 days (Figure 17D and F). Moreover, on sixth day, the remaining cells displayed an abnormally elongated morphology compared to cells treated with DMSO (Figure 17A). ISRIB did not rescue growth in any concentration of this metabolite. Compared to octyl-R-2-HG, NHA cells were more sensitive to octyl-α-KG as no proliferation was observed for up to 2 days (Figure 17B and C). Cells treated with 0.5mM and 1mM octyl-α-KG respectively showed complete and partial growth rescue with ISRIB. Similar to octyl-S-2-HG treatment, cells in octyl-α-KG showed abnormal morphological elongation between day 4 to day 6 of treatment (Figure 17A). NHA showed least sensitivity to octyl-R-2-HG in contrast to similar concentrations of the other two metabolites (Figure 17B, C and D). Blocking ISR showed a significantly partial and complete rescue in cell growth at 2mM and 1mM octyl-R-2-HG, respectively, without any elongated morphology (Figure 17A, C and E). An explanation for this elongated morphology is the reactive astrogliosis, a defence mechanism induced by stress (Zhou et al., 2019). U2OS cells were also affected by octyl-R-2-HG treatment and rescued with ISRIB (Figure 18B). The results demonstrate that NHA cells are resilient to the accumulation of R-2-HG compared to the enantiomer S-2-HG and α-KG. It appears, however, that ISR activation may be a common cellular response to the treatment with octyl-metabolites.

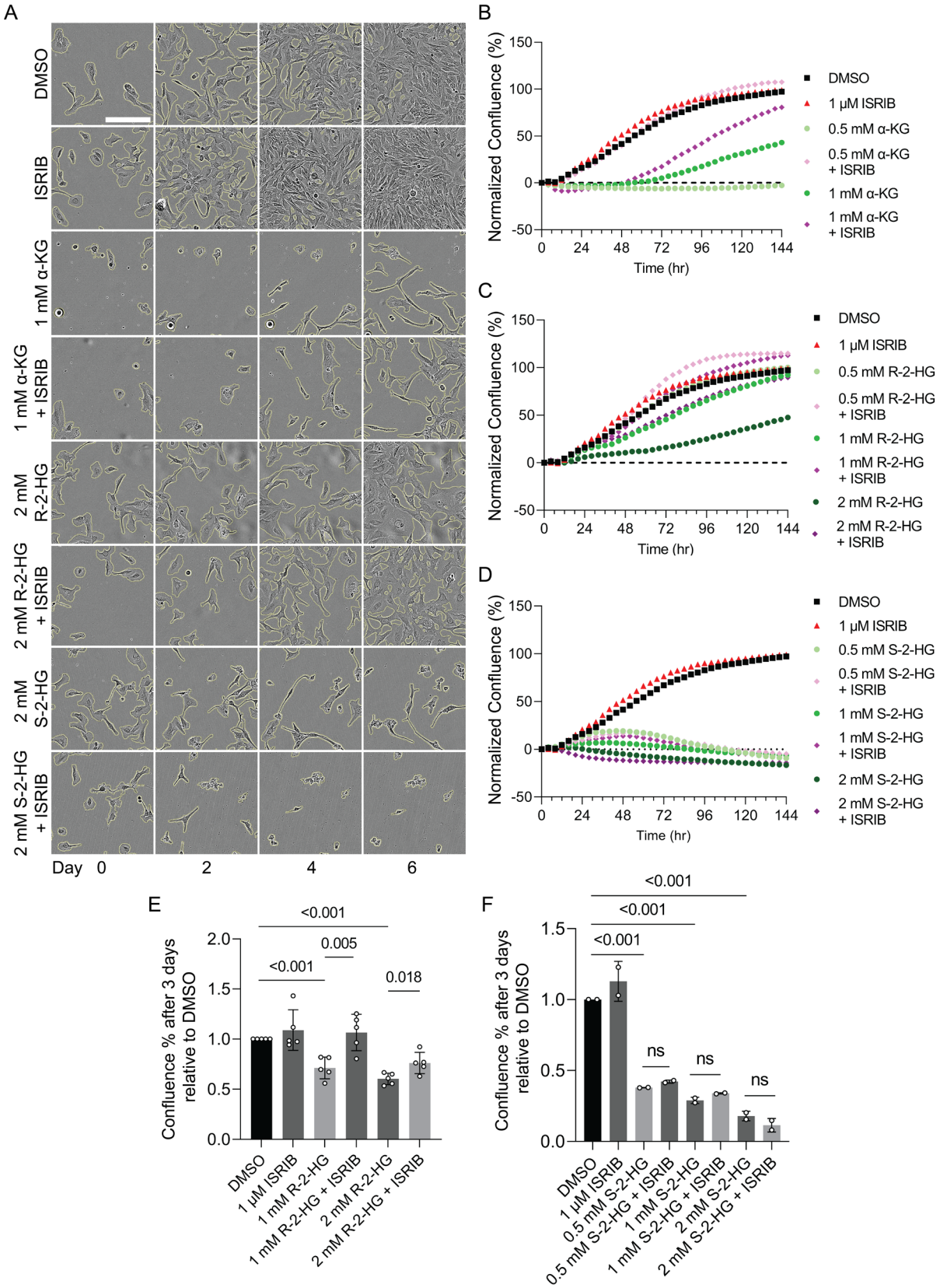
A
DMSO
ISRIB
1 mM α-KG
1 mM α-KG + ISRIB
2 mM R-2-HG
2 mM R-2-HG + ISRIB
2 mM S-2-HG
2 mM S-2-HG + ISRIB
Day 0
2
4
6
B
Normalized Confluence (%)
Time (hr)
DMSO
1 μM ISRIB
0.5 mM α-KG
0.5 mM α-KG + ISRIB
1 mM α-KG
1 mM α-KG + ISRIB
C
Normalized Confluence (%)
Time (hr)
DMSO
1 μM ISRIB
0.5 mM R-2-HG
0.5 mM R-2-HG + ISRIB
1 mM R-2-HG
1 mM R-2-HG + ISRIB
2 mM R-2-HG
2 mM R-2-HG + ISRIB
D
Normalized Confluence (%)
Time (hr)
DMSO
1 μM ISRIB
0.5 mM S-2-HG
0.5 mM S-2-HG + ISRIB
1 mM S-2-HG
1 mM S-2-HG + ISRIB
2 mM S-2-HG
2 mM S-2-HG + ISRIB
E
Confluence % after 3 days relative to DMSO
<0.001
0.005
<0.001
0.018
DMSO
1 μM ISRIB
1 mM R-2-HG
1 mM R-2-HG + ISRIB
2 mM R-2-HG
2 mM R-2-HG + ISRIB
F
Confluence % after 3 days relative to DMSO
<0.001
<0.001
<0.001
ns
ns
ns
DMSO
1 μM ISRIB
0.5 mM S-2-HG
0.5 mM S-2-HG + ISRIB
1 mM S-2-HG
1 mM S-2-HG + ISRIB
2 mM S-2-HG
2 mM S-2-HG + ISRIB

Figure 17 – Octyl-metabolites inhibit NHA cell growth in a dose-dependent manner and blocking ISR signalling rescues the growth defect in octyl-R-2-HG.

A) Time-course representation of NHA cells treated with DMSO, ISRIB, and octyl-metabolites with and without ISRIB using Incucyte cell proliferation assay. The yellow line surrounding a cell indicated cell segmentation utilized for the confluence percent analysis. The scale bar shown in the DMSO day 0 image represents 200µm. **(B, C, D)** Normalized confluence percent analysis (calculation described in materials and methods) comparing the growth curve of cells treated with different concentrations of octyl-α-KG (B), octyl-R-2-HG (C) and octyl-S-2-HG (D) in combination with ISRIB. **(E, F)** The mean of confluence percent relative to DMSO was obtained from five independent experiments for octyl-R-2-HG (E) and two independent experiments for octyl-S-2-HG (F). In each experiment with octyl-S-2-HG, the relative confluence percent was calculated by taking the average of technical replicates. The confluence percent obtained from the Incucyte Basic Analyzer for each sample was divided by the confluence percent of DMSO. The adjusted p-values were obtained from multiple unpaired t-tests using the Holm-Šídák method. The definition of statistical significance is $p < 0.05$.

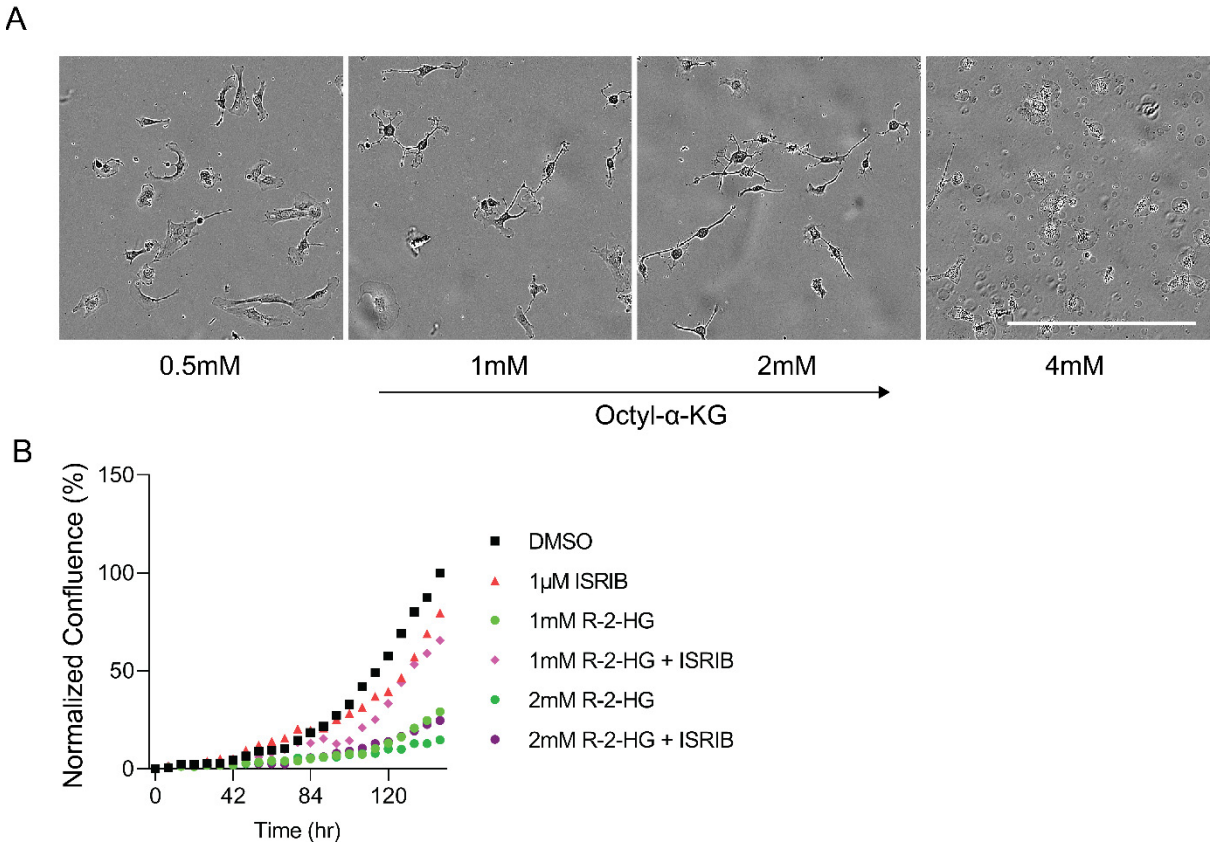

Figure 18 – Octyl-metabolites impairs cell growth.

A) Representative images of NHA cells after an hour of octyl-α-KG. The scale bar on the bottom right represents 400μm. **B)** Normalized confluence percent analysis comparing the growth curve of U2OS cells with treatment as labelled for 6 days (144 hours).

Cancer-relevant IDH2-mutant overexpression slows NHA proliferation

To eliminate the artefacts resulting from octyl processing inside the cells due to exogenous treatment of octyl-metabolites, IDH mutations, specifically IDH1 R132H functioning in the cytoplasm and IDH2 R172K functioning in the mitochondria, were introduced into NHA (Benlabiod et al., 2022; de Jong & Bovée, 2018). The Tet-On inducible system was selected for gene overexpression thereby ruling out the cellular adaptation to excessive accumulation of metabolites which might occur in cells constitutively expressing mutant IDH1/2 genes (Figure 19). To generate NHA cell lines, lentiviral vectors with GFP, FLAG-tagged IDH1, IDH2, IDH1 R132H, and IDH2 R172K genes were used to transduce cells. Gene induced by doxycycline was validated by quantifying the GFP and FLAG levels using immunoblots and immunofluorescence flow cytometry (Figure 20A and B). Compared to IDH1(wildtype and mutant), the median intensity of IDH2 FLAG was higher implying more protein expression or easier detection of the protein epitope. Moreover, the doxycycline concentration used for induction itself did not cause ISR activation in NHA cells as confirmed by analysing the ATF4 protein in the NHA GFP cell lines (Figure 20C). To reproduce the growth defect caused by exogenous octyl-R-2-HG treatment, we overexpressed wildtype and mutant IDH 1 and 2 genes and monitored the growth curve for six days following induction. In the presence of doxycycline, NHA cells with IDH2 R172K, but not IDH1 R132H exhibited a significant growth defect (Figure 20D, E and F), consistent with a recent study highlighting higher R-2-HG levels in mitochondrial IDH2 R172K versus cytoplasmic IDH1 R132H overexpression (Parker et al., 2021).

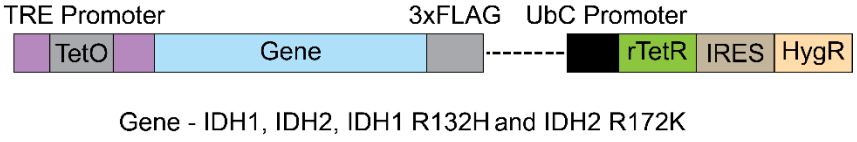

Figure 19 – Schematic of wild-type and mutant IDH1/2 genes overexpression.
A section of expression plasmids used for NHA cell transduction is shown. The gene of interest is expressed under TRE promoter that is, in the presence of tetracycline or doxycycline. The selection marker hygromycin is ubiquitously expressed under the UbC promoter. The plasmid with the GFP gene without 3xFLAG was used as an expression control.

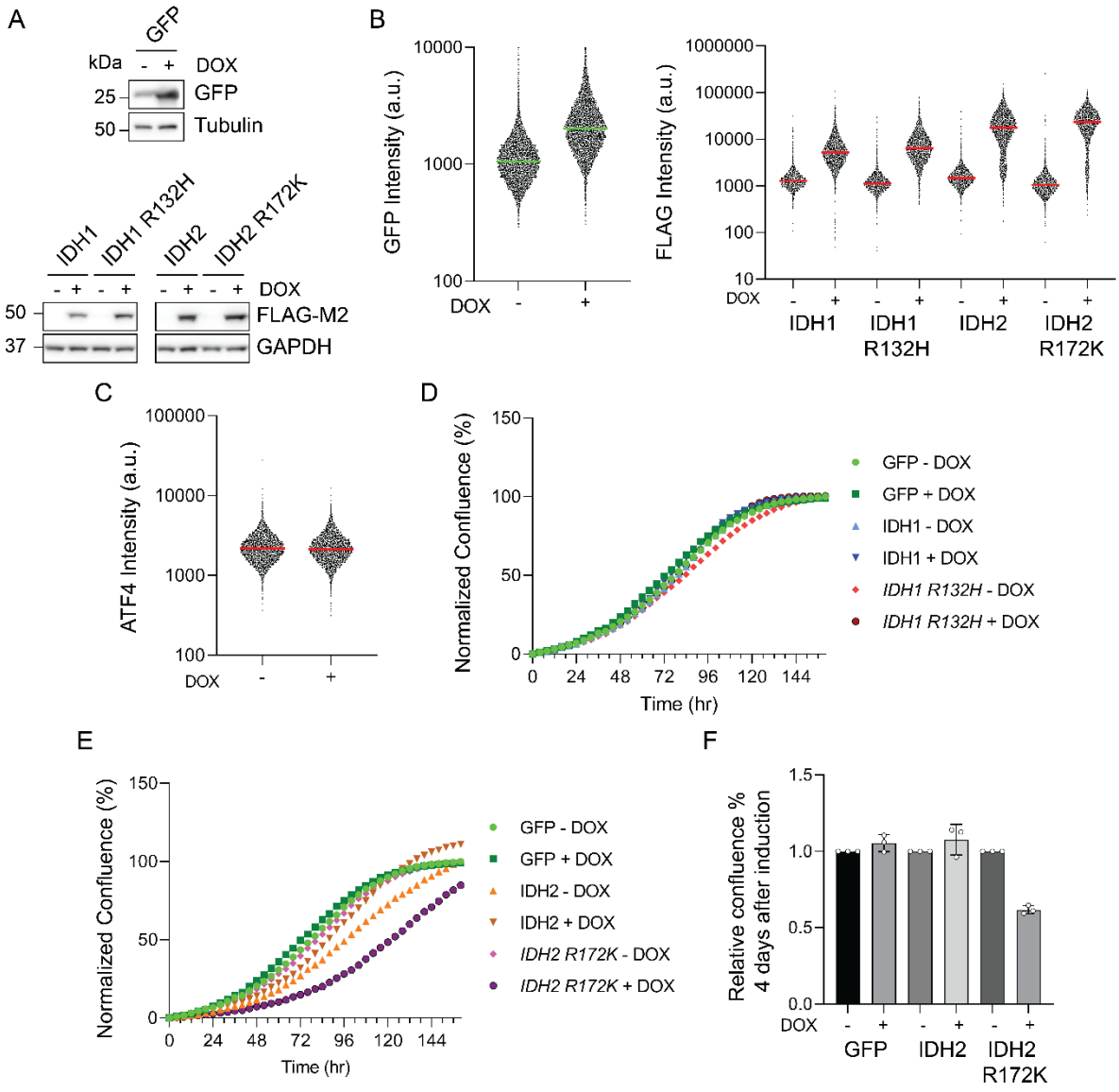

Figure 20 – Overexpressing IDH2 R172K gene inhibits NHA cell growth.

A) Immunoblot analyses of NHA cells overexpressing IDH1, IDH2, IDH1 R132H, and IDH2 R172K FLAG-tagged genes induced with 1µg/mL doxycycline (DOX) for 24 hours. NHA overexpressing GFP (without FLAG tag) was used as an expression control cell line. **(B, C)** Whole-cell GFP, FLAG (B) and ATF4 (C) intensity from all phases of the cell cycle upon induction as described in (A) using immunofluorescence flow cytometry. **(D, E)** Normalized confluence percent analysis of cells with and without doxycycline-induced overexpression of IDH1, IDH2, IDH1 R132H, and IDH2 R172K FLAG-tagged genes for 160 hours (6.6 days) using Incucyte cell proliferation assay. **F)** Mean of confluence percent relative to cells without doxycycline was calculated from two independent experiments.

IDH2-mutant overexpression impairs DNA replication

To evaluate whether mIDH-derived R-2-HG impairs DNA replication as well as to question whether R-2-HG-based ISR activation was responsible for the DNA synthesis defect, we induced wildtype and mutant IDH2 gene overexpression using doxycycline for 3 days in combination with ISRIB followed by an EdU incorporation assay. FLAG-tagged protein levels were evaluated with and without doxycycline to validate protein induction (Figure 21A). Overexpression of IDH2 R172K in NHA cells reduced the incorporation of EdU in replicating DNA consistent with our previous findings (Figure 21B and C). In contrast, IDH2 overexpression was found to increase EdU incorporation in S-phase cells. When the ISR signalling was inhibited in NHA cells with IDH2 R172K overexpression, EdU incorporation was partially improved. However, this was not the case in IDH2 overexpression. The stress-induced transcription factor ATF4 was found elevated in both IDH2 and IDH2 R172K induced overexpression compared to cells without induction. However, ISRIB slightly reduced the levels of ATF4 in wild-type IDH2 overexpression and remained unaffected in IDH2 R172K expressing cells (Figure 21D). The cell proliferation assay for NHA wildtype IDH2 and IDH2 R172K overexpression showed growth inhibition in ISRIB alone, suggesting that a basal activation of ISR may promote cell proliferation (Figure 21E and F). Our results indicate that DNA replication is impaired upon overexpression of IDH2 R172K, which is consistent with our findings when NHA were exogenously treated with octyl-R-2-HG. On the other hand, IDH2 overexpression, resulting in α-KG accumulation improved DNA replication in contrast to octyl-α-KG treatment. The data presented here are preliminary in nature and will need to be replicated.

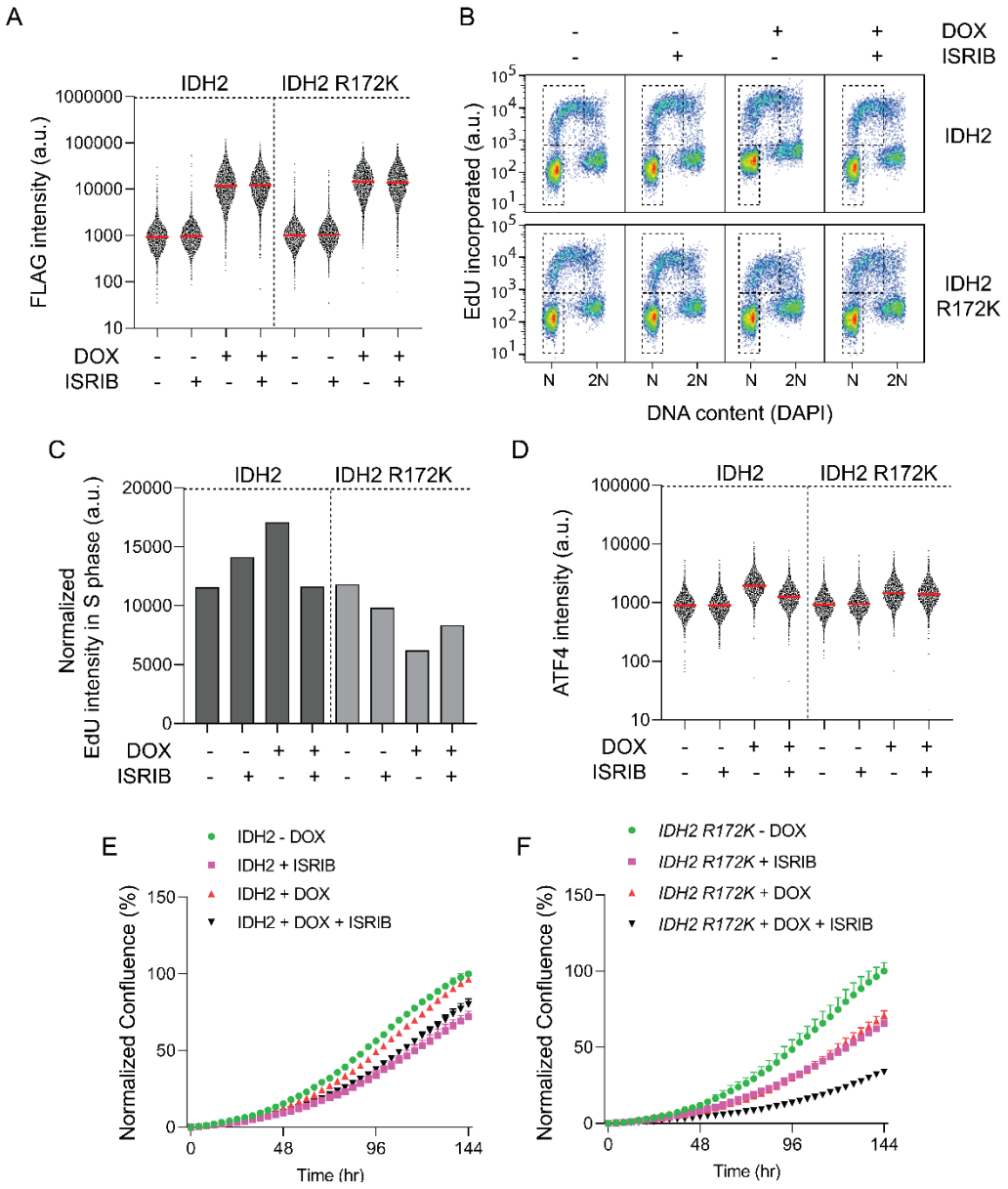

Figure 21 – IDH2 and IDH2 R172K overexpression promote and impair DNA replication, respectively.

(A, D) Whole-cell FLAG (A) and ATF4 (D) intensity of NHA cells overexpressing IDH2 and IDH2 R172K FLAG-tagged genes upon 1µg/mL doxycycline induction for 3 days with and without 1µM ISRIB obtained by immunofluorescence flow cytometry. **B)** A dot plot of EdU incorporation versus DNA content for cells overexpressing IDH2 and IDH2 R172K FLAG-tagged genes as described in (A) using immunofluorescence flow cytometry. 10 µM EdU was added 30 minutes before the completion of the 3-day timepoint. A dashed line represents the gating for the G1 and S phases and is used for analysis in (C). **C)** Normalized EdU intensity in the S phase calculated for cells in (A) using the gates labelled in (B) from a single experiment. **(E, F)** Normalized confluence

percent analysis to compare growth curves between different conditions as referred to in (A) for wildtype IDH2 (E) and IDH2 R172K cells from two independent experiments.

Chapter 4 – Discussion

A majority of low-grade gliomas possess mutations in the IDH enzyme (Y. Liu et al., 2020). As a result, the oncometabolite R-2-HG accumulates in cells and inhibits several enzymatic activities including ten-eleven translocation (TET) and Jumonji C (JmjC) domain proteins which mediates DNA and histone demethylation, respectively. The loss of specific histones and DNA modifications has been suggested to cause DNA replicative stress (Kang et al., 2020; Rondinelli et al., 2015). It has also been shown that tumours with IDH mutations are susceptible to genotoxic therapies due to defective homologous recombination (Sulkowski et al., 2017b), an essential repair pathway employed during S-phase. The impact of R-2-HG on DNA replication nevertheless remains poorly understood. Our data suggests that R-2-HG impairs DNA replication causing replicative stress in NHA cell lines. We explored the ISR activation upon R-2-HG accumulation as an underlying mechanism that modulates DNA replication in IDH-mutant pathologies.

We quantified replication fork and S-phase progression in normal and cancer cell lines treated with the cell-permeable oncometabolite octyl-R-2-HG for one hour. Our results on the dose-dependent DNA replication defect indicate that this oncometabolite reduces fork progression and DNA synthesis (Figure 9 and 10). Chromatin-associated PCNA was slightly reduced in the early S-phase of the cell cycle upon octyl-R-2-HG treatment (Figure 10). The decrease in chromatin-associated PCNA might result from the absence of critical demethylase activity necessary for PCNA recruitment, a process hindered by the presence of the metabolite (Rondinelli et al., 2015). However, unlike the replication-blocking agent hydroxyurea, octyl-R-2-HG showed no increase in replication stress response markers. This metabolite did not result in the significant buildup of RPA-coated single-stranded DNA (ssDNA), which is typically responsible for initiating the activation of the ATR and CHK1 kinases (Toledo et al., 2013). As a consequence, inhibiting ATR or CHK1 kinase did not aggravate the extent of DNA synthesis impairment. It must be acknowledged, however, that monitoring the replicative stress response in 4mM octyl-R-2-HG treated cells for one hour may not be sufficient to confirm the signalling activation. It is also crucial to quantify R-2-HG cellular intake which would strengthen the argument that the replication defect is the direct result of R-2-HG accumulation. A metabolite analysis could be conducted, for example by NMR, GC/MS and LC-MS/MS.

R-2-HG accumulation is known to activate ER stress signalling via unfolded protein response (Sasaki et al., 2012) which impairs replication fork progression without the RSR activation (Choo et al., 2020b). Following octyl-R-2-HG treatment for one hour we observed elevated ATF4 protein and reduced global protein synthesis, however, lack of changes in eIF2α phosphorylation limits us from concluding the role of a specific ISR kinase (Figure 11). However, since ISRIB rescued both the ISR activation markers (ATF4 and global protein synthesis) as well as EdU incorporation in octyl-R-2-HG treatment, we suspect a possible link between R-2-HG and ISR (Figure 13 and 14). The levels of ATF4 were unexpectedly increased in U2OS cells when ISRIB was combined with octyl-R-2-HG (Figure 12), despite an expected rescue in the global protein synthesis, implying that either the experimental timeline was not sufficient to observe a rescue in ATF4 levels or a basal ISR activation via feedback mechanism is essential for cancer cell survival (McConkey, 2017; Tameire et al., 2019; Tian et al., 2021). Perhaps ISRIB concentration can be increased according to its IC_{50} to test whether ISR signalling activation is solely responsible for the upregulation of ATF4 protein.

Octyl-R-2-HG acidifies the growth medium. This observation is consistent with the octyl-conjugated ester associated pH alteration studied in Parker et al., 2021. We questioned whether this change in extracellular pH impacted DNA synthesis. We compared the EdU incorporation of cells treated with octyl-R-2-HG and cells in growth medium that was pH-adjusted to the same final pH as the metabolite mix using sulfuric acid. The DNA synthesis or the upregulation of ATF4 were not significantly affected in cells grown in a pH-altered medium, suggesting that extracellular pH changes caused by the metabolite do not cause defects in DNA replication (Figure 15). However, repeating the experiments with different organic acid such as glacial acetic acid can accentuate our observations.

To determine the specificity of the R-2-HG/ISR effect on DNA replication, cells were exposed to octyl-α-KG, a physiologically normal metabolite. It has been demonstrated in several studies that histone tail demethylation by KDMs contributes to DNA replication, RSR, DNA damage response, and telomere replication (Gaillard et al., 2021; Rondinelli et al., 2015; Udugama et al., 2021; Wu et al., 2017). Accordingly, we anticipated that octyl-α-KG treatment could promote DNA replication by increasing demethylation activity. In contrast, astrocytes were extremely sensitive to octyl-α-KG within one hour of treatment as observed by a decrease in DNA synthesis as well as

elevated ATF4 protein, both in a dose-dependent manner (Figure 16). With increasing octyl-α-KG concentrations, H2AX phosphorylation increased markedly, suggesting that cells sense replication stress. It will be necessary to investigate the levels of other replication stress response markers such as CHK1 and RPA phosphorylation to support this finding in the future. According to a recent study, octyl-conjugated esters may have off-target effects, which may explain the cellular stress response induced by both normal and oncometabolite octyl esters used in our study (Parker et al., 2021).

The specificity of the oncometabolite activity in NHA was further tested via a long-term octyl-R-2-HG treatment. We considered that R-2-HG would impair NHA proliferation in an ISR-dependent manner. In response to the presence of octyl-R-2-HG, NHA as well as U2OS showed slow growth for up to six days, and the addition of ISRIB significantly rescued the growth defect (Figure 17 and 18). It is important to note that ISRIB's ability to rescue growth was dependent on metabolite concentration. Taken together, our results indicate that octyl-R-2-HG can regulate ISR activation and may promote tumour growth by exploiting translational alterations. Furthermore, the extreme sensitivity of NHA towards the enantiomer octyl-S-2-HG emphasizes the specificity of R-2-HG in favouring cell proliferation.

Using lentiviral transduction, we created an inducible IDH wildtype and mutant gene overexpression system to eliminate potential artifacts associated with octyl-conjugated ester processing inside cells (Figure 19). We speculated that the accumulation of R-2-HG by IDH1/2-mutant overexpression would alter cell proliferation as well as EdU incorporation, and that blocking the ISR would partially restore these defects. Although both IDH1 R132H and IDH2 R172K mutations drive the accumulation of R-2-HG (Ye et al., 2013c), NHA cells overexpressing IDH1 R132H exhibited no growth defect in six days. This could stem, for example, from the low expression levels of Flag-tagged IDH1 R132H protein or from cytosolic R-2-HG accumulation and associated signaling that are too low to cause deleterious effects. We also examined the mitochondrial IDH2 R172K overexpressed cell lines, which grew slowly likely as a result of R-2-HG production (Figure 20). ISRIB treatment, in contrast to our previous findings, aggravated the slow growth of IDH2 R172K overexpressing cells. As a matter of fact, ISRIB alone impaired cell proliferation, suggesting that basal activation of the ISR may be crucial for cellular homeostasis and survival. Such possibility will, however, require further investigation. The EdU incorporation

experiments showed that wildtype IDH2 and IDH2 R172K induced overexpression positively and negatively modulate DNA synthesis, respectively. Consistent with previous observations, ISRIB rescued the EdU incorporation in IDH2 R172K overexpressed cells (Figure 21). However, the similar upregulation of ATF4 protein observed in the wildtype IDH2 and IDH2 R172K overexpression system could result from UPR activation or mitochondrial dysfunction. Hence, in order to identify the specificity of R-2-HG's effect in upregulating ATF4, exploring the exact mechanism of ATF4 upregulation, whether eIF2α-dependent or independent, will be insightful.

The experiments utilizing transduced cell lines were conducted only once, and involving cells cultured for a month. Given that a substantial portion of these cells could have reached the stationary/senescence phase, as per the Hayflick phenomenon, it is crucial to repeat these experiments using newly thawed cells to ensure accuracy and validity (Groten et al., 2018; Verma, 2013). We also did not quantify the α-KG as well as R-2-HG accumulated in IDH2 wildtype and R172K inducible cell lines and these quantifications could reinforce our findings. Exogenous treatment of metabolite may cause significant R-2-HG accumulation in the cytoplasm whereas the mitochondrial IDH2 R172K overexpression cause R-2-HG accumulation in the mitochondria (Parker et al., 2021). This mitochondrial R-2-HG accumulation location could potentially lead to ATF4 upregulation through a mechanism unrelated to ISR. As a result, the inhibition of ER-induced ISR did not lead to a reduction in ATF4 levels (Figure 21). Finally, it is necessary to repeat cell growth and EdU incorporation assay associated with transduced NHA cells to strengthen the conclusion of our innovative findings for research purposes.

Chapter 5 – Conclusion

This study explored how oncometabolite R-2-HG accumulation impacts DNA replication primarily in human astrocytes. Both octyl-R-2-HG and octyl-S-2-HG impaired DNA synthesis, slowing replication forks and S-phase progression. Cancer-relevant IDH2 R172K mutation, likely causing R-2-HG accumulation, similarly hindered DNA replication process. In contrast, normal metabolite octyl-α-KG reduced DNA synthesis but increased H2AX phosphorylation, highlighting that octyl-R-2-HG influences replication without triggering the replication stress response.

We aimed to correlate ISR activation with R-2-HG-associated DNA replication defect and observed partial rescue in DNA replication by blocking ISR signalling. This observation was consistent in both octyl-R-2-HG treatment and cells with induced IDH2 R172K overexpression. In fact, the ISR markers were also reduced upon adding ISRIB in octyl-R-2-HG treatment. However, this reduction of ISR markers by ISRIB was much less pronounced in IDH2 R172K overexpressed cells. Taken together, our data implies that R-2-HG prompts ISR-dependent as well as independent (or eIF2α phosphorylation-dependent/independent) pathways, influencing replication fork progression.

While IDH1/2 mutations as well as R-2-HG accumulation are oncogenic in nature, our study confirmed an R-2-HG-triggered anti-tumor response (Su et al., 2018b). Exogenous octyl-R-2-HG treatment and induced IDH2 R172K overexpression slowed NHA growth. Blocking ISR rescued NHA growth in the octyl-R-2-HG treatment. However, the effect of ISRIB on the growth of IDH2 R172K-overexpressing cells awaits further investigation.

Future Outlook

Precisely how R-2-HG impedes DNA synthesis in the context of global epigenetic reprogramming, presumably via its impact on histone demethylase activity, remains to be determined. Quantifying specific histone methylation markers (Table 4) with and without induced overexpression of the IDH2 R172K gene in NHA, followed by overexpression of KDM proteins could reveal the genetic networks influencing replication in IDH-mutant brain cancers. R-2-HG inhibits demethylase activity (e.g. KDM4D), which is implicated in the initiation and elongation of DNA replication (Wu et al., 2017), so it is possible that increased methylation markers are responsible for the slow

RF progression when the IDH2 R172K gene is overexpressed. Overexpression of KDM proteins could then rescue the R-2-HG-mediated fork progression defect.

An attempt was made to link ISR activation as a mechanism by which R-2-HG modulated DNA synthesis. A distinct observation of elevated ATF4 expression and partial rescue effect of ISRIB were the key findings linking R-2-HG with slow RF progression. This defect in RF progression may also be explained by quantifying the DNA: RNA hybrids likely to form due to ATF4 function as a transcription factor during S phase. There are two major questions arising from this novel discovery of the R-2-HG/ATF4/DNA replication axis.

1. **Molecular mechanism behind ATF4 upregulation**: ATF4 is upregulated in response to mitochondrial stress, ER stress and mTOR signalling sensors. This study did not identify the mechanism by which R-2-HG induces upregulation of the ATF4 protein other than through ISR. Thus, further studies such as the inhibition of mTORC signaling by Torin 1 as well as the knockdown of specific ISR kinases by siRNA may provide further evidence (Y. Park et al., 2017; Tabata et al., 2023).
2. **Histone pool depletion by ISR signalling**: A direct mechanism underlying a slowed replisome activity can be explained by R-2-HG induced ISR activation. During the S phase, replication-dependent histone proteins are actively expressed (Armstrong & Spencer, 2021; Gajdušková et al., 2020). Therefore, by blocking protein synthesis, ISR activation may deplete histone pools resulting in slow progression of the replication fork (Groth et al., 2007b). Therefore, immunostaining the free nuclear histones following octyl-R-2-HG treatment or overexpression of IDH2 R172K gene may prove insightful.

A crucial observation arises from the fact that the octyl moiety present in octyl-R-2-HG experiences cleavage facilitated by esterase activity (Parker et al., 2021). The accumulation of the amphiphilic compound octanol within the cytosol may interact with the lipid membranes of cellular organelles, leading to disruptive effects (Amézqueta et al., 2019; Bahmani et al., 2017). These disturbances in the membrane structure have been demonstrated to activate cellular stress responses, notably the unfolded protein response (UPR) (Jarc & Petan, 2019; Thibault et al., 2012). To gain a comprehensive understanding of the specificity inherent to the R-2-HG/ATF4 axis, it becomes imperative to conduct a meticulous and thorough characterization of these unintended impacts stemming from octyl-R-2-HG.

One possibility of the fate of slow-growing cells due R-2-HG accumulation is that they are undergoing cell reprogramming which is associated with compromised replication process and ATF4 protein elevation as observed in our study (Ruiz et al., 2015; X. Yang et al., 2018; Y. Zhao et al., 2015). This can be characterized in the future, by testing for increased levels of reprogramming markers such as OCT4, SOX2, KLF4 and MYC proteins (Buganim et al., 2012). R-2-HG production consumes a significant amount of NAPDH (described in the introduction) which is normally utilized in ROS detoxification (Dang et al., 2009; Gelman et al., 2018). Elevated ROS levels have been implicated as a hallmark of cancer (Arfin et al., 2021; Hanahan, 2022). Accordingly, slow-growing NHA cells may also result from excessive ROS which could eventually induce cell cycle arrest, senescence, or apoptosis, all of which remain to be clarified in the context of the accumulation of R-2-HG.

The present study indicates that oncometabolite accumulation is associated with impaired replication fork progression and leads to the upregulation of stress induced ATF4 transcription factor in normal as well as cancer cell lines. Blocking ISR along with other stress signalling pathways as a pre-treatment may restore the rate of DNA replication in R-2-HG producing cells. As a result, genotoxic chemotherapies as well as combination therapy with PARP inhibitor could more effectively damage the replicating DNA (Figure 22). Thus, the strategy of blocking ISR may be used in addition to the current therapies to increase the killing efficiency of IDH-mutant tumors originating from both brain and non-central nervous system.

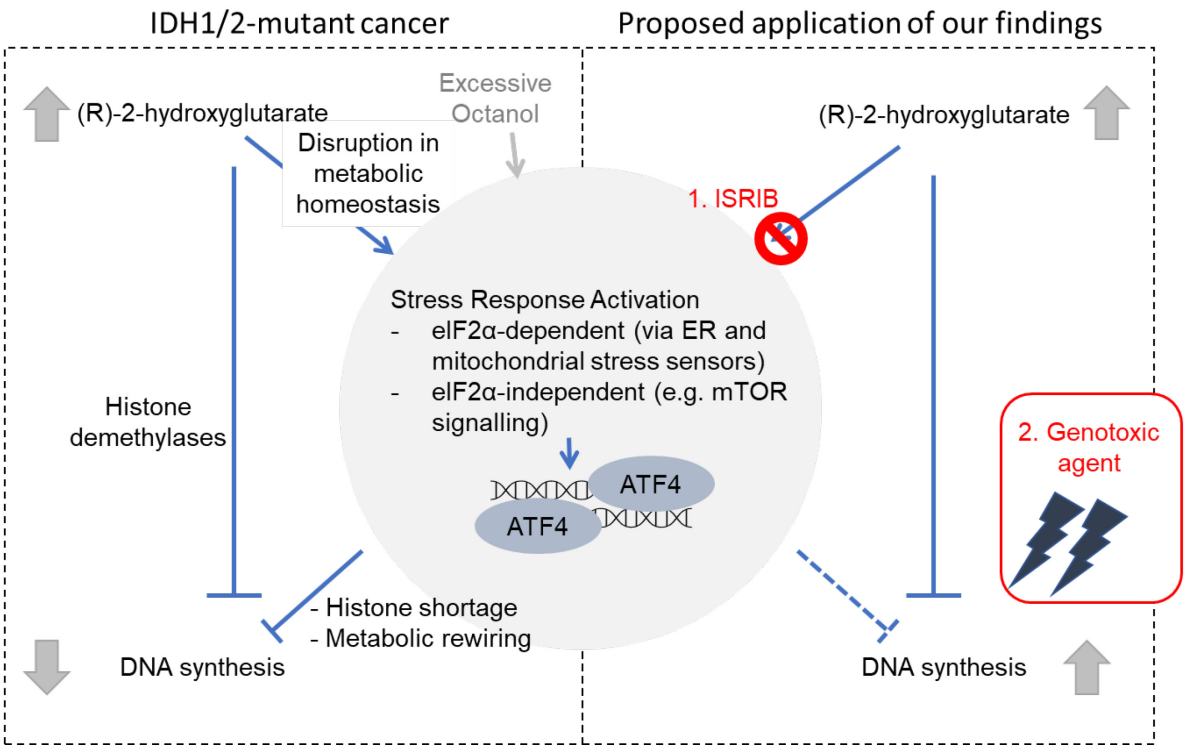

Figure 22 – Possible mechanism of R-2-HG modulating DNA replication.

In the left box, there are two ways of R-2-HG modulating DNA synthesis, either via the direct effect on histone demethylases inhibition or indirectly via activating cellular stress response. In case of octyl-R-2-HG treatment, 'octyl' processing by esterase reaction may result in octanol build-up, in turn activates cellular stress response (Parker et al., 2021). In the right box, ISRIB blocking activity alleviates DNA replication defect caused by R-2-HG. By exploiting ISRIB pre-treatment represented as step 1, enhanced genotoxic effects (step 2) can sensitize IDH-mutant cancers.

References

Aas, P. A., Otterlei, M., Falnes, P., Vågbø, C. B., Skorpen, F., Akbari, M., Sundheim, O., Bjørås, M., Slupphaug, G., Seeberg, E., & Krokan, H. E. (2003). Human and bacterial oxidative demethylases repair alkylation damage in both RNA and DNA. *Nature 2003 421:6925*, *421*(6925), 859–863. https://doi.org/10.1038/nature01363

Adelman, J. L., Chodera, J. D., Kuo, L. F. W., Miller, T. F., & Barsky, D. (2010). The mechanical properties of PCNA: Implications for the loading and function of a DNA sliding clamp. *Biophysical Journal*, *98*(12), 3062–3069. https://doi.org/10.1016/J.BPJ.2010.03.056

Aguilera, P., & López-Contreras, A. J. (2023). *ATRX, a guardian of chromatin*. https://doi.org/10.1016/j.tig.2023.02.009

Alberts, B., Johnson, A., Lewis, J., Raff, M., Roberts, K., & Walter, P. (2002). *DNA Replication Mechanisms*. https://www.ncbi.nlm.nih.gov/books/NBK26850/

Alonso-De Vega, I., Paz-Cabrera, M. C., Rother, M. B., Wiegant, W. W., Checa-Rodríguez, C., Hernández-Fernaud, J. R., Huertas, P., Freire, R., Van Attikum, H., & Smits, V. A. J. (2020). PHF2 regulates homology-directed DNA repair by controlling the resection of DNA double strand breaks. *Nucleic Acids Research*, *48*(9), 4915–4927. https://doi.org/10.1093/NAR/GKAA196

Amézqueta, S., Subirats, X., Fuguet, E., Roses, M., & Rafols, C. (2019). Octanol-water partition constant. *Liquid-Phase Extraction*, 183–208. https://doi.org/10.1016/B978-0-12-816911-7.00006-2

Aprelikova, O., Chandramouli, G. V. R., Wood, M., Vasselli, J. R., Riss, J., Maranchie, J. K., Linehan, W. M., & Barrett, J. C. (2004). Regulation of HIF prolyl hydroxylases by hypoxia-inducible factors. *Journal of Cellular Biochemistry*, *92*(3), 491–501. https://doi.org/10.1002/JCB.20067

Arfin, S., Jha, N. K., Jha, S. K., Kesari, K. K., Ruokolainen, J., Roychoudhury, S., Rathi, B., & Kumar, D. (2021). Oxidative Stress in Cancer Cell Metabolism. *Antioxidants 2021, Vol. 10, Page 642*, *10*(5), 642. https://doi.org/10.3390/ANTIOX10050642

Armstrong, C., & Spencer, S. L. (2021). Replication-dependent histone biosynthesis is coupled to cell-cycle commitment. *Proceedings of the National Academy of Sciences of the United States of America*, *118*(31), e2100178118. https://doi.org/10.1073/PNAS.2100178118/SUPPL_FILE/PNAS.2100178118.SAPP.PDF

Badur, M. G., Muthusamy, T., Parker, S. J., Magana, J. H., Guan, K.-L., & Metallo Correspondence, C. M. (2018). Oncogenic R132 IDH1 Mutations Limit NADPH for De Novo Lipogenesis through (D)2-Hydroxyglutarate Production in Fibrosarcoma Cells Graphical Abstract Highlights d D2HG production competes with reductive biosynthesis for NADPH in IDH1-mutant cells d 2 H tracing resolves L2HG and D2HG production pathways d IDH1 mutation slows cell growth when biosynthetic NADPH demands are increased. *Cell Reports*, *25*. https://doi.org/10.1016/j.celrep.2018.09.074

Bahmani, A., Saaidpour, S., & Rostami, A. (2017). A Simple, Robust and Efficient Computational Method for n-Octanol/Water Partition Coefficients of Substituted Aromatic Drugs. *Scientific Reports*, *7*(1). https://doi.org/10.1038/S41598-017-05964-Z

Baird, T. D., & Wek, R. C. (2012). Eukaryotic Initiation Factor 2 Phosphorylation and Translational Control in Metabolism. *Advances in Nutrition*, *3*(3), 307–321. https://doi.org/10.3945/AN.112.002113

Barrio, L., Dekanty, A., & Milán, M. (2014). MicroRNA-Mediated Regulation of Dp53 in the Drosophila Fat Body Contributes to Metabolic Adaptation to Nutrient Deprivation. *Cell Reports*, *8*(2), 528–541. https://doi.org/10.1016/J.CELREP.2014.06.020

Bartosovic, M., Molares, H. C., Gregorova, P., Hrossova, D., Kudla, G., & Vanacova, S. (2017). N6-methyladenosine demethylase FTO targets pre-mRNAs and regulates alternative splicing and 3′-end processing. *Nucleic Acids Research*, *45*(19), 11356–11370. https://doi.org/10.1093/NAR/GKX778

Beggs, R., & Yang, E. S. (2019). Targeting DNA repair in precision medicine. *Advances in Protein Chemistry and Structural Biology*, *115*, 135–155. https://doi.org/10.1016/BS.APCSB.2018.10.005

Bellelli, R., & Boulton, S. J. (2021). Spotlight on the Replisome: Aetiology of DNA Replication-Associated Genetic Diseases. *Trends in Genetics*, *37*(4), 317–336.

https://doi.org/10.1016/J.TIG.2020.09.008

Benlabiod, C., Dagher, T., Marty, C., & Villeval, J. L. (2022). Lessons from mouse models of MPN. *International Review of Cell and Molecular Biology*, *366*, 125–185. https://doi.org/10.1016/bs.ircmb.2021.02.009

Berger, R. S., Ellmann, L., Reinders, J., Kreutz, M., Stempfl, T., Oefner, P. J., & Dettmer, K. (2019). Degradation of D-2-hydroxyglutarate in the presence of isocitrate dehydrogenase mutations. *Scientific Reports 2019 9:1*, *9*(1), 1–11. https://doi.org/10.1038/s41598-019-43891-3

Bhat, K. P., Bétous, R., & Cortez, D. (2015). High-affinity DNA-binding Domains of Replication Protein A (RPA) Direct SMARCAL1-dependent Replication Fork Remodeling. *Journal of Biological Chemistry*, *290*(7), 4110–4117. https://doi.org/10.1074/JBC.M114.627083

Boila, L. D., Ghosh, S., Bandyopadhyay, S. K., Jin, L., Murison, A., Zeng, A. G. X., Shaikh, W., Bhowmik, S., Muddineni, S. S. N. A., Biswas, M., Sinha, S., Chatterjee, S. S., Mbong, N., Gan, O. I., Bose, A., Chakraborty, S., Arruda, A., Kennedy, J. A., Mitchell, A., … Sengupta, A. (2023). KDM6 demethylases integrate DNA repair gene regulation and loss of KDM6A sensitizes human acute myeloid leukemia to PARP and BCL2 inhibition. *Leukemia 2023 37:4*, *37*(4), 751–764. https://doi.org/10.1038/s41375-023-01833-z

Boiteux, S., & Laval, J. (1982). Mutagenesis by alkylating agents: coding properties for DNA polymerase of poly (dC) template containing 3-methylcytosine. *Biochimie*, *64*(8–9), 637–641. https://doi.org/10.1016/S0300-9084(82)80103-X

Brown, E. J., & Baltimore, D. (2003). Essential and dispensable roles of ATR in cell cycle arrest and genome maintenance. *Genes & Development*, *17*(5), 615. https://doi.org/10.1101/GAD.1067403

Bueno, M. T. D., Baldascini, M., Richard, S., & Lowndes, N. F. (2018). Recruitment of lysine demethylase 2A to DNA double strand breaks and its interaction with 53BP1 ensures genome stability. *Oncotarget*, *9*(22), 15915. https://doi.org/10.18632/ONCOTARGET.24636

Buganim, Y., Faddah, D. A., Cheng, A. W., Itskovich, E., Markoulaki, S., Ganz, K., Klemm, S. L., Van Oudenaarden, A., & Jaenisch, R. (2012). Single-Cell Expression Analyses during

Cellular Reprogramming Reveal an Early Stochastic and a Late Hierarchic Phase. *Cell*, *150*(6), 1209–1222. https://doi.org/10.1016/J.CELL.2012.08.023

Byun, T. S., Pacek, M., Yee, M. C., Walter, J. C., & Cimprich, K. A. (2005). Functional uncoupling of MCM helicase and DNA polymerase activities activates the ATR-dependent checkpoint. *Genes & Development*, *19*(9), 1040–1052. https://doi.org/10.1101/GAD.1301205

Cabrera, E., Hernández-Pérez, S., Koundrioukoff, S., Debatisse, M., Kim, D., Smolka, M. B., Freire, R., & Gillespie, D. A. (2016). PERK inhibits DNA replication during the Unfolded Protein Response via Claspin and Chk1. *Oncogene 2017 36:5*, *36*(5), 678–686. https://doi.org/10.1038/onc.2016.239

Cabrera, E., Hernández-Pérez, S., Koundrioukoff, S., Debatisse, M., Kim, D., Smolka, M. B., Freire, R., & Gillespie, D. A. (2017). PERK inhibits DNA replication during the Unfolded Protein Response via Claspin and Chk1. *Oncogene*, *36*(5), 678–686. https://doi.org/10.1038/ONC.2016.239

Carbonneau, M., Gagne, L. M., Lalonde, M. E., Germain, M. A., Motorina, A., Guiot, M. C., Secco, B., Vincent, E. E., Tumber, A., Hulea, L., Bergeman, J., Oppermann, U., Jones, R. G., Laplante, M., Topisirovic, I., Petrecca, K., Huot, M. É., & Mallette, F. A. (2016). The oncometabolite 2-hydroxyglutarate activates the mTOR signalling pathway. *Nature Communications*, *7*. https://doi.org/10.1038/ncomms12700

Castelli, S., De Falco, P., Ciccarone, F., Desideri, E., & Ciriolo, M. R. (2021). Lipid Catabolism and ROS in Cancer: A Bidirectional Liaison. *Cancers*, *13*(21). https://doi.org/10.3390/CANCERS13215484

Castellini, L., Moon, E. J., Razorenova, O. V., Krieg, A. J., Von Eyben, R., & Giaccia, A. J. (2017). KDM4B/JMJD2B is a p53 target gene that modulates the amplitude of p53 response after DNA damage. *Nucleic Acids Research*, *45*(7), 3674. https://doi.org/10.1093/NAR/GKW1281

Çelik, H., Bulut, G., Han, J., Graham, G. T., Minas, T. Z., Conn, E. J., Hong, S. H., Pauly, G. T., Hayran, M., Li, X., Özdemirli, M., Ayhan, A., Rudek, M. A., Toretsky, J. A., & Üren, A. (2016). Ezrin inhibition up-regulates stress response gene expression. *Journal of Biological Chemistry*, *291*(25), 13257–13270. https://doi.org/10.1074/jbc.M116.718189

Chen, F., Bian, K., Tang, Q., Fedeles, B. I., Singh, V., Humulock, Z. T., Essigmann, J. M., & Li, D. (2017). Oncometabolites d- and l-2-Hydroxyglutarate Inhibit the AlkB Family DNA Repair Enzymes under Physiological Conditions. *Chemical Research in Toxicology*, *30*(4), 1102–1110. https://doi.org/10.1021/ACS.CHEMRESTOX.7B00009

Chong, J. P. J., Hayashi, M. K., Simon, M. N., Xu, R. M., & Stillman, B. (2000). A double-hexamer archaeal minichromosome maintenance protein is an ATP-dependent DNA helicase. *Proceedings of the National Academy of Sciences of the United States of America*, *97*(4), 1530–1535. https://doi.org/10.1073/PNAS.030539597/ASSET/09256C51-967A-4CF3-9E2D-74004D0F7D4A/ASSETS/GRAPHIC/PQ0305395006.JPEG

Choo, J. A. M. Y., Schlösser, D., Manzini, V., Magerhans, A., & Dobbelstein, M. (2020a). The integrated stress response induces R-loops and hinders replication fork progression. *Cell Death & Disease 2020 11:7*, *11*(7), 1–16. https://doi.org/10.1038/s41419-020-2727-2

Choo, J. A. M. Y., Schlösser, D., Manzini, V., Magerhans, A., & Dobbelstein, M. (2020b). The integrated stress response induces R-loops and hinders replication fork progression. *Cell Death & Disease 2020 11:7*, *11*(7), 1–16. https://doi.org/10.1038/s41419-020-2727-2

Chowdhury, R., Yeoh, K. K., Tian, Y. M., Hillringhaus, L., Bagg, E. A., Rose, N. R., Leung, I. K. H., Li, X. S., Woon, E. C. Y., Yang, M., McDonough, M. A., King, O. N., Clifton, I. J., Klose, R. J., Claridge, T. D. W., Ratcliffe, P. J., Schofield, C. J., & Kawamura, A. (2011). The oncometabolite 2-hydroxyglutarate inhibits histone lysine demethylases. *EMBO Reports*, *12*(5), 463–469. https://doi.org/10.1038/EMBOR.2011.43

Clynes, D., Jelinska, C., Xella, B., Ayyub, H., Taylor, S., Mitson, M., Bachrati, C. Z., Higgs, D. R., & Gibbons, R. J. (2014). ATRX Dysfunction Induces Replication Defects in Primary Mouse Cells. *PLOS ONE*, *9*(3), e92915. https://doi.org/10.1371/JOURNAL.PONE.0092915

Cooper, G. M. (2000). *DNA Replication*. https://www.ncbi.nlm.nih.gov/books/NBK9940/

Costa-Mattioli, M., & Walter, P. (2020). The integrated stress response: From mechanism to disease. *Science (New York, N.Y.)*, *368*(6489). https://doi.org/10.1126/SCIENCE.AAT5314

Dang, L., White, D. W., Gross, S., Bennett, B. D., Bittinger, M. A., Driggers, E. M., Fantin, V. R., Jang, H. G., Jin, S., Keenan, M. C., Marks, K. M., Prins, R. M., Ward, P. S., Yen, K. E., Liau,

L. M., Rabinowitz, J. D., Cantley, L. C., Thompson, C. B., Vander Heiden, M. G., & Su, S. M. (2009). Cancer-associated IDH1 mutations produce 2-hydroxyglutarate. *Nature*, *462*(7274), 739–744. https://doi.org/10.1038/NATURE08617

de Jong, Y., & Bovée, J. V. M. G. (2018). Molecular drivers in chondrosarcoma. *Chordomas and Chondrosarcomas of the Skull Base and Spine*, 31–41. https://doi.org/10.1016/B978-0-12-804257-1.00004-9

Duncan, T., Trewick, S. C., Koivisto, P., Bates, P. A., Lindahl, T., & Sedgwick, B. (2002). Reversal of DNA alkylation damage by two human dioxygenases. *Proceedings of the National Academy of Sciences of the United States of America*, *99*(26), 16660–16665. https://doi.org/10.1073/PNAS.262589799/ASSET/D2DDBD87-3A17-4418-9448-70F89BD6DEAA/ASSETS/GRAPHIC/PQ0135897005.JPEG

Fan, L., Xu, S., Zhang, F., Cui, X., Fazli, L., Gleave, M., Clark, D. J., Yang, A., Hussain, A., Rassool, F., & Qi, J. (2020). Histone demethylase JMJD1A promotes expression of DNA repair factors and radio-resistance of prostate cancer cells. *Cell Death & Disease*, *11*(4). https://doi.org/10.1038/S41419-020-2405-4

Faubert, B., Solmonson, A., & DeBerardinis, R. J. (2020). Metabolic reprogramming and cancer progression. *Science (New York, N.Y.)*, *368*(6487). https://doi.org/10.1126/SCIENCE.AAW5473

Ferguson, L. R., Chen, H., Collins, A. R., Connell, M., Damia, G., Dasgupta, S., Malhotra, M., Meeker, A. K., Amedei, A., Amin, A., Ashraf, S. S., Aquilano, K., Azmi, A. S., Bhakta, D., Bilsland, A., Boosani, C. S., Chen, S., Ciriolo, M. R., Fujii, H., … Maxwell, C. A. (2015). Genomic instability in human cancer: Molecular insights and opportunities for therapeutic attack and prevention through diet and nutrition. *Seminars in Cancer Biology*, *35*, S5–S24. https://doi.org/10.1016/J.SEMCANCER.2015.03.005

Ferreira, M. S. V., Sørensen, M. D., Pusch, S., Beier, D., Bouillon, A. S., Kristensen, B. W., Brümmendorf, T. H., Beier, C. P., & Beier, F. (2020). Alternative lengthening of telomeres is the major telomere maintenance mechanism in astrocytoma with isocitrate dehydrogenase 1 mutation. *Journal of Neuro-Oncology*, *147*(1), 1. https://doi.org/10.1007/S11060-020-03394-Y

Figueroa, M. E., Abdel-Wahab, O., Lu, C., Ward, P. S., Patel, J., Shih, A., Li, Y., Bhagwat, N., Vasanthakumar, A., Fernandez, H. F., Tallman, M. S., Sun, Z., Wolniak, K., Peeters, J. K., Liu, W., Choe, S. E., Fantin, V. R., Paietta, E., Löwenberg, B., … Melnick, A. (2010). Leukemic IDH1 and IDH2 Mutations Result in a Hypermethylation Phenotype, Disrupt TET2 Function, and Impair Hematopoietic Differentiation. *Cancer Cell*, *18*(6), 553–567. https://doi.org/10.1016/J.CCR.2010.11.015

Fletcher, S. C., Hall, C. L., Kennedy, T. J., Pajusalu, S., Wojcik, M. H., Boora, U., Li, C., Oja, K. T., Hendrix, E., Westrip, C. A. E., Andrijes, R., Piasecka, S. K., Singh, M., El-Asrag, M. E., Ptasinska, A., Tillmann, V., Higgs, M. R., Carere, D. A., Beggs, A. D., … Coleman, M. L. (2023). Impaired protein hydroxylase activity causes replication stress and developmental abnormalities in humans. *The Journal of Clinical Investigation*, *133*(7). https://doi.org/10.1172/JCI152784

Fragkos, M., Ganier, O., Coulombe, P., & Méchali, M. (2015). DNA replication origin activation in space and time. *Nature Reviews Molecular Cell Biology 2015 16:6*, *16*(6), 360–374. https://doi.org/10.1038/nrm4002

Frank, C. L., Ge, X., Xie, Z., Zhou, Y., & Tsai, L. H. (2010). Control of activating transcription factor 4 (ATF4) persistence by multisite phosphorylation impacts cell cycle progression and neurogenesis. *Journal of Biological Chemistry*, *285*(43), 33324–33337. https://doi.org/10.1074/jbc.M110.140699

Fugger, K., Mistrik, M., Danielsen, J. R., Dinant, C., Falck, J., Bartek, J., Lukas, J., & Mailand, N. (2009). Human Fbh1 helicase contributes to genome maintenance via pro- and anti-recombinase activities. *Journal of Cell Biology*, *186*(5), 655–663. https://doi.org/10.1083/JCB.200812138

Gaillard, S., Charasson, V., Ribeyre, C., Salifou, K., Pillaire, M. J., Hoffmann, J. S., Constantinou, A., Trouche, D., & Vandromme, M. (2021). Kdm5a and kdm5b histone-demethylases contribute to hu-induced replication stress response and tolerance. *Biology Open*, *10*(5). https://doi.org/10.1242/BIO.057729/268370

Gajdušková, P., Ruiz de los Mozos, I., Rájecký, M., Hluchý, M., Ule, J., & Blazek, D. (2020). CDK11 is required for transcription of replication-dependent histone genes. *Nature Structural*

& Molecular Biology 2020 27:5, *27*(5), 500–510. https://doi.org/10.1038/s41594-020-0406-8

Gelman, S. J., Naser, F., Mahieu, N. G., McKenzie, L. D., Dunn, G. P., Chheda, M. G., & Patti, G. J. (2018). Consumption of NADPH for 2-HG Synthesis Increases Pentose Phosphate Pathway Flux and Sensitizes Cells to Oxidative Stress. *Cell Reports*, *22*(2), 512. https://doi.org/10.1016/J.CELREP.2017.12.050

Gerace, E. L., & Moazed, D. (2010). Histone Demethylation and Timely DNA Replication. In *Molecular Cell* (Vol. 40, Issue 5, pp. 683–684). https://doi.org/10.1016/j.molcel.2010.11.036

Ghaddar, N., Wang, S., Woodvine, B., Krishnamoorthy, J., van Hoef, V., Darini, C., Kazimierczak, U., Ah-son, N., Popper, H., Johnson, M., Officer, L., Teodósio, A., Broggini, M., Mann, K. K., Hatzoglou, M., Topisirovic, I., Larsson, O., Le Quesne, J., & Koromilas, A. E. (2021). The integrated stress response is tumorigenic and constitutes a therapeutic liability in KRAS-driven lung cancer. *Nature Communications 2021 12:1*, *12*(1), 1–15. https://doi.org/10.1038/s41467-021-24661-0

Gilbert, D. M. (2002). Replication timing and transcriptional control: Beyond cause and effect. *Current Opinion in Cell Biology*, *14*(3), 377–383. https://doi.org/10.1016/S0955-0674(02)00326-5

Gilljam, K. M., Feyzi, E., Aas, P. A., Sousa, M. M. L., Müller, R., Vågbø, C. B., Catterall, T. C., Liabakk, N. B., Slupphaug, G., Drabløs, F., Krokan, H. E., & Otterlei, M. (2009). Identification of a novel, widespread, and functionally important PCNA-binding motif. *The Journal of Cell Biology*, *186*(5), 645–654. https://doi.org/10.1083/JCB.200903138

Gómez-Escoda, B., & Jenny Wu, P. Y. (2017). Roles of CDK and DDK in Genome Duplication and Maintenance: Meiotic Singularities. *Genes*, *8*(3). https://doi.org/10.3390/GENES8030105

Gouirand, V., Guillaumond, F., & Vasseur, S. (2018). Influence of the tumor microenvironment on cancer cells metabolic reprogramming. *Frontiers in Oncology*, *8*(APR), 363474. https://doi.org/10.3389/FONC.2018.00117/BIBTEX

Gralewska, P., Gajek, A., Marczak, A., & Rogalska, A. (2020). Participation of the ATR/CHK1

pathway in replicative stress targeted therapy of high-grade ovarian cancer. *Journal of Hematology & Oncology 2020 13:1*, *13*(1), 1–16. https://doi.org/10.1186/S13045-020-00874-6

Gross, S., Cairns, R. A., Minden, M. D., Driggers, E. M., Bittinger, M. A., Jang, H. G., Sasaki, M., Jin, S., Schenkein, D. P., Su, S. M., Dang, L., Fantin, V. R., & Mak, T. W. (2010). Cancer-associated metabolite 2-hydroxyglutarate accumulates in acute myelogenous leukemia with isocitrate dehydrogenase 1 and 2 mutations. *The Journal of Experimental Medicine*, *207*(2), 339–344. https://doi.org/10.1084/JEM.20092506

Groten, J., Venkatraman, A., & Mertelsmann, R. (2018). Modeling and Simulating Carcinogenesis. *Precision Medicine: Tools and Quantitative Approaches*, 277–295. https://doi.org/10.1016/B978-0-12-805364-5.00012-3

Groth, A., Corpet, A., Cook, A. J. L., Roche, D., Bartek, J., Lukas, J., & Almouzni, G. (2007a). Regulation of replication fork progression through histone supply and demand. *Science*, *318*(5858), 1928–1931. https://doi.org/10.1126/SCIENCE.1148992

Groth, A., Corpet, A., Cook, A. J. L., Roche, D., Bartek, J., Lukas, J., & Almouzni, G. (2007b). Regulation of replication fork progression through histone supply and demand. *Science (New York, N.Y.)*, *318*(5858), 1928–1931. https://doi.org/10.1126/SCIENCE.1148992

Gruber, E., So, J., Lewis, A. C., Shortt, J., Johnstone, R. W., Kats Correspondence, L. M., Franich, R., Cole, R., Martelotto, L. G., Rogers, A. J., Vidacs, E., Fraser, P., Stanley, K., Jones, L., Trigos, A., Thio, N., Li, J., Nicolay, B., Daigle, S., … Kats, L. M. (2022). Inhibition of mutant IDH1 promotes cycling of acute myeloid leukemia stem cells. *CellReports*, *40*, 111182. https://doi.org/10.1016/j.celrep.2022.111182

Han, J., Back, S. H., Hur, J., Lin, Y. H., Gildersleeve, R., Shan, J., Yuan, C. L., Krokowski, D., Wang, S., Hatzoglou, M., Kilberg, M. S., Sartor, M. A., & Kaufman, R. J. (2013). ER-stress-induced transcriptional regulation increases protein synthesis leading to cell death. *Nature Cell Biology*, *15*(5), 481. https://doi.org/10.1038/NCB2738

Han, S., Liu, Y., Cai, S. J., Qian, M., Ding, J., Larion, M., Gilbert, M. R., & Yang, C. (2020). IDH mutation in glioma: molecular mechanisms and potential therapeutic targets. *British Journal of Cancer 2020 122:11*, *122*(11), 1580–1589. https://doi.org/10.1038/s41416-020-0814-x

Hanahan, D. (2022). Hallmarks of Cancer: New Dimensions. In *Cancer Discovery* (Vol. 12, Issue 1). https://doi.org/10.1158/2159-8290.CD-21-1059

Hanahan, D., & Weinberg, R. A. (2000). The Hallmarks of Cancer. *Cell*, *100*(1), 57–70. https://doi.org/10.1016/S0092-8674(00)81683-9

Hanahan, D., & Weinberg, R. A. (2011). Hallmarks of cancer: The next generation. In *Cell* (Vol. 144, Issue 5). https://doi.org/10.1016/j.cell.2011.02.013

Harding, H. P., Zhang, Y., Zeng, H., Novoa, I., Lu, P. D., Calfon, M., Sadri, N., Yun, C., Popko, B., Paules, R., Stojdl, D. F., Bell, J. C., Hettmann, T., Leiden, J. M., & Ron, D. (2003). An Integrated Stress Response Regulates Amino Acid Metabolism and Resistance to Oxidative Stress. *Molecular Cell*, *11*(3), 619–633. https://doi.org/10.1016/S1097-2765(03)00105-9

Hartmann, C., Meyer, J., Balss, J., Capper, D., Mueller, W., Christians, A., Felsberg, J., Wolter, M., Mawrin, C., Wick, W., Weller, M., Herold-Mende, C., Unterberg, A., Jeuken, J. W. M., Wesseling, P., Reifenberger, G., & von Deimling, A. (2009). Type and frequency of IDH1 and IDH2 mutations are related to astrocytic and oligodendroglial differentiation and age: A study of 1,010 diffuse gliomas. *Acta Neuropathologica*, *118*(4), 469–474. https://doi.org/10.1007/S00401-009-0561-9/TABLES/3

Heller, R. C., Kang, S., Lam, W. M., Chen, S., Chan, C. S., & Bell, S. P. (2011). Eukaryotic origin-dependent DNA replication in vitro reveals sequential action of DDK and S-CDK kinases. *Cell*, *146*(1), 80–91. https://doi.org/10.1016/j.cell.2011.06.012

Hiramatsu, N., Messah, C., Han, J., LaVail, M. M., Kaufman, R. J., & Lin, J. H. (2014). A Highlights from MBoC Selection: Translational and posttranslational regulation of XIAP by eIF2α and ATF4 promotes ER stress–induced cell death during the unfolded protein response. *Molecular Biology of the Cell*, *25*(9), 1411. https://doi.org/10.1091/MBC.E13-11-0664

Hu, X., Li, L., Eid, J. E., Liu, C., Yu, J., Yue, J., & Trent, J. C. (2022). IDH1 Mutation Induces HIF-1 α and Confers Angiogenic Properties in Chondrosarcoma JJ012 Cells. *Disease Markers*, *2022*. https://doi.org/10.1155/2022/7729968

Huang, B., Wang, B., Yuk-Wai Lee, W., Chang Chan, H., Li, G., & Jiang, X. (2019). KDM3A and KDM4C Regulate Mesenchymal Stromal Cell Senescence and Bone Aging via Condensin-

mediated Heterochromatin Reorganization. *ISCIENCE*, *21*, 375–390. https://doi.org/10.1016/j.isci.2019.10.041

Hustedt, N., Gasser, S. M., & Shimada, K. (2013). Replication Checkpoint: Tuning and Coordination of Replication Forks in S Phase. *Genes*, *4*(3), 388. https://doi.org/10.3390/GENES4030388

Inoue, S., Li, W. Y., Tseng, A., Beerman, I., Elia, A. J., Bendall, S. C., Lemonnier, F., Kron, K. J., Cescon, D. W., Hao, Z., Lind, E. F., Takayama, N., Planello, A. C., Shen, S. Y., Shih, A. H., Larsen, D. M., Li, Q., Snow, B. E., Wakeham, A., … Mak, T. W. (2016). Mutant IDH1 Downregulates ATM and Alters DNA Repair and Sensitivity to DNA Damage Independent of TET2. *Cancer Cell*, *30*(2), 337–348. https://doi.org/10.1016/j.ccell.2016.05.018

Intlekofer, A. M., Wang, B., Liu, H., Shah, H., Carmona-Fontaine, C., Rustenburg, A. S., Salah, S., Gunner, M. R., Chodera, J. D., Cross, J. R., & Thompson, C. B. (2017). L-2-hydroxyglutarate production arises from non-canonical enzyme function at acidic pH. *Nature Chemical Biology*, *13*(5), 494. https://doi.org/10.1038/NCHEMBIO.2307

Janke, R., Iavarone, A. T., & Rine, J. (2017). Oncometabolite d-2-hydroxyglutarate enhances gene silencing through inhibition of specific h3k36 histone demethylases. *ELife*, *6*. https://doi.org/10.7554/ELIFE.22451

Jarc, E., & Petan, T. (2019). Focus: Organelles: Lipid Droplets and the Management of Cellular Stress. *The Yale Journal of Biology and Medicine*, *92*(3), 435. /pmc/articles/PMC6747940/

Ježek, P. (2020). 2-hydroxyglutarate in cancer cells. *Antioxidants and Redox Signaling*, *33*(13), 903–926. https://doi.org/10.1089/ARS.2019.7902/ASSET/IMAGES/LARGE/ARS.2019.7902_FIGURE7.JPEG

Jia, G., Fu, Y., Zhao, X., Dai, Q., Zheng, G., Yang, Y., Yi, C., Lindahl, T., Pan, T., Yang, Y. G., & He, C. (2011). N6-Methyladenosine in Nuclear RNA is a Major Substrate of the Obesity-Associated FTO. *Nature Chemical Biology*, *7*(12), 885. https://doi.org/10.1038/NCHEMBIO.687

Jin, G., Pirozzi, C. J., Chen, L. H., Duncan, C. G., Lopez, G. Y., Feng, J., Spasojevic, I., Bigner,

D. D., He, Y., Yan, H., Jin, G., Pirozzi, C. J., Chen, L. H., Duncan, C. G., Lopez, G. Y., Feng, J., Spasojevic, I., Bigner, D. D., He, Y., & Yan, H. (2012). Mutant IDH1 is required for IDH1 mutated tumor cell growth. *Oncotarget*, *3*(8), 774–782. https://doi.org/10.18632/ONCOTARGET.577

Jin, Y., Elalaf, H., Watanabe, M., Tamaki, S., Hineno, S., Matsunaga, K., Woltjen, K., Kobayashi, Y., Nagata, S., Ikeya, M., Kato, T., Okamoto, T., Matsuda, S., & Toguchida, J. (2015). Mutant IDH1 Dysregulates the Differentiation of Mesenchymal Stem Cells in Association with Gene-Specific Histone Modifications to Cartilage- and Bone-Related Genes. *PLOS ONE*, *10*(7), e0131998. https://doi.org/10.1371/JOURNAL.PONE.0131998

Joberty, G., Boesche, M., Brown, J. A., Eberhard, D., Garton, N. S., Humphreys, P. G., Mathieson, T., Muelbaier, M., Ramsden, N. G., Reader, V., Rueger, A., Sheppard, R. J., Westaway, S. M., Bantscheff, M., Lee, K., Wilson, D. M., Prinjha, R. K., & Drewes, G. (2016). Interrogating the Druggability of the 2-Oxoglutarate-Dependent Dioxygenase Target Class by Chemical Proteomics. *ACS Chemical Biology*, *11*(7), 2002–2010. https://doi.org/10.1021/ACSCHEMBIO.6B00080/SUPPL_FILE/CB6B00080_SI_004.PDF

Kang, J. Y., Park, J. W., Hahm, J. Y., Jung, H., & Seo, S. B. (2020). Histone H3K79 demethylation by KDM2B facilitates proper DNA replication through PCNA dissociation from chromatin. *Cell Proliferation*, *53*(11). https://doi.org/10.1111/cpr.12920

Kapur, I., Boulier, E. L., & Francis, N. J. (2022). Regulation of Polyhomeotic Condensates by Intrinsically Disordered Sequences That Affect Chromatin Binding. *Epigenomes*, *6*(4). https://doi.org/10.3390/epigenomes6040040

Kayabolen, A., Sahin, G. N., Seker-Polat, F., Cingoz, A., Isik, B., Acar, S., Wakimoto, H., Cahill, D. P., Solaroglu, I., Cribbs, A., Oppermann, U., & Bagci-Onder, T. (2020). Combined inhibition of KDM6A/B and HDACs exacerbates integrated stress response and mediates therapeutic effects in IDH1-mutant glioma. *BioRxiv*, 2020.11.26.400234. https://doi.org/10.1101/2020.11.26.400234

Kickingereder, P., Sahm, F., Radbruch, A., Wick, W., Heiland, S., Von Deimling, A., Bendszus, M., & Wiestler, B. (2015). IDH mutation status is associated with a distinct hypoxia/angiogenesis transcriptome signature which is non-invasively predictable with rCBV

imaging in human glioma. *Scientific Reports 2015 5:1*, *5*(1), 1–9. https://doi.org/10.1038/srep16238

Kim, C., Jin, J., Ye, Z., Jadhav, R. R., Gustafson, C. E., Hu, B., Cao, W., Tian, L., Weyand, C. M., & Goronzy, J. J. (2021). Histone deficiency and accelerated replication stress in T cell aging. *The Journal of Clinical Investigation*, *131*(11). https://doi.org/10.1172/JCI143632

Klein, H. L. (2020). Stressed DNA replication generates stressed DNA. *Proceedings of the National Academy of Sciences of the United States of America*, *117*(19), 10108. https://doi.org/10.1073/PNAS.2005160117

Klusmann, I., Rodewald, S., Müller, L., Friedrich, M., Wienken, M., Li, Y., Schulz-Heddergott, R., & Dobbelstein, M. (2016). p53 Activity Results in DNA Replication Fork Processivity. *Cell Reports*, *17*(7), 1845–1857. https://doi.org/10.1016/J.CELREP.2016.10.036

Kohlschütter, A., Behbehani, A., Langenbeck, U., Albani, M., Heidemann, P., Hoffmann, G., Kleineke, J., Lehnert, W., & Wendel, U. (1982). A familial progressive neurodegenerative disease with 2-oxoglutaric aciduria. *European Journal of Pediatrics*, *138*(1), 32–37. https://doi.org/10.1007/BF00442325

Kranendijk, M., Struys, E. A., Salomons, G. S., Van Der Knaap, M. S., & Jakobs, C. (2012). Progress in understanding 2-hydroxyglutaric acidurias. *Journal of Inherited Metabolic Disease*, *35*(4), 571–587. https://doi.org/10.1007/S10545-012-9462-5

Lauber, S. (2013). *SDS PAGE Protein Electrophoresis*. OpenWetWare. https://openwetware.org/wiki/Sean_Lauber:SDS_PAGE_Protein_Electrophoresis

Lemay, J. F., St-Hilaire, E., Ronato, D. A., Gao, Y., Bélanger, F., Gezzar-Dandashi, S., Kimenyi Ishimwe, A. B., Sawchyn, C., Lévesque, D., McQuaid, M., Boisvert, F. M., Mallette, F. A., Masson, J. Y., Drobetsky, E. A., & Wurtele, H. (2022). A genome-wide screen identifies SCAI as a modulator of the UV-induced replicative stress response. *PLOS Biology*, *20*(10), e3001543. https://doi.org/10.1371/JOURNAL.PBIO.3001543

Leonardi, R., Subramanian, C., Jackowski, S., & Rock, C. O. (2012). Cancer-associated isocitrate dehydrogenase mutations inactivate NADPH-dependent reductive carboxylation. *Journal of Biological Chemistry*, *287*(18), 14615–14620. https://doi.org/10.1074/jbc.C112.353946

Li, F., He, X., Ye, D., Lin, Y., Yu, H., Yao, C., Huang, L., Zhang, J., Wang, F., Xu, S., Wu, X., Liu, L., Yang, C., Shi, J., He, X., Liu, J., Qu, Y., Guo, F., Zhao, J., … Zhao, S. (2015). NADP+-IDH Mutations Promote Hypersuccinylation that Impairs Mitochondria Respiration and Induces Apoptosis Resistance. *Molecular Cell*, *60*(4), 661–675. https://doi.org/10.1016/J.MOLCEL.2015.10.017

Li, H., Zhou, J., Sun, H., Qiu, Z., Gao, X., & Xu, Y. (2020). CaMeRe: A Novel Tool for Inference of Cancer Metabolic Reprogramming. *Frontiers in Oncology*, *10*, 518675. https://doi.org/10.3389/FONC.2020.00207/BIBTEX

Li, K., Ouyang, L., He, M., Luo, M., Cai, W., Tu, Y., Pi, R., Liu, A., Li, K., Ouyang, L., He, M., Luo, M., Cai, W., Tu, Y., Pi, R., & Liu, A. (2017). IDH1 R132H mutation regulates glioma chemosensitivity through Nrf2 pathway. *Oncotarget*, *8*(17), 28865–28879. https://doi.org/10.18632/ONCOTARGET.15868

Li, N., Gao, N., & Zhai, Y. (2023). DDK promotes DNA replication initiation: Mechanistic and structural insights. *Current Opinion in Structural Biology*, *78*, 102504. https://doi.org/10.1016/J.SBI.2022.102504

Li, S., Sun, C., Gu, Y., Gao, X., Zhao, Y., Yuan, Y., Zhang, F., Hu, P., Liang, W., Cao, K., Zhang, J., Wang, Z., & Ye, J. (2019). Mutation of IDH1 aggravates the fatty acid-induced oxidative stress in HCT116 cells by affecting the mitochondrial respiratory chain. *Molecular Medicine Reports*, *19*(4), 2509–2518. https://doi.org/10.3892/MMR.2019.9903/HTML

Li, Y., Chen, X., & Lu, C. (2021). The interplay between DNA and histone methylation: molecular mechanisms and disease implications. *EMBO Reports*, *22*(5), e51803. https://doi.org/10.15252/EMBR.202051803

Liberti, M. V., & Locasale, J. W. (2016). The Warburg Effect: How Does it Benefit Cancer Cells? *Trends in Biochemical Sciences*, *41*(3), 211. https://doi.org/10.1016/J.TIBS.2015.12.001

Lin, C.-Y. G., Näger, A. C., Lunardi, T., Vančevska, A., Lossaint, G., & Lingner, J. (2021). The human telomeric proteome during telomere replication. *Nucleic Acids Research*, *1*. https://doi.org/10.1093/NAR/GKAB1015

Liu, C. L., He, Y. Y., Li, X., Li, R. J., He, K. L., & Wang, L. L. (2014). Inhibition of

serine/threonine protein phosphatase PP1 protects cardiomyocytes from tunicamycin-induced apoptosis and I/R through the upregulation of p-eIF2α. *International Journal of Molecular Medicine*, *33*(3), 499–506. https://doi.org/10.3892/IJMM.2013.1603

Liu, L., Hu, K., Feng, J., Wang, H., Fu, S., Wang, B., Wang, L., Xu, Y., Yu, X., & Huang, H. (2021). The oncometabolite R-2-hydroxyglutarate dysregulates the differentiation of human mesenchymal stromal cells via inducing DNA hypermethylation. *BMC Cancer*, *21*(1), 1–12. https://doi.org/10.1186/S12885-020-07744-X/FIGURES/6

Liu, Y., Lang, F., Chou, F. J., Zaghloul, K. A., & Yang, C. (2020). Isocitrate Dehydrogenase Mutations in Glioma: Genetics, Biochemistry, and Clinical Indications. *Biomedicines*, *8*(9). https://doi.org/10.3390/BIOMEDICINES8090294

Liu, Y., Lu, Y., Celiku, O., Li, A., Wu, Q., Zhou, Y., & Yang, C. (2019). Targeting IDH1-mutated malignancies with NRF2 blockade. *Journal of the National Cancer Institute*, *111*(10), 1033–1041. https://doi.org/10.1093/jnci/djy230

Losman, J. A., Looper, R. E., Koivunen, P., Lee, S., Schneider, R. K., McMahon, C., Cowley, G. S., Root, D. E., Ebert, B. L., & Kaelin, W. G. (2013). (R)-2-hydroxyglutarate is sufficient to promote leukemogenesis and its effects are reversible. *Science (New York, N.Y.)*, *339*(6127), 1621–1625. https://doi.org/10.1126/SCIENCE.1231677

Lu, C., Ward, P. S., Kapoor, G. S., Rohle, D., Turcan, S., Abdel-Wahab, O., Edwards, C. R., Khanin, R., Figueroa, M. E., Melnick, A., Wellen, K. E., Oĝrourke, D. M., Berger, S. L., Chan, T. A., Levine, R. L., Mellinghoff, I. K., & Thompson, C. B. (2012). IDH mutation impairs histone demethylation and results in a block to cell differentiation. *Nature*, *483*(7390), 474. https://doi.org/10.1038/NATURE10860

Ma, L., Tao, Y., Duran, A., Llado, V., Galvez, A., Barger, J. F., Castilla, E. A., Chen, J., Yajima, T., Porollo, A., Medvedovic, M., Brill, L. M., Plas, D. R., Riedl, S. J., Leitges, M., Diaz-Meco, M. T., Richardson, A. D., & Moscat, J. (2013). Control of nutrient stress-induced metabolic reprogramming by PKCζ in tumorigenesis. *Cell*, *152*(3), 599–611. https://doi.org/10.1016/J.CELL.2012.12.028

Ma, T., Peng, Y., Huang, W., Liu, Y., & Ding, J. (2017). *The β and γ subunits play distinct functional roles in the α 2 βγ heterotetramer of human NAD-dependent isocitrate*

dehydrogenase. https://doi.org/10.1038/srep41882

Mallette, F. A., Moiseeva, O., Calabrese, V., Mao, B., Gaumont-Leclerc, M. F., & Ferbeyre, G. (2010). Transcriptome analysis and tumor suppressor requirements of STAT5-induced senescence. *Annals of the New York Academy of Sciences*, *1197*(1), 142–151. https://doi.org/10.1111/J.1749-6632.2010.05192.X

Márton, M., Bánhegyi, G., Gyöngyösi, N., Kálmán, E. É., Pettkó-Szandtner, A., Káldi, K., & Kapuy, O. (2022). A systems biological analysis of the ATF4-GADD34-CHOP regulatory triangle upon endoplasmic reticulum stress. *FEBS Open Bio*, *12*(11), 2065–2082. https://doi.org/10.1002/2211-5463.13484

Matsumoto, H., Miyazaki, S., Matsuyama, S., Takeda, M., Kawano, M., Nakagawa, H., Nishimura, K., & Matsuo, S. (2013). Selection of autophagy or apoptosis in cells exposed to ER-stress depends on ATF4 expression pattern with or without CHOP expression. *Biology Open*, *2*(10), 1084. https://doi.org/10.1242/BIO.20135033

McBrayer, S. K., Mayers, J. R., DiNatale, G. J., Shi, D. D., Khanal, J., Chakraborty, A. A., Sarosiek, K. A., Briggs, K. J., Robbins, A. K., Sewastianik, T., Shareef, S. J., Olenchock, B. A., Parker, S. J., Tateishi, K., Spinelli, J. B., Islam, M., Haigis, M. C., Looper, R. E., Ligon, K. L., … Kaelin, W. G. (2018). Transaminase Inhibition by 2-Hydroxyglutarate Impairs Glutamate Biosynthesis and Redox Homeostasis in Glioma. *Cell*, *175*(1), 101-116.e25. https://doi.org/10.1016/J.CELL.2018.08.038

McCann, C., & Kerr, E. M. (2021). Metabolic Reprogramming: A Friend or Foe to Cancer Therapy? *Cancers*, *13*(13). https://doi.org/10.3390/CANCERS13133351

McConkey, D. J. (2017). The integrated stress response and proteotoxicity in cancer therapy. In *Biochemical and Biophysical Research Communications* (Vol. 482, Issue 3). https://doi.org/10.1016/j.bbrc.2016.11.047

Mejlvang, J., Feng, Y., Alabert, C., Neelsen, K. J., Jasencakova, Z., Zhao, X., Lees, M., Sandelin, A., Pasero, P., Lopes, M., & Groth, A. (2014). New histone supply regulates replication fork speed and PCNA unloading. *The Journal of Cell Biology*, *204*(1), 29. https://doi.org/10.1083/JCB.201305017

Mishra, S., Van Rechem, C., Pal, S., Clarke, T. L., Chakraborty, D., Mahan, S. D., Black, J. C., Lawrence, M. S., Daniels, D. L., & Whetstine, J. R. (2018). Cross-talk between Lysine-Modifying Enzymes Controls Site-Specific DNA Amplifications. *Cell*, *174*(4), 803-817.e16. https://doi.org/10.1016/J.CELL.2018.06.018

Mohan, M., Pandya, V., & Anindya, R. (2018). Escherichia coli AlkB and single-stranded DNA binding protein SSB interaction explored by Molecular Dynamics Simulation. *Journal of Molecular Graphics & Modelling*, *84*, 29–35. https://doi.org/10.1016/J.JMGM.2018.05.007

Molinaro, A. M., Taylor, J. W., Wiencke, J. K., & Wrensch, M. R. (2019). Genetic and molecular epidemiology of adult diffuse glioma. *Nature Reviews. Neurology*, *15*(7), 405–417. https://doi.org/10.1038/S41582-019-0220-2

Nagata, M., Ishino, S., Yamagami, T., & Ishino, Y. (2019). Replication protein A complex in Thermococcus kodakarensis interacts with DNA polymerases and helps their effective strand synthesis. *Bioscience, Biotechnology and Biochemistry*, *83*(4), 695–704. https://doi.org/10.1080/09168451.2018.1559722/SUPPL_FILE/TBBB_A_1559722_SM2896.PDF

Nedelcheva-Veleva, M. N., Krastev, D. B., & Stoynov, S. S. (2006). Coordination of DNA synthesis and replicative unwinding by the S-phase checkpoint pathways. *Nucleic Acids Research*, *34*(15), 4138. https://doi.org/10.1093/NAR/GKL528

Negrini, S., Gorgoulis, V. G., & Halazonetis, T. D. (2010). Genomic instability — an evolving hallmark of cancer. *Nature Reviews Molecular Cell Biology 2010 11:3*, *11*(3), 220–228. https://doi.org/10.1038/nrm2858

Nigam, R., Mohan, M., Shivange, G., Dewangan, P. K., & Anindya, R. (2018). Escherichia coli AlkB interacts with single-stranded DNA binding protein SSB by an intrinsically disordered region of SSB. *Molecular Biology Reports*, *45*(5), 865–870. https://doi.org/10.1007/s11033-018-4232-6

Nobusawa, S., Watanabe, T., Kleihues, P., & Ohgaki, H. (2009). IDH1 mutations as molecular signature and predictive factor of secondary glioblastomas. *Clinical Cancer Research : An Official Journal of the American Association for Cancer Research*, *15*(19), 6002–6007. https://doi.org/10.1158/1078-0432.CCR-09-0715

Noushmehr, H., Weisenberger, D. J., Diefes, K., Phillips, H. S., Pujara, K., Berman, B. P., Pan, F., Pelloski, C. E., Sulman, E. P., Bhat, K. P., Verhaak, R. G. W., Hoadley, K. A., Hayes, D. N., Perou, C. M., Schmidt, H. K., Ding, L., Wilson, R. K., Van Den Berg, D., Shen, H., … Aldape, K. (2010). Identification of a CpG Island Methylator Phenotype that Defines a Distinct Subgroup of Glioma. *Cancer Cell*, *17*(5), 510–522. https://doi.org/10.1016/J.CCR.2010.03.017

Oermann, E. K., Wu, J., Guan, K. L., & Xiong, Y. (2012). Alterations of Metabolic Genes and Metabolites in Cancer. *Seminars in Cell & Developmental Biology*, *23*(4), 370. https://doi.org/10.1016/J.SEMCDB.2012.01.013

Pakos-Zebrucka, K., Koryga, I., Mnich, K., Ljujic, M., Samali, A., & Gorman, A. M. (2016). The integrated stress response. *EMBO Reports*, *17*(10), 1374–1395. https://doi.org/10.15252/EMBR.201642195

Pappa, S., Padilla, N., Iacobucci, S., Vicioso, M., De La Campa, E. Á., Navarro, C., Marcos, E., De La Cruz, X., & Martínez-Balbás, M. A. (2019). PHF2 histone demethylase prevents DNA damage and genome instability by controlling cell cycle progression of neural progenitors. *Proceedings of the National Academy of Sciences of the United States of America*, *116*(39), 19464–19473. https://doi.org/10.1073/PNAS.1903188116/SUPPL_FILE/PNAS.1903188116.SAPP.PDF

Park, J. W., & Turcan, Ş. (2019). Epigenetic Reprogramming for Targeting IDH-Mutant Malignant Gliomas. *Cancers*, *11*(10). https://doi.org/10.3390/CANCERS11101616

Park, Y., Reyna-Neyra, A., Philippe, L., & Thoreen, C. C. (2017). mTORC1 Balances Cellular Amino Acid Supply with Demand for Protein Synthesis through Post-transcriptional Control of ATF4. *Cell Reports*, *19*(6), 1083–1090. https://doi.org/10.1016/j.celrep.2017.04.042

Parker, S. J., Encarnación-Rosado, J., Hollinshead, K. E. R., Hollinshead, D. M., Ash, L. J., Rossi, J. A. K., Lin, E. Y., Sohn, A. S. W., Philips, M. R., Jones, D. R., & Kimmelman, A. C. (2021). Spontaneous hydrolysis and spurious metabolic properties of α-ketoglutarate esters. *Nature Communications*, *12*(1). https://doi.org/10.1038/s41467-021-25228-9

Pasero, P., & Gasser, S. M. (1998). New systems for replicating DNA in vitro. *Current Opinion in Cell Biology*, *10*(3), 304–310. https://doi.org/10.1016/S0955-0674(98)80004-5

Podust, L. M., Krezel, A. M., & Kim, Y. (2001). Crystal structure of the CCAAT box/enhancer-binding protein beta activating transcription factor-4 basic leucine zipper heterodimer in the absence of DNA. *The Journal of Biological Chemistry*, *276*(1), 505–513. https://doi.org/10.1074/JBC.M005594200

Pommier, Y., Sun, Y., Huang, S. Y. N., & Nitiss, J. L. (2016). Roles of eukaryotic topoisomerases in transcription, replication and genomic stability. *Nature Reviews Molecular Cell Biology 2016 17:11*, *17*(11), 703–721. https://doi.org/10.1038/nrm.2016.111

Popovici-Muller, J., Lemieux, R. M., Artin, E., Saunders, J. O., Salituro, F. G., Travins, J., Cianchetta, G., Cai, Z., Zhou, D., Cui, D., Chen, P., Straley, K., Tobin, E., Wang, F., David, M. D., Penard-Lacronique, V., Quivoron, C., Saada, V., De Botton, S., … Yen, K. (2018). Discovery of AG-120 (Ivosidenib): A First-in-Class Mutant IDH1 Inhibitor for the Treatment of IDH1 Mutant Cancers. *ACS Medicinal Chemistry Letters*, *9*(4), 300–305. https://doi.org/10.1021/ACSMEDCHEMLETT.7B00421/SUPPL_FILE/ML7B00421_SI_001.PDF

Popovici-Muller, J., Saunders, J. O., Salituro, F. G., Travins, J. M., Yan, S., Zhao, F., Gross, S., Dang, L., Yen, K. E., Yang, H., Straley, K. S., Jin, S., Kunii, K., Fantin, V. R., Zhang, S., Pan, Q., Shi, D., Biller, S. A., & Su, S. M. (2012). Discovery of the FirstPotent Inhibitors of MutantIDH1 That Lower Tumor 2-HG in Vivo. *ACS Medicinal Chemistry Letters*, *3*(10), 850. https://doi.org/10.1021/ML300225H

Ré mi Buisson, A., Boisvert, J. L., Benes, C. H., & Zou Correspondence, L. (2015). Distinct but Concerted Roles of ATR, DNA-PK, and Chk1 in Countering Replication Stress during S Phase. *Molecular Cell*, *59*. https://doi.org/10.1016/j.molcel.2015.07.029

Read, A., & Schröder, M. (2021). The Unfolded Protein Response: An Overview. *Biology*, *10*(5). https://doi.org/10.3390/BIOLOGY10050384

Richardson, R. T., Alekseev, O. M., Grossman, G., Widgren, E. E., Thresher, R., Wagner, E. J., Sullivan, K. D., Marzluff, W. F., & O'Rand, M. G. (2006). Nuclear autoantigenic sperm protein (NASP), a linker histone chaperone that is required for cell proliferation. *Journal of Biological Chemistry*, *281*(30), 21526–21534. https://doi.org/10.1074/jbc.M603816200

Rodriguez-Fernandez, M., Iii, F. J. D., Kreutz, C., & Timmer, J. (2013). Oxidative Stress, Protein

Damage. *Encyclopedia of Systems Biology*, 1619–1620. https://doi.org/10.1007/978-1-4419-9863-7_650

Rojas, M., Vasconcelos, G., & Dever, T. E. (2015). An eIF2α-binding motif in protein phosphatase 1 subunit GADD34 and its viral orthologs is required to promote dephosphorylation of eIF2α. *Proceedings of the National Academy of Sciences of the United States of America*, *112*(27), E3466–E3475. https://doi.org/10.1073/PNAS.1501557112/SUPPL_FILE/PNAS.201501557SI.PDF

Rondinelli, B., Schwerer, H., Antonini, E., Gaviraghi, M., Lupi, A., Frenquelli, M., Cittaro, D., Segalla, S., Lemaitre, J. M., & Tonon, G. (2015). H3K4me3 demethylation by the histone demethylase KDM5C/JARID1C promotes DNA replication origin firing. *Nucleic Acids Research*, *43*(5), 2560–2574. https://doi.org/10.1093/NAR/GKV090

Rouschop, K. M., Dubois, L. J., Keulers, T. G., Van Den Beucken, T., Lambin, P., Bussink, J., Van Der Kogel, A. J., Koritzinsky, M., & Wouters, B. G. (2013). PERK/eIF2α signaling protects therapy resistant hypoxic cells through induction of glutathione synthesis and protection against ROS. *Proceedings of the National Academy of Sciences of the United States of America*, *110*(12), 4622–4627. https://doi.org/10.1073/PNAS.1210633110/SUPPL_FILE/PNAS.201210633SI.PDF

Ruiz, S., Lopez-Contreras, A. J., Gabut, M., Marion, R. M., Gutierrez-Martinez, P., Bua, S., Ramirez, O., Olalde, I., Rodrigo-Perez, S., Li, H., Marques-Bonet, T., Serrano, M., Blasco, M. A., Batada, N. N., & Fernandez-Capetillo, O. (2015). Limiting replication stress during somatic cell reprogramming reduces genomic instability in induced pluripotent stem cells. *Nature Communications*, *6*. https://doi.org/10.1038/NCOMMS9036

Saavedra, F., Gurard-Levin, Z. A., Rojas-Villalobos, C., Vassias, I., Quatrini, R., Almouzni, G., & Loyola, A. (2020). JMJD1B, a novel player in histone H3 and H4 processing to ensure genome stability. *Epigenetics & Chromatin*, *13*(1). https://doi.org/10.1186/S13072-020-00331-1

Sabatinos, S. A., & Forsburg, S. L. (2015). Managing Single-Stranded DNA during Replication Stress in Fission Yeast. *Biomolecules*, *5*(3), 2123. https://doi.org/10.3390/BIOM5032123

Sasaki, M., Knobbe, C. B., Itsumi, M., Elia, A. J., Harris, I. S., Chio, I. I. C., Cairns, R. A., Mccracken, S., Wakeham, A., Haight, J., Ten, A. Y., Snow, B., Ueda, T., Inoue, S.,

Yamamoto, K., Ko, M., Rao, A., Yen, K. E., Su, S. M., & Mak, T. W. (2012). D-2-hydroxyglutarate produced by mutant IDH1 perturbs collagen maturation and basement membrane function. *Genes & Development*, *26*(18), 2038–2049. https://doi.org/10.1101/GAD.198200.112

Schindelin, J., Arganda-Carreras, I., Frise, E., Kaynig, V., Longair, M., Pietzsch, T., Preibisch, S., Rueden, C., Saalfeld, S., Schmid, B., Tinevez, J. Y., White, D. J., Hartenstein, V., Eliceiri, K., Tomancak, P., & Cardona, A. (2012). Fiji: an open-source platform for biological-image analysis. *Nature Methods 2012 9:7*, *9*(7), 676–682. https://doi.org/10.1038/nmeth.2019

Schrecker, M., Castaneda, J. C., Devbhandari, S., Kumar, C., Remus, D., & Hite, R. K. (2022). Multistep loading of a DNA sliding clamp onto DNA by replication factor C. *ELife*, *11*. https://doi.org/10.7554/ELIFE.78253

Schvartzman, J.-M., Forsyth, G., Walch, H., Chatila, W., Santella, A., Menghrajani, K., Sánchez-Vega, F., Koche, R., & Thompson, C. B. (2022). Oncogenic IDH mutations increase heterochromatin-related replication stress without impacting tumor mutation burden. *BioRxiv*, 2022.08.04.502834. https://doi.org/10.1101/2022.08.04.502834

Selak, M. A., Armour, S. M., MacKenzie, E. D., Boulahbel, H., Watson, D. G., Mansfield, K. D., Pan, Y., Simon, M. C., Thompson, C. B., & Gottlieb, E. (2005). Succinate links TCA cycle dysfunction to oncogenesis by inhibiting HIF-α prolyl hydroxylase. *Cancer Cell*, *7*(1), 77–85. https://doi.org/10.1016/j.ccr.2004.11.022

Shan, J., Örd, D., Örd, T., & Kilberg, M. S. (2009). Elevated ATF4 Expression, in the Absence of Other Signals, Is Sufficient for Transcriptional Induction via CCAAT Enhancer-binding Protein-activating Transcription Factor Response Elements. *The Journal of Biological Chemistry*, *284*(32), 21241. https://doi.org/10.1074/JBC.M109.011338

Shechter, D., Ying, C. Y., & Gautier, J. (2004). DNA unwinding is an MCM complex-dependent and ATP hydrolysis-dependent process. *Journal of Biological Chemistry*, *279*(44), 45586–45593. https://doi.org/10.1074/jbc.M407772200

Shen, J., Xiang, X., Chen, L., Wang, H., Wu, L., Sun, Y., Ma, L., Gu, X., Liu, H., Wang, L., Yu, Y., Shao, J., Huang, C., & Chin, Y. E. (2017). JMJD5 cleaves monomethylated histone H3 N-tail under DNA damaging stress. *EMBO Reports*, *18*(12), 2131–2143.

https://doi.org/10.15252/EMBR.201743892

Shi, H., Wang, X., Lu, Z., Zhao, B. S., Ma, H., Hsu, P. J., Liu, C., & He, C. (2017). YTHDF3 facilitates translation and decay of N6-methyladenosine-modified RNA. *Cell Research 2017 27:3*, *27*(3), 315–328. https://doi.org/10.1038/cr.2017.15

Sidrauski, C., McGeachy, A. M., Ingolia, N. T., & Walter, P. (2015). The small molecule ISRIB reverses the effects of eIF2α phosphorylation on translation and stress granule assembly. *ELife*, *2015*(4). https://doi.org/10.7554/ELIFE.05033

Singh, D., Vishnoi, T., & Kumar, A. (2013). Effect of alpha-ketoglutarate on growth and metabolism of cells cultured on three-dimensional cryogel matrix. *International Journal of Biological Sciences*, *9*(5), 521–530. https://doi.org/10.7150/ijbs.4962

Smith, Z. D., & Meissner, A. (2013). DNA methylation: roles in mammalian development. *Nature Reviews Genetics 2013 14:3*, *14*(3), 204–220. https://doi.org/10.1038/nrg3354

Stenlund, A. (2003). Initiation of DNA replication: lessons from viral initiator proteins. *Nature Reviews Molecular Cell Biology 2003 4:10*, *4*(10), 777–785. https://doi.org/10.1038/nrm1226

Su, R., Dong, L., Li, C., Nachtergaele, S., Wunderlich, M., Qing, Y., Deng, X., Wang, Y., Weng, X., Hu, C., Yu, M., Skibbe, J., Dai, Q., Zou, D., Wu, T., Yu, K., Weng, H., Huang, H., Ferchen, K., … Chen, J. (2018a). R-2HG Exhibits Anti-tumor Activity by Targeting FTO/m 6 A/MYC/CEBPA Signaling. *Cell*, *172*(1–2), 90-105.e23. https://doi.org/10.1016/J.CELL.2017.11.031

Su, R., Dong, L., Li, C., Nachtergaele, S., Wunderlich, M., Qing, Y., Deng, X., Wang, Y., Weng, X., Hu, C., Yu, M., Skibbe, J., Dai, Q., Zou, D., Wu, T., Yu, K., Weng, H., Huang, H., Ferchen, K., … Chen, J. (2018b). R-2HG Exhibits Anti-tumor Activity by Targeting FTO/m6A/MYC/CEBPA Signaling. *Cell*, *172*(1–2), 90-105.e23. https://doi.org/10.1016/J.CELL.2017.11.031/ATTACHMENT/48868333-A7A4-41AE-BE63-D15E2BF2D01A/MMC3.XLSX

Subramanian, D., & Griffith, J. D. (2005). p53 Monitors Replication Fork Regression by Binding to “Chickenfoot” Intermediates. *Journal of Biological Chemistry*, *280*(52), 42568–42572. https://doi.org/10.1074/JBC.M506348200

Sulkowski, P. L., Corso, C. D., Robinson, N. D., Scanlon, S. E., Purshouse, K. R., Bai, H., Liu, Y., Sundaram, R. K., Hegan, D. C., Fons, N. R., Breuer, G. A., Song, Y., Mishra-Gorur, K., De Feyter, H. M., De Graaf, R. A., Surovtseva, Y. V., Kachman, M., Halene, S., Günel, M., … Bindra, R. S. (2017a). 2-Hydroxyglutarate produced by neomorphic IDH mutations suppresses homologous recombination and induces PARP inhibitor sensitivity. *Science Translational Medicine*, *9*(375). https://doi.org/10.1126/SCITRANSLMED.AAL2463/SUPPL_FILE/AAL2463_SM.PDF

Sulkowski, P. L., Corso, C. D., Robinson, N. D., Scanlon, S. E., Purshouse, K. R., Bai, H., Liu, Y., Sundaram, R. K., Hegan, D. C., Fons, N. R., Breuer, G. A., Song, Y., Mishra-Gorur, K., De Feyter, H. M., De Graaf, R. A., Surovtseva, Y. V., Kachman, M., Halene, S., Günel, M., … Bindra, R. S. (2017b). 2-Hydroxyglutarate produced by neomorphic IDH mutations suppresses homologous recombination and induces PARP inhibitor sensitivity. *Science Translational Medicine*, *9*(375). https://doi.org/10.1126/SCITRANSLMED.AAL2463

Sulkowski, P. L., Corso, C. D., Robinson, N. D., Scanlon, S. E., Purshouse, K. R., Bai, H., Liu, Y., Sundaram, R. K., Hegan, D. C., Fons, N. R., Breuer, G. A., Song, Y., Mishra-Gorur, K., De Feyter, H. M., De Graaf, R. A., Surovtseva, Y. V., Kachman, M., Halene, S., Günel, M., … Bindra, R. S. (2017c). 2-Hydroxyglutarate produced by neomorphic IDH mutations suppresses homologous recombination and induces PARP inhibitor sensitivity. *Science Translational Medicine*, *9*(375). https://doi.org/10.1126/SCITRANSLMED.AAL2463

Sulkowski, P. L., Oeck, S., Dow, J., Economos, N. G., Mirfakhraie, L., Liu, Y., Noronha, K., Bao, X., Li, J., Shuch, B. M., King, M. C., Bindra, R. S., & Glazer, P. M. (2020). Oncometabolites suppress DNA repair by disrupting local chromatin signalling. *Nature 2020 582:7813*, *582*(7813), 586–591. https://doi.org/10.1038/s41586-020-2363-0

Tabata, S., Kojima, Y., Sakamoto, T., Igarashi, K., Umetsu, K., Ishikawa, T., Hirayama, A., Kajino-Sakamoto, R., Sakamoto, N., Yasumoto, K. ichi, Okano, K., Suzuki, Y., Yachida, S., Aoki, M., & Soga, T. (2023). L-2hydroxyglutaric acid rewires amino acid metabolism in colorectal cancer via the mTOR-ATF4 axis. *Oncogene 2023 42:16*, *42*(16), 1294–1307. https://doi.org/10.1038/s41388-023-02632-7

Tameire, F., Verginadis, I. I., Leli, N. M., Polte, C., Conn, C. S., Ojha, R., Salas Salinas, C., Chinga,

F., Monroy, A. M., Fu, W., Wang, P., Kossenkov, A., Ye, J., Amaravadi, R. K., Ignatova, Z., Fuchs, S. Y., Diehl, J. A., Ruggero, D., & Koumenis, C. (2019). ATF4 couples MYC-dependent translational activity to bioenergetic demands during tumour progression. *Nature Cell Biology*, *21*(7). https://doi.org/10.1038/s41556-019-0347-9

Tanaka, M., & Chock, P. B. (2021). Oxidative Modifications of RNA and Its Potential Roles in Biosystem. *Frontiers in Molecular Biosciences*, *8*, 685331. https://doi.org/10.3389/FMOLB.2021.685331/BIBTEX

Técher, H., & Pasero, P. (2021a). The Replication Stress Response on a Narrow Path Between Genomic Instability and Inflammation. *Frontiers in Cell and Developmental Biology*, *9*. https://doi.org/10.3389/FCELL.2021.702584

Técher, H., & Pasero, P. (2021b). The Replication Stress Response on a Narrow Path Between Genomic Instability and Inflammation. *Frontiers in Cell and Developmental Biology*, *9*, 1671. https://doi.org/10.3389/FCELL.2021.702584/BIBTEX

Teng, Y. C., Sundaresan, A., O'Hara, R., Gant, V. U., Li, M., Martire, S., Warshaw, J. N., Basu, A., & Banaszynski, L. A. (2021). ATRX promotes heterochromatin formation to protect cells from G-quadruplex DNA-mediated stress. *Nature Communications 2021 12:1*, *12*(1), 1–14. https://doi.org/10.1038/s41467-021-24206-5

Thibault, G., Shui, G., Kim, W., McAlister, G. C., Ismail, N., Gygi, S. P., Wenk, M. R., & Ng, D. T. W. (2012). The Membrane Stress Response Buffers Lethal Effects of Lipid Disequilibrium by Reprogramming the Protein Homeostasis Network. *Molecular Cell*, *48*(1), 16–27. https://doi.org/10.1016/J.MOLCEL.2012.08.016

Tian, X., Zhang, S., Zhou, L., Seyhan, A. A., Hernandez Borrero, L., Zhang, Y., & El-Deiry, W. S. (2021). Targeting the Integrated Stress Response in Cancer Therapy. In *Frontiers in Pharmacology* (Vol. 12). https://doi.org/10.3389/fphar.2021.747837

Toledo, L. I., Altmeyer, M., Rask, M. B., Lukas, C., Larsen, D. H., Povlsen, L. K., Bekker-Jensen, S., Mailand, N., Bartek, J., & Lukas, J. (2013). ATR Prohibits Replication Catastrophe by Preventing Global Exhaustion of RPA. *Cell*, *155*(5), 1088–1103. https://doi.org/10.1016/J.CELL.2013.10.043

Torrence, M. E., Macarthur, M. R., Hosios, A. M., Valvezan, A. J., Asara, J. M., Mitchell, J. R., & Manning, B. D. (2021). The mtorc1-mediated activation of atf4 promotes protein and glutathione synthesis downstream of growth signals. *ELife*, *10*. https://doi.org/10.7554/ELIFE.63326

Turcan, S., Rohle, D., Goenka, A., Walsh, L. A., Fang, F., Yilmaz, E., Campos, C., Fabius, A. W. M., Lu, C., Ward, P. S., Thompson, C. B., Kaufman, A., Guryanova, O., Levine, R., Heguy, A., Viale, A., Morris, L. G. T., Huse, J. T., Mellinghoff, I. K., & Chan, T. A. (2012). IDH1 mutation is sufficient to establish the glioma hypermethylator phenotype. *Nature*, *483*(7390), 479–483. https://doi.org/10.1038/NATURE10866

Tyler, J. K., Adams, C. R., Chen, S. R., Kobayashi, R., Kamakaka, R. T., & Kadonaga, J. T. (1999). The RCAF complex mediates chromatin assembly during DNA replication and repair. *Nature*, *402*(6761), 555–560. https://doi.org/10.1038/990147

Udugama, M., Hii, L., Garvie, A., Cervini, M., Vinod, B., Chan, F. L., Das, P. P., Mann, J. R., Collas, P., Voon, H. P. J., & Wong, L. H. (2021). Mutations inhibiting KDM4B drive ALT activation in ATRX-mutated glioblastomas. *Nature Communications 2021 12:1*, *12*(1), 1–11. https://doi.org/10.1038/s41467-021-22543-z

Van Houten, B., Santa-Gonzalez, G. A., & Camargo, M. (2018). DNA repair after oxidative stress: Current challenges. *Current Opinion in Toxicology*, *7*, 9–16. https://doi.org/10.1016/j.cotox.2017.10.009

Vasudevan, D., Neuman, S. D., Yang, A., Lough, L., Brown, B., Bashirullah, A., Cardozo, T., & Ryoo, H. D. (2020). Translational induction of ATF4 during integrated stress response requires noncanonical initiation factors eIF2D and DENR. *Nature Communications 2020 11:1*, *11*(1), 1–11. https://doi.org/10.1038/s41467-020-18453-1

Verma, A. (2013). Animal Tissue Culture: Principles and Applications. *Animal Biotechnology: Models in Discovery and Translation*, 211–231. https://doi.org/10.1016/B978-0-12-416002-6.00012-2

Vicioso-Mantis, M., Aguirre, S., & Martínez-Balbás, M. A. (2022). JmjC Family of Histone Demethylases Form Nuclear Condensates. *International Journal of Molecular Sciences*, *23*(14), 7664. https://doi.org/10.3390/IJMS23147664/S1

Waitkus, M. S., Diplas, B. H., Yan, H., Preston, T., Tisch, R., & Tumor, B. (2016). Isocitrate dehydrogenase mutations in gliomas. *Neuro-Oncology*, *18*(1), 16–26. https://doi.org/10.1093/NEUONC/NOV136

Wang, P., Wu, J., Ma, S., Zhang, L., Yao, J., Hoadley, K. A., Wilkerson, M. D., Perou, C. M., Guan, K. L., Ye, D., & Xiong, Y. (2015). Oncometabolite D-2-Hydroxyglutarate Inhibits ALKBH DNA Repair Enzymes and Sensitizes IDH Mutant Cells to Alkylating Agents. *Cell Reports*, *13*(11), 2353–2361. https://doi.org/10.1016/J.CELREP.2015.11.029

Watanabe, T., Nobusawa, S., Kleihues, P., & Ohgaki, H. (2009). IDH1 mutations are early events in the development of astrocytomas and oligodendrogliomas. *American Journal of Pathology*, *174*(4), 1149–1153. https://doi.org/10.2353/ajpath.2009.080958

Wolzak, K., Nölle, A., Farina, M., Abbink, T. E., Knaap, M. S. van der, Verhage, M., & Scheper, W. (2022). Neuron-specific translational control shift ensures proteostatic resilience during ER stress. *The EMBO Journal*, *41*(16), 110501. https://doi.org/10.15252/EMBJ.2021110501

Wortel, I. M. N., van der Meer, L. T., Kilberg, M. S., & van Leeuwen, F. N. (2017). Surviving Stress: Modulation of ATF4-Mediated Stress Responses in Normal and Malignant Cells. *Trends in Endocrinology and Metabolism: TEM*, *28*(11), 794. https://doi.org/10.1016/J.TEM.2017.07.003

Wu, R., Wang, Z., Zhang, H., Gan, H., & Zhang, Z. (2017). H3K9me3 demethylase Kdm4d facilitates the formation of pre-initiative complex and regulates DNA replication. *Nucleic Acids Research*, *45*(1), 169–180. https://doi.org/10.1093/NAR/GKW848

Xie, S.-Z., Pan, J.-J., Xu, J.-F., Zhu, W.-W., Qin, L.-X., & Feng, J.-. (2022). The critical function of metabolic reprogramming in cancer metastasis. *Aging and Cancer*, *3*(1), 20–43. https://doi.org/10.1002/AAC2.12044

Xu, W., Yang, H., Liu, Y., Yang, Y., Wang, P., Kim, S. H., Ito, S., Yang, C., Wang, P., Xiao, M. T., Liu, L. X., Jiang, W. Q., Liu, J., Zhang, J. Y., Wang, B., Frye, S., Zhang, Y., Xu, Y. H., Lei, Q. Y., … Xiong, Y. (2011). Oncometabolite 2-hydroxyglutarate is a competitive inhibitor of α-ketoglutarate-dependent dioxygenases. *Cancer Cell*, *19*(1), 17–30. https://doi.org/10.1016/J.CCR.2010.12.014

Yan, H., Parsons, D. W., Jin, G., McLendon, R., Rasheed, B. A., Yuan, W., Kos, I., Batinic-Haberle, I., Jones, S., Riggins, G. J., Friedman, H., Friedman, A., Reardon, D., Herndon, J., Kinzler, K. W., Velculescu, V. E., Vogelstein, B., & Bigner, D. D. (2009). IDH1 and IDH2 Mutations in Gliomas . *New England Journal of Medicine*, *360*(8), 765–773. https://doi.org/10.1056/NEJMOA0808710/SUPPL_FILE/NEJM_YAN_765SA1.PDF

Yang, B., Liu, Y., & Steinacker, J. M. (2023). α-Ketoglutarate stimulates cell growth through the improvement of glucose and glutamine metabolism in C2C12 cell culture. *Frontiers in Nutrition*, *10*. https://doi.org/10.3389/fnut.2023.1145236

Yang, X., Xia, R., Yue, C., Zhai, W., Du, W., Yang, Q., Cao, H., Chen, X., Obando, D., Zhu, Y., Chen, X., Chen, J. J., Piganelli, J., Wipf, P., Jiang, Y., Xiao, G., Wu, C., Jiang, J., & Lu, B. (2018). ATF4 Regulates CD4+ T Cell Immune Responses through Metabolic Reprogramming. *Cell Reports*, *23*(6), 1754–1766. https://doi.org/10.1016/J.CELREP.2018.04.032

Ye, D., Ma, S., Xiong, Y., & Guan, K. L. (2013a). R-2-hydroxyglutarate as the key effector of IDH mutations promoting oncogenesis. *Cancer Cell*, *23*(3), 274. https://doi.org/10.1016/J.CCR.2013.03.005

Ye, D., Ma, S., Xiong, Y., & Guan, K. L. (2013b). R-2-hydroxyglutarate as the key effector of IDH mutations promoting oncogenesis. *Cancer Cell*, *23*(3), 274. https://doi.org/10.1016/J.CCR.2013.03.005

Ye, D., Ma, S., Xiong, Y., & Guan, K. L. (2013c). R-2-hydroxyglutarate as the key effector of IDH mutations promoting oncogenesis. *Cancer Cell*, *23*(3), 274. https://doi.org/10.1016/J.CCR.2013.03.005

Yeeles, J. T. P., Deegan, T. D., Janska, A., Early, A., & Diffley, J. F. X. (2015). Regulated eukaryotic DNA replication origin firing with purified proteins. *Nature 2015 519:7544*, *519*(7544), 431–435. https://doi.org/10.1038/nature14285

Yheskel, M., Sidoli, S., & Secombe, J. (2023). Proximity labeling reveals a new in vivo network of interactors for the histone demethylase KDM5. *Epigenetics and Chromatin*, *16*(1), 1–16. https://doi.org/10.1186/S13072-023-00481-Y/FIGURES/4

Zeman, M. K., & Cimprich, K. A. (2013). Causes and consequences of replication stress. *Nature Cell Biology 2014 16:1*, *16*(1), 2–9. https://doi.org/10.1038/ncb2897

Zhang, Q. (2018). It takes two to tango: IDH mutation and glutaminase inhibition in glioma. *Science Translational Medicine*, *10*(460). https://doi.org/10.1126/SCITRANSLMED.AAV0344

Zhao, E., Ding, J., Xia, Y., Liu, M., Ye, B., Choi, J. H., Yan, C., Dong, Z., Huang, S., Zha, Y., Yang, L., Cui, H., & Ding, H. F. (2016). KDM4C and ATF4 Cooperate in Transcriptional Control of Amino Acid Metabolism. *Cell Reports*, *14*(3), 506. https://doi.org/10.1016/J.CELREP.2015.12.053

Zhao, Y., Zhou, J., Liu, D., Dong, F., Cheng, H., Wang, W., Pang, Y., Wang, Y., Mu, X., Ni, Y., Li, Z., Xu, H., Hao, S., Wang, X., Ma, S., Wang, Q. F., Xiao, G., Yuan, W., Liu, B., & Cheng, T. (2015). ATF4 plays a pivotal role in the development of functional hematopoietic stem cells in mouse fetal liver. *Blood*, *126*(21), 2383–2391. https://doi.org/10.1182/BLOOD-2015-03-633354

Zhou, B., Zuo, Y. X., & Jiang, R. T. (2019). Astrocyte morphology: Diversity, plasticity, and role in neurological diseases. *CNS Neuroscience & Therapeutics*, *25*(6), 665. https://doi.org/10.1111/CNS.13123

Zhuang, X., Pei, H. Z., Li, T., Huang, J., Guo, Y., Zhao, Y., Yang, M., Zhang, D., Chang, Z., Zhang, Q., Yu, L., He, C., Zhang, L., Pan, Y., Chen, C., & Chen, Y. (2022). The Molecular Mechanisms of Resistance to IDH Inhibitors in Acute Myeloid Leukemia. *Frontiers in Oncology*, *12*. https://doi.org/10.3389/FONC.2022.931462

Zyryanova, A. F., Kashiwagi, K., Rato, C., Shirouzu, M., Ito, T., & Ron, D. (2021). *ISRIB Blunts the Integrated Stress Response by Allosterically Antagonising the Inhibitory Effect of Phosphorylated eIF2 on eIF2B*. https://doi.org/10.1016/j.molcel.2020.10.031